MATERIALS CHEMISTRY
FRONTIERS

REVIEW

View Article Online
View Journal | View Issue

Cite this: *Mater. Chem. Front.*, 2023, **7**, 405

Metal–organic framework (MOF)-based fluorescence "turn-on" sensors

Tapan K. Pal

Received 18th October 2022,
Accepted 2nd December 2022

DOI: 10.1039/d2qm01070d

rsc.li/frontiers-materials

Metal–organic frameworks (MOFs) are a novel category of hybrid porous multifunctional materials with excellent qualitative features. These properties can be fine-tuned *via* the judicial choice of organic ligands and metal ions and by changing the synthetic reaction conditions. Among the various excellent applications exhibited by MOFs, the photoluminescence behaviour is very appealing and originates from their metal ions, linker, or entrapped guest molecules in their cavity. Thus, due to the tuneable luminescent properties of MOFs, they can act as sensors, enabling the selective and sensitive detection of a diverse range of analytes. In general, the sensing of analytes by MOFs can be accomplished either through a fluorescence "turn-on" (fluorescence intensity increases) or "turn-off" (fluorescence intensity decreases) process. Between them, the former is more important and significant in terms of real-time applications. This is because the "turn-on" emission occurs with the signal lighting (increases the fluorescence intensity) against a dark background. Therefore, this review summarizes the recent advances in MOFs as "turn-on" sensors for the recognition of a wide range of analytes (hazardous compounds, volatile organic molecules, cations, biomolecule, anions, *etc.*) and their sensing mechanism.

1. Introduction

MOFs are an emerging class of coordination polymers that consist of voids with micro/mesoporous channels and a highly crystalline network.[1] Over the last few decades, MOFs have attracted attention from scientists, especially in the fields of materials science, industrial engineering, and chemistry. MOFs possess unique and fascinating structural chemistry such as inorganic-organic hybrid network,[2] high surface area,[3] controllable pore size,[4] flexibility,[5] easy functionalization,[6] smooth tuning of their host–guest interaction[7] and good stability.[8] All these qualitative features of MOFs make them suitable for several potential applications such as sensing,[9–11] catalysis,[12–14] CO_2 sequestration,[15,16] magnetism,[17] gas adsorption,[18,19] separation,[20–22] bio-imaging,[23] drug delivery,[24] energy storage,[25] and proton conductance.[26] Interestingly, MOFs can potentially act as luminescent sensors and this application has been flourishing significantly.[27–30]

Generally, the main components of any sensor are a transducer and receptor, which passes a signal through several pathways. Among the various sensing pathways, the luminescence sensing process is straightforward, friendly, can be quantified by the naked eye and has great flexibility.[31] The crystalline MOF network is synthesized through the self-assembly of an organic linker consisting of multiple binding sites and a single metal ion or metal ion clusters (metal node or SBU).[32,33] Generally, the organic ligand possesses an aromatic surface area with free movement of π electrons, giving rise to luminescence activity upon excitation at a particular wavelength. In addition, the role of metal ions is crucial to the photoluminescence property. Particularly, the d10 transition metal ions or clusters and lanthanide ions are fascinating.[34,35] Specifically, the permutation and combination of organic ligands and metal ions can be adjusted to modulate the sensing property of MOFs. In comparison to the contemporary sensory polymeric materials, MOFs demonstrate various potential benefits, as follows: (a) the direct visualization of the crystalline network, which helps to establish their structural-property correlation, (b) atomistic location of the guest interaction site, which makes easier to confirm the sensing mechanism, (c) their porous nature allows the smooth transfer of the analytes through their voids, *i.e.*, a larger concentration of the analyte in their pores, which brings the analytes in close proximity to the guest interaction site, resulting in a very low limit of detection, and (d) highly luminescent MOFs offer ultra-selectivity, ultra-sensitivity, and rapid response time. Additionally, MOFs show a colorimetric response, which enables the naked eye recognition of the desired analytes. Thus, MOFs as luminescence sensors have excelled in diverse sensing fields (Fig. 1).

In principle, the recognition of analytes can be read out according to the changes in the emission wavelength of MOFs either by a decrease/increase in their emission intensity and/or shift in their emission wavelength peak. However, depending

Department of Chemistry, Pandit Deendayal Energy University, Gandhinagar 382426, Gujarat, India. E-mail: tapan.pal@sot.pdpu.ac.in

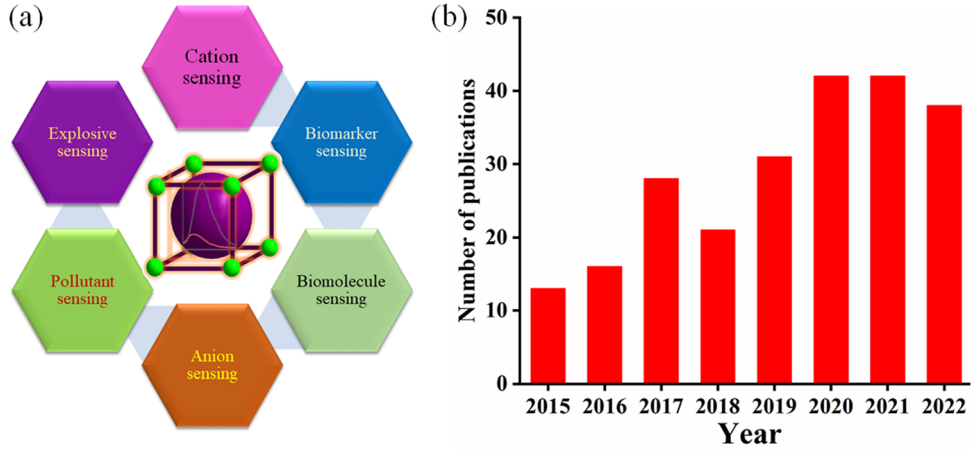

Fig. 1 (a) Various sensing applications using MOFs and (b) "turn-on" sensor application by MOFs for the recognition of diverse analytes (source: SciFinder, accession date: 31st August 2022 and keyword: MOF as "turn-on" sensor).

on the electronic nature of the analyte, MOFs can show either quenching of their emission intensity (turn-off response) or the enhancement in their emission intensity (turn-on response).[36,37] The "turn-on" sensing event is an interesting research motif in terms of sensitivity and real-time applicability, given that the response signal can be denoted as an optical indicator by illuminating light in a dark environment. Alternatively, the "turn-off" sensing event reduces the optical colorimetric response against a bright background. Typically, most of the sensing by MOFs is based on the quenching of luminescence intensity, whereas sensing through "turn-on" by MOFs is very scarce and challenging. A SciFinder survey revealed that the number of MOF-based "turn-on" sensors developed for the detection of various analytes has gradually increased from 2015 to 2022 (Fig. 1, accession date 31st August 2022 and searched using the term MOF as "turn-on" sensor).

Most of the published reviews are focused on MOF-based luminescence sensors[38–41] for all types of analytes, regardless of the sensing event or mechanism. However, although each review article has its own importance and purpose, the approach of this current review is different. Also, a timely review with updated research developments can forecast the past realization, present growth, and further improvement in any research field. Thus, in this review article, attention is devoted to the recent developments for the fluorescence "turn-on" detection of all types of analytes using MOF-based sensors. Various analytes including (a) neutral molecules (biological active molecules/biomarkers, toxic compounds, and volatile organic molecules), (b) cations and (c) anions that induce a luminescence "turn-on" event are discussed thoroughly. Before we summarize the research progress on "turn-on" sensing using MOFs, initially, the fundamental features of luminescence in MOFs are briefly discussed.

2. Luminescence in MOFs

The luminescence process involves the emission of light upon irradiation with a certain wavelength, which can be classed as two types, *i.e.*, fluorescence and phosphorescence. Upon the absorption of incident light, the molecule jumps from the ground state to excited state, and then come down to the ground state either by fluorescence or phosphorescence, *i.e.*, radiative transition. The fluorescence is a very fast process (10^{-15} s) and occurs among energy levels of equal spin multiplicity ($S_1 \rightarrow S_0$). Alternatively, phosphorescence is a delay luminescence process, generally taking microsecond to seconds, and the emission wavelength occurs between the energy states of different spin multiplicity ($T_1 \rightarrow S_0$). Besides this radiative transition, some non-radiative processes are also associated with the luminescence process such as vibrational relaxation, internal conversion and intersystem crossing. This non-radiative process can be clearly comprehended using the well-known Jablonski diagram.[42]

The luminescence process of a fluorophore can be assessed using various factors, as follows: (a) the changes in its luminescence spectrum (or emission wavelength), *i.e.*, either a change in intensity or shift in the peak position, (b) quantum yield, which can be described as the number of photons emitted with respect to the number of quanta absorbed, and (c) average lifetime of the excited state, which indicates the time the fluorophore molecule spends in the excited state before emitting and depends on the rate constant of the non-radiative (k_{nr}) and radiative process (k_r) according to the following equation:[43]

$$\tau = \frac{1}{k_f + k_{nr}} \quad (1)$$

Based on the investigation of numerous luminescent MOFs, the luminescence can originate from different sources such as the ligand alone (mostly π conjugated organic ligands), metal-based emission (mostly noticed from lanthanide metal ions by feature of antenna effect) and due to several types of charge transfer (MMCT, LMCT, MMCT and LLCT).[44] Moreover, the presence of fluorophore molecules in the empty space of MOFs can generate luminescence in MOFs. Each luminescence source are explained in the following sections.

2.1. Emission from ligand

According to the design perspective of the ligands for the construction of MOFs, ligands possessing a large π conjugated aromatic surface area (*i.e.*, rigid backbone) functionalized with carboxylic moieties or heterocyclic groups for coordination to metal ions are generally preferred. This type of organic linker provides stability to the network. In addition, the presence of free π electrons, which freely move throughout the MOF network, reduces the HOMO–LUMO energy gap and delivers interesting photophysical properties to the system. Generally, the emission of free ligands and their solution-based luminescence behaviour are the emission of electrons from the lowermost singlet excited level to the singlet ground level, where the transitions involved are π*→ n and/or π* → π. However, the emission behaviour of the ligand in MOFs with respect to the free organic ligand is very different in terms of emission peak shift, emission peak intensity, lifetime and quantum yield. This is because the binding site of the ligand strongly holds the metal ion to form a coordinated network. Therefore, due to the lack of flexibility of the ligand in the MOF, the excited state is stabilised, and hence the non-radiative decay rate is reduced. In addition, the MOF network allows the various MOF-forming components to be in close proximity, making intramolecular or intermolecular interactions between them feasible, which results in changes in the emission intensity, peak shifting and broadening of the emission peak. Moreover, exposure to external stimuli will also affect the ligand emission. Therefore, it is vital to monitor these various interactions and external stimuli for tuning the emission properties of MOFs. The utilization of these strategies to fine-tune the luminescence properties of MOFs has been nicely demonstrated in the following examples. Ma and coworkers synthesized highly luminescent porous 3D zinc-based MOFs, $[Zn_7(TPPE)_2(SO_4^{2-})_7](DMF{\cdot}H_2O)$ and $[Zn_7(TPPE)_{3/2}(NO_3^-)(OH^-)(H_2O)](DMF{\cdot}2H_2O)$, which displayed strong emission peaks at 497 and 510 nm, respectively, upon excitation at 420 nm.[45] The emission spectrum of the free ligand TPPE showed a peak at 480 nm under the same excitation wavelength. The emission peak of these two MOFs is almost close to the emission peak of the ligand, which may be due to the intra or inter ligand charge transfer transition. Neogi and co-workers synthesized a 3D porous, highly stable nickel-based MOF, CSMCRI-3 under solvothermal conditions.[46] The electronic-rich linker tpim and H_2azdc contain potential binding sites for nickel ions. Consequently, a blue-shift of 17 nm and red-shift of 5 nm for the free linkers H_2azdc (λ_{ex} = 331 nm) and tpim (λ_{ex} = 309 nm) were observed compared to the emission of the MOF (λ_{ex} = 314 nm), respectively. Importantly, in water dispersed medium, the MOF CSMCRI-3 exhibited an emission peak at 395 nm under excitation at 314 nm and the maximum emission peak of the MOF is close to that of the free linker. This is owing to the n–π* and π–π* transition in the electronic-rich ligands in CSMCRI-3. Allendorf and co-workers showed that the ligand-based emission is affected by the local environment in the MOF.[47] They reported the preparation of two porous zinc-based MOFs, *i.e.*, one is a 2D MOF and the other is a 3D MOF. Obviously, the ligand environment in these two MOFs was very different, which influenced their emission property. The 3D and 2D MOFs under UV light showed purple/blue and blue emission, respectively.

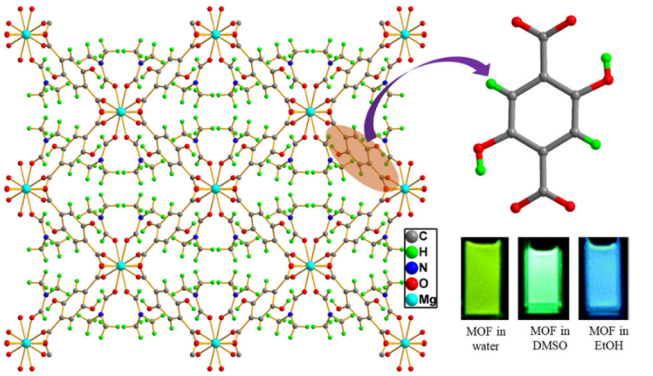

Fig. 2 H_2DHT ligand and its three-dimensional MOF network $Mg(DHT)(DMF)_2$ (inset: solution colour of MOF dispersed in different solvents).

Also, alterations in the luminescence of the ligand may occur due to changes in the excitation level of the linker. Two significant process are excited-state proton transfer (ESPT) and excited-state electron transfer (ESET). In the former process, the proton is attached or leaves the molecule in the excited state, whereas in the latter case, the relocation of the electron occurs from the electron-rich ligand to the electron-deficient ligand. Maji and co-workers used the H_2DHT ligand to construct a magnesium-based MOF, $Mg(DHT)(DMF)_2$, which showed a prominent intramolecular ESPT process (Fig. 2).[48] The free linker H_2DHT showed a UV absorption peak at around 360 nm and its emission peaks appeared at different positions depending on the polarity of the solvent molecules. For instance, the ligand showed blue emission (at 440 nm) in ethanol solvent (polar protic) and green emission (at 510 nm) in DMSO/DMF solvent (polar aprotic). This is ascribed to the keto–enol tautomerism of H_2DHT. Interestingly, given that the H_2DHT ligand can show fluorescence changes due to ESIPT, the MOF also exhibited luminescence changes with a variation in the solvent polarity. The MOF showed blue emission at 429 and 404 nm in ethanol, while in DMSO, these peaks were red-shifted and appeared at 508 nm. Also, in water the emission peak was strongly red-shifted and the maximum emission was observed at 532 nm. Remarkably, in the presence of TFA, the emission peak of MOF was blue-shifted, which is due to the formation of intermolecular hydrogen bonding between H_2DHT and TFA, effectively stopping the ESIPT mechanism. Canivet and co-workers synthesized an Al-MIL-101-NH_2 MOF for the ''turn-on'' detection of H_2S.[49] They first post-synthetically converted the $-NH_2$ group of the linker (NH_2-BDC) in Al-MIL-101-NH_2 to an $-N_3$ group for the construction of Al-MIL-101-N_3. Consequently, the luminescence intensity of the daughter MOF was significantly reduced. In the presence of H_2S, the azide group was converted to an amino group, and hence the fluorescence intensity of the MOF was recovered. Thus, the emission peak and its intensity during the sensing process is entirely ligand based.

2.2. Emission from metal

Besides the role of the ligand in tuning the luminescence properties of MOFs, the involvement of metal ions (nodes) or clusters in their luminescence properties is crucial and has been investigated thoroughly. The construction of MOFs is possible using ligands and a variety of metal ions such as s/p block elements,[50] d block metals[51] and lanthanide metal ions.[52] MOFs synthesized using d block elements particularly d10 metal ions play a vital role in the photoluminescent properties.[53,54] The d10 metal ions contain a closed shell electronic configuration, and thus the d–d electronic transition is very difficult. The network formed from the d10 metal ion shows high luminescent intensity. This can be attributed to the chelation of the metal ion by the ligand, which successfully enhances the rigidity of the ligand and diminishes the non-radiative decay.[55] Generally, to obtain MOFs with significant luminescent properties, zinc and cadmium transition metal ions are widely used. For example, Tai and co-worker synthesized zinc- and cadmium-based MOFs under solvothermal conditions using the H_3L and 2,2-bipy ligands.[56] The free H_3L ligand displayed an emission peak at 448 nm upon excitation at 330 nm. In contrast, the two d10-based MOFs exhibited an emission peak at 528 nm (zinc-based MOF, λ_{ex} = 335 nm) and 532 nm (cadmium-based MOF, λ_{ex} = 330), which are red-shifted by 80 and 84 nm with respect to the emission of the free ligand, respectively. Interestingly, the luminescence intensity of both MOFs was superior with respect to the emission intensity of the free ligand.

Besides, d10 transition metal ions, lanthanide metal ions and/or their clusters are the main contributors to the metal-based emission in MOFs. In the periodic table, the lanthanide metal ions are identified by the regular filling of electrons in the 4f orbitals, from $4f^0$ (for La^{3+}) to $4f^{14}$ (for Lu^{3+}) with the general electronic configuration $[Xe]4f^n$ (n = 0–14). This electronic configuration produces various well-defined energy levels, leading to interesting luminescent properties.[57–59] The 4f orbitals are well shielded by 5s and 5d shells, and thus the electron in the 4f orbital is less sensitive to the outer electronic environment. Moreover, the f–f transition is forbidden, offering sharp, narrow and signature emission peaks. Most of the lanthanide metal ions except Lu^{3+} and La^{3+} show characteristic emission colours. The Tb^{3+}, Tm^{3+}, Eu^{3+} and Sm^{3+} lanthanide metal ions produce green, blue, red and orange emissive colour, respectively. In contrast, the Nd^{3+}, Yb^{3+} and Er^{3+} lanthanide metal ions emit in the near-infrared region.

Considering that the f–f transition in lanthanides metal ions is forbidden, their molar absorption coefficients are very low. The direct electronic transition in lanthanide metal ions is very inefficient, which can sometimes be achieved using a high power laser source. However, this difficulty can be overcome using a foreign compound that can transfer energy to the lanthanide metal ions, where this process is widely known as the antenna effect or sensitization.[60–62] This antenna effect generally occurs in three steps. In the first step, upon light irradiation the organic ligand present in the lanthanide complex or MOF gets excited. In the second step, intramolecular energy relocation is accomplished from the excited level of the ligand to the lanthanide ions. The final step involves the occurrence of emission from the lanthanide metal ions. This movement of energy in the antenna or sensitization process can be clearly understood according to the following path: the initial migration of energy is the spin-allowed ligand-based transition, and then the spin-forbidden energy relocation from the excited singlet level (S_1) to the excited triplet level (T_1), followed by the transfer of energy from the excited triplet state T_1 to the lanthanide metal ion. Finally, the metal-based emission occurs (Fig. 3). Another way of energy relocation is the direct allocation of energy from the excited singlet level of the linker to the excited energy level of the lanthanide metal, where the metal-entered emission occurs (Fig. 3). This direct transfer of energy generally observed for Tb^{3+} and Eu^{3+}.[63] If the energy transfer from the ligand to the lanthanide metal ion is very efficient, then phosphorescence and fluorescence from the ligand may not occur. If the energy relocation is occurs partially, then the both the ligand-based and metal-based (lanthanide) emission will be observed. In this context, the energy relocation from the ligand to lanthanide metal ions usually occurs at higher energy levels than the emission level for the metal-based emission, otherwise the back transfer of energy will occur.

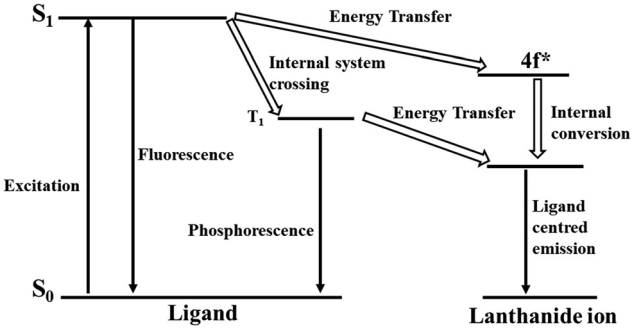

Fig. 3 Schematic presentation of the absorption, emission and sensitization process occurring in lanthanide-based MOFs (S_0 = ground singlet level, S_1 = ground excited level, and T_1 = triplet singlet level).

Therefore, to achieve lanthanide-based emission in MOFs, the role of the organic linkers is crucial. In addition, the triplet energy state of the linker should be energetically equal or higher than the resonance energy state of the lanthanide metal ion, and thus the linker can maximize the energy transfer and decrease the back-transfer. Therefore, the design of the organic ligand is crucial to generate the luminescent lanthanide-based MOFs.[64]

Another important transition shown by lanthanide metal ions is the ''hypersensitive transition'', in which the intensity of the transition is influenced by the local symmetry and environment.[65] Although, the f–f transition is less intense, when lanthanide metal ions are introduced in a new chemical environment, the non-centrosymmetric interaction enables the mixing of the different parity wave functions. This results in ''hypersensitive transitions.[66] Various Eu^{3+} ion-based lanthanide MOFs show hypersensitive transitions and based on these

transitions, the coordination environment and symmetry of the chemical environment around the metal ion can be understood.[67,68]

The quantum yield is a very significant parameter to assess the luminescence quality of MOFs. The quantum yield can be defined as the ratio of the number of photons released to the number of photon absorbed. The quantum yield of lanthanide MOFs sometimes decreases due to the vibration of the environmental ligands, and particularly, the high energy vibration of carbon–hydrogen, nitrogen–hydrogen and oxygen–hydrogen bonds.[69] Significant progress has been made in the reduction of non-radiative transitions. The replacement of the high-energy O–H bond vibration by the low energy O–D bond vibration results the shrinkage of the vibronic de-excitation process.[70] This indicates that if we remove this high energy bond vibration, then the luminescent properties of lanthanide MOFs can be significantly improved. For example, Tb^{3+}, Eu^{3+}, and Tb^{3+} metal ions have been complexed with macrocyclic polyamine ligands, and then the complex used to construct MOFs.[71] In this case, the coordination environment of the lanthanides are fulfilled, and hence the vibration effect from the environmental water molecules is blocked. Consequently, the MOFs show highly luminescence features in the visible and NIR regions. Therefore, the aforementioned discussion clearly reveals that the judicial design and proper understanding of the energy transfer in lanthanide-based MOFs are key features to develop lanthanide-based luminescent MOFs.

2.3. Emission due to charge transfer

The emission of a molecule is due to charge transfer, which generally occurs by the transfer of charge from the higher excited state to the ground state. This type of emission usually gives a high-intensity band and is an internal redox process. Four types of charge transfer transitions are observed including LMCT, MLCT, MMCT and LLCT. LMCT involves the transfer of charge from the linker-centered orbital to metal-localized orbital. Alternatively, MLCT represents the transfer of charge from the metal-localized orbital to the linker-centered orbital. Similarly, MMCT and LLCT are the transfer of charge from the metal to metal centered orbital and ligand to ligand localized orbital, respectively. A generalized schematic diagram is presented in Fig. 4a, which shows the various mode of charge transfer occurring in the complex, where t_{2g} and e_g indicate the HOMO and LUMO of the metal ion in the complex and π_L and π_L^* represent the bonding and antibonding π orbitals of the ligand, respectively.

Commonly, the intense colour of complexes can be easily explained by these transitions. For example, the pink colour of $KMnO_4$ and orange colour of $K_2Cr_2O_7$ can be attributed to the LMCT process, where the charge relocation occurs from the oxygen (2p orbital) ion to the vacant d orbital on Mn^{7+} and Cr^{6+}, respectively. Similarly, with the help of MLCT, the colour of a tris(bipyridyl)iron(III) complex can be explained by the charge transfer occurring from the iron metal centre to the π*-orbital of bipyridyl.[72] The deep-blue colour of a Prussian blue complex can be explain by MMCT.[73] LLCT is also observed in a variety of coordination compounds.[74]

In the case of MOFs, their network is developed through strong bonds between their ligand and metal ion. However, not all metal–ligand bonds are very strong, and the labile nature between them sometimes produces new important chemistry. Occasionally, the flexible nature of the ligand can endow flexibility to the MOF system. As discussed, the tuneable porous nature of MOFs can enable several fluorophore molecules to be embedded inside their cavity (Fig. 4b). These features enable the design of the desired MOF with interesting luminescent properties. In MOFs, the above-mentioned charge transfer process may occur very smoothly (Fig. 4b). Here, a few examples are presented where the involvement of these charge transfer processes was obviously observed.

Pei and co-workers reported an interesting work, where they demonstrated that an alternation in LMCT led to fluoro-switching in an MOF.[75] By using an AIE-inactive fluorophore as the linker, they synthesized two MOFs, Gd-ETTC and Cu-

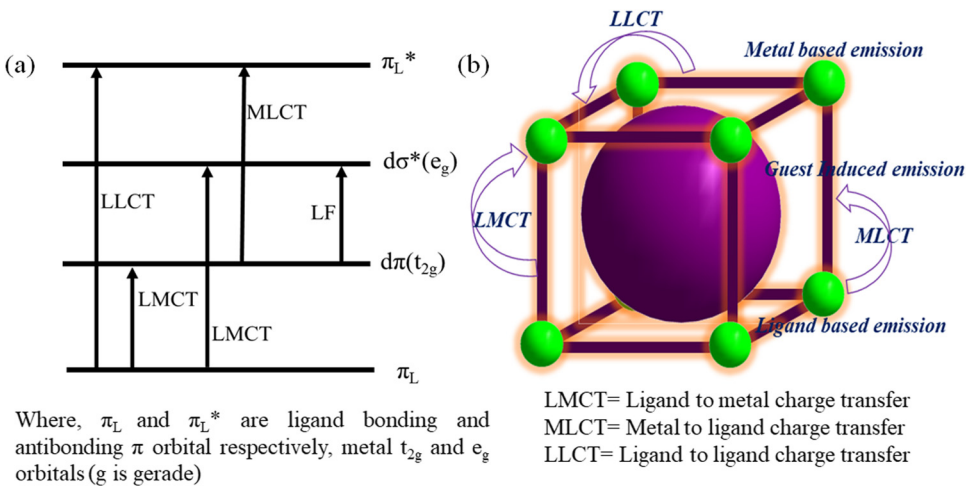

Fig. 4 (a) Diverse charge transfer in metal ligand complex (octahedral) and (b) operation of various types of charge transfer in MOFs.

ETTC (Fig. 5). Specifically, Gd-ETTC was fluorescent in nature with a high intense emission band at 455 nm, whereas the Cu-ETTC is non-fluorescent. The XPS analysis revealed that due to the efficient LMCT process in Cu-ETTC, a redox reaction occurred, which led to changes in the oxidation state of copper from +2 to +1. This process triggered a matrix coordination-induced quenching process,[76] which caused luminescence quenching of Cu-ETTC. In the presence of GSH (electron donor moiety), the reduction of the Cu^{2+} to Cu^{+} state occurred, which stops the LMCT process effectively. Therefore, the fluorescence property of Cu-ETTC was recovered.

Xu and co-workers synthesized two d10-based MOFs, *i.e.*, $[Zn(2,3\text{-pydc})(bpp)(H_2O)]\cdot 2.5H_2O$ and $[Cd(2,3\text{-pydc})(bpp)(H_2O)]\cdot 3H_2O$, under solvothermal conditions.[77] The cadmium- and zinc-based MOFs exhibited emission peaks at 438 and 436 nm upon excitation at 370 and 372 nm, respectively. The free ligand 2,3-pydcH_2 showed a very feeble emission peak upon excitation at 370 nm. Therefore, the origin of the high-intensity fluorescence peak in these two MOFs is due to the LMCT process. Furthermore, the strong chelation ability of the linker to the metal node reduced the ligand flexibility, and thus the luminescence intensity of the MOFs was significantly enhanced.

Zhu and co-workers synthesized two new d10 metal ion MOFs, $[Zn(L_1)(bpy)_{0.5}].(H_2O)_{0.25}$ and $[Cd_4(L_1)_4(bpy)_2]\cdot(H_2O)$, under solvothermal conditions for the detection of H_2S.[78] The solid-state luminescence spectra of both complexes exhibited the maximum emission peak at 560 nm under excitation at 466 nm. With respect to the free ligand (λ_{em} = 518 nm), the emission peak of the complexes was red-shifted by about 42 nm. This is ascribed to the MLCT or cluster to ligand charge transfer. Guo and co-workers reported the preparation of two MOFs, *i.e.*, a copper-based $Cu_3(L_2)_2\cdot 3H_2O$ and mixed-metal $CuAg_2(L_2)_2$ MOF.[79] The emission spectra of the free ligand L_2 and $CuAg_2(L_2)_2$ MOF showed a green luminescence peak at 526 nm and 515 nm under excitation at 365 nm and 358 nm, respectively. In contrast, the copper-based $Cu_3(L_2)_2\cdot 3H_2O$ MOF displayed blue luminescence at 478 and 398 nm under excitation at 333 nm. This MOF exhibited a large blue shift of 48 and 59 nm with respect to the emission peak of the ligand, respectively, whereas the mixed MOF only showed an 11 nm blue shift in its emission peak. Therefore, the origin of the luminescence in $Cu_3(L_2)_2\cdot 3H_2O$ is the MLCT and the source of the emission in $CuAg_2(L)_2$ is the $\pi\cdots\pi^*$ electronic transition of L_2.

2.4. Guest-induced emission

As mentioned previously (*vide supra*), the porous nature, high stability, and tunable pore size of MOFs make them an important rigid/flexible podium for the inclusion of luminescence guest molecules. Generally, guest molecules such as carbon dots,[80] dyes,[81] luminescent organic/inorganic complexes[82] and lanthanide metal ions[83] can be easily incorporated in the porous cavity of MOFs. Consequently, the quantum yield of the MOF material is augmented.

The inclusion of a lanthanide metal ion either by the de-novo or PSM method is an interesting strategy to induce luminescent properties in the daughter MOF. For example, Qian and co-workers described the preparation of a zirconium-based MOF, UiO-66-$(COOH)_2$, using $ZrCl_4$ and H_4btec under solvothermal reaction conditions. This MOF contained free carboxylic acids, which act as guest interaction sites to facilitate the post-synthetic incorporation of Eu^{3+} and Cu^{2+} to deliver Eu^{3+}/Cu^{2+}@UiO-66-$(COOH)_2$.[84] The emission spectrum of the composite displayed the ligand-centered emission at 393 nm and metal-centred emission of Eu^{3+} at 615 nm. Due to the strong antenna effect of H_4btec, Eu^{3+} demonstrated a strong peak at 615 nm. In the presence of Cu^{2+}, the antenna effect of H_4btec decreased, *i.e.*, the degree of charge transfer from the ligand to Eu^{3+} significantly declined given that Cu^{2+} (d^9) is an electron-deficient system, which withdraws more energy from the ligand. Thus, in the composite, the emission intensity at 615 nm decreased. Interestingly, the composite showed the very fast recognition of H_2S (Fig. 6) with an LOD value of 5.45 μM. The soft sulphide ion interacted strongly with the soft Cu^{2+} ion, and thereby reduced the energy transfer from the linker to Cu^{2+}. Therefore, the energy transfer increased

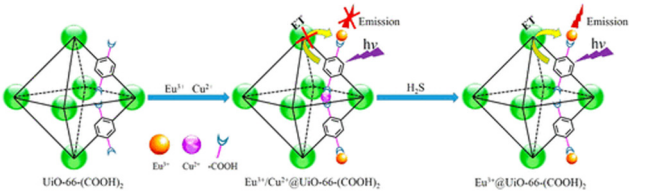

Fig. 6 Post-synthetic incorporation of Eu^{3+} and Cu^{2+} in UiO-66-$(COOH)_2$ to from Eu^{3+}/Cu^{2+}@UiO-66-$(COOH)_2$, followed by the detection of H_2S. Reproduced with permission from ref. 84, the American Chemical Society, Copyright 2016.

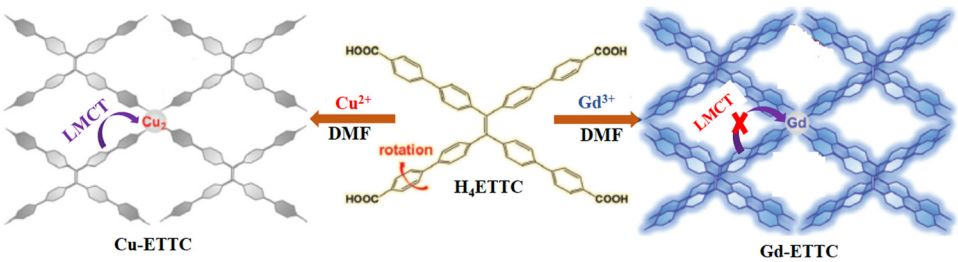

Fig. 5 Synthetic scheme for Cu-ETTC and Gd-ETTC with the occurrence of LMCT in the former from the ligand to copper centre, while in the latter case, there is no LMCT, which aids to the illumination of the ligand.

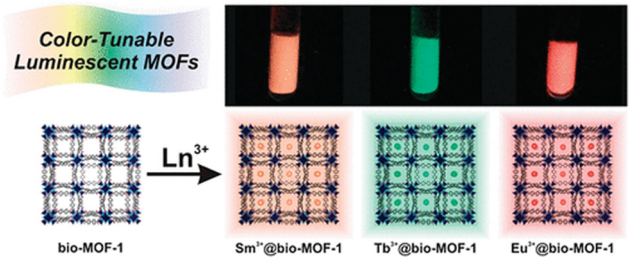

Fig. 7 Doping of Tb^{3+}, Sm^{3+}, and Eu^{3+} in bio-MOF-1 and the respective colour of the doped MOFs. Reproduced with permission from ref. 85, the American Chemical Society, Copyright 2019.

from the ligand to Eu^{3+}. Consequently, the emission of Eu^{3+} sharply increased.

In an early report, Rosi and co-workers reported the synthesis of lanthanide-based luminescent MOFs, Ln^{3+}@bio-MOF-1, by doping lanthanide metal ions (Ln^{3+} = Tb^{3+}, Sm^{3+}, and Eu^{3+}) *via* post-synthetic cation exchange in bio-MOF-1 (Fig. 7).[85] All the doped MOFs showed a distinct colour upon excitation at 365 nm. Specifically, Eu^{3+}@bio-MOF-1, Sm^{3+}@bio-MOF-1 and Tb^{3+}@bio-MOF-1 emitted red, orange-pink and green color, respectively which could be clearly observed by the bare eye. Importantly, all these doped MOFs showed characteristic emission wavelengths, where Eu^{3+}@bio-MOF-1, Sm^{3+}@bio-MOF-1 and Tb^{3+}@bio-MOF-1 produced an emission at 614, 640 and 545 nm, respectively. Simultaneously, all these complexes exhibited a common peak at 340 nm, indicating that the energy transfer occurs from the same electronic state situated in the doped lanthanide complexes. Importantly, the lanthanide-doped MOFs were found to be highly luminescent in water solvent, despite the strong quenching effect of the aqua molecules. This illustrates that bio-MOF-1 efficiently sensitized the guest lanthanide ion. In addition, all the lanthanide metal ions nicely fitted inside the pore, which resulted in a high quantum yield for these doped MOFs.

Carbon dots (CDs) are well-known fluorophore compounds, which can be nicely incorporated in the cavity of MOFs to generate new fluorescence MOF entities.[86] Chi and coworkers reported the inclusion of BPEI-CQDs in ZIF-8 and the new MOF composite (BPEI-CQDs/ZIF-8) showed a high quantum yield. The composite exhibited strong blue emission at 440 nm upon excitation at 385 nm and it could detect copper ions.[87] Similalrly, Wang and co-worker used the ZIF-8 framework to encapsulate CDs in its cavity to form CDs@ZIF-8 for the recognition of quercetin.[88] The luminescence intensity of CDs@ZIF-8 appeared at 480 nm upon excitation at 365 nm. The ZIF-8 did not show any peak at 480 nm, indicating that the emission originated from the CD moiety. Besides CDs, the inclusion of dye and luminescent organic molecules in the MOF cavity, the luminescence properties of the MOF composite could be tuned. Li and co-workers incorporated three different dyes (fluorescein (green), rhodamine B (red) and coumarin C-151 (blue)) molecules in the cavity of ZIF-8 (Fig. 8).[89] The judicial tuning of the ratio of these dyes caused the MOF composite (model 3) to show white light emission upon excitation at 365 nm. The increase in the quantum yield of dye@ZIF-8 is due to the reduction in the aggregation-caused quenching process.

Su and co-workers described the construction of a highly luminescent MOF composite (Rh6@NENU-519) *via* the post-synthetic encapsulation of dye molecules (Rhodamine 6G and Rh6) in the cavity of the anionic MOF, NENU-519.[90] Under excitation at 350 nm, the Rh6@NENU-519 material exhibited emission peaks at 406 nm and 565 nm, which correspond to the emission from NENU-519 and Rh6 molecule, respectively. By comparing the emission intensity ratio at 565 nm and 406 nm of Rh6@NENU-519 in the presence of various analytes, it was found that the composite was selective for the recognition of *para*, *meta* and *ortho*-xylene. The differences in the intensity ratio of Rh6@NENU-519 is owing the diverse amount of charge transfer between the composite and the organic analytes.

The inclusion of organic molecules or inorganic complexes in MOF composites enables the creation of a fluorophore entity. In this regard, Wang and co-worker described the encapsulation of $Ru(bpy)_3^{2+}$ in UiO-66-NH_2.[91] The MOF composite demonstrated two peaks at 437 nm and 604 nm, which correspond to the emission of UiO-66-NH_2 and $Ru(bpy)_3^{2+}$, respectively. However, by comparing the emission intensity ratio of the composite in the presence of various analytes, the composite could recognize Hg^{2+} ions. Importantly, the authors also demonstrated the formation of a hydrogel composite, where the luminescence intensity of the network remained intact. Although the gel composite contained the maximum percentage of water and despite the resilient quenching influence of the aqua molecule, the MOF-based gel composite showed luminescence activity. This indicates that the MOF composite could sufficiently protect the guest molecule $Ru(bpy)_3^{2+}$, causing it to show luminescence behaviour. Interestingly, the gel composite also enabled the colorimetric detection of mercury ions. Recently, Chen and co-workers published an important work in which the fluorescence property of the encapsulated fluorophore molecule could be tuned (photo-switchable phenomena) in the presence external stimuli (light).[92] They synthesized a photo-switchable Eu^{3+}-based MOF by capturing diarylethene (DAE) moiety in its porous cavity. In the presence of light, the DAE unit underwent a ring-closing reaction. Thus, the ring-opening and ring-closing form of DAE displayed distinct colours. This colour-changing phenomena is also reversible, and this technique is used to demonstrate reversible data storage application.

3. Turn-on sensing by MOFs

It is clear that MOF can detect the target analyte either by a fluorescence ''turn-on'' or ''turn-off'' process. In the ''turn-on'' method, a luminescence enhancement occurs in the MOF, whereas in the case of a ''turn-off'' event, the fluorescence intensity of the MOF declines. Remarkably, the former is superior for real-time sensing application. In the case of luminescence enhancement, the illumination occurs against a dark background and is easier to monitor than the quenching

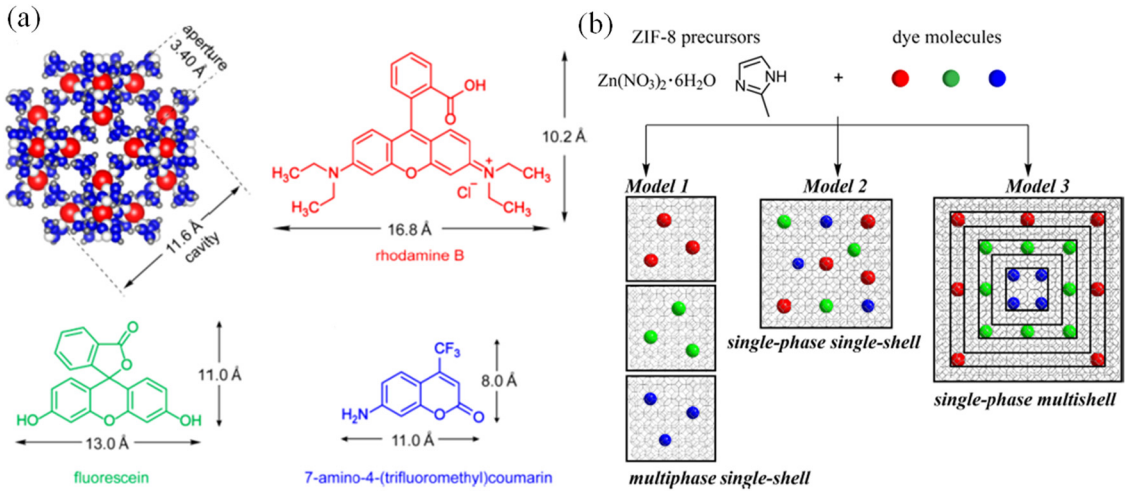

Fig. 8 (a) Cavity size of ZIF-8 and the dimensions of C-151, fluorescein and rhodamine B and (b) synthetic methodologies for dye-encapsulated ZIF-8. Reproduced with permission from ref. 89, the American Chemical Society, Copyright 2019.

(turn-off) event. Additionally, the "turn-off" event can be caused by interfering analytes instead of the target analyte, which often leads to the wrong prediction and is the main obstacle for real-time application. Furthermore, in biological systems, the "turn-on" process is very desirable, given that a luminescence enhancement is required in the dark background. This results in the facile monitoring of the analyte detection through the emission enhancement. In contrast, this positive information is absent in the "turn-off" event.[93] The following sections present the use of MOFs as fluorescence "turn-on" probes for the detection of various analytes.

3.1. Turn-on sensing of organic molecules including solvents

As previously mentioned, MOFs and their composites have exceled as fluorescence "turn-on" probes for the recognition of several pollutants. The volatile organic molecules including organic solvent molecules have a high vapor pressure and are very hazardous to human health.[94] Therefore, the recognition of these molecules is extremely important. In this regard, Zhang and co-workers performed an excellent study on the multi-colored "turn-on" detection of a variety of VOCs using a silver-chalcogenolate cluster-based MOF, Ag_{12}bpy.[95] In the present study, the silver(I) chalcogenide cluster (Ag_{12}) was very unstable and contained coordinated acetonitrile molecules. When the cluster was reacted with bpy, it replaced the acetonitrile molecules to form the highly stable Ag_{12}bpy, in which the Ag_{12} cluster transformed into quasi-isomers. Firstly, Ag_{12}bpy showed a "turn-off" luminescence response in the presence of molecular oxygen, which was intercalated inside the pores of the MOF. Interestingly, in the presence of VOCs, a "turn-on" luminescence response was observed. The ultra-fast "turn-on" luminescence response by Ag_{12}bpy can be attributed to the following reasons. Firstly, the easy ingression of the VOCs in the microporous pores of the framework, while maintaining their structural integrity, which maximized the host–guest interaction. Secondly, the chromophores were nicely organized inside the framework. According to the solvatofluorochromism study, it was revealed that Ag_{12}bpy possesses a large dipole moment. All the VOCs gathered around the linker and the high dipole movement of the framework established a strong host–guest interaction with the VOCs, imparting diverse emission colors. The precise location of the VOCs in the porous network was also confirmed from the single crystal diffraction data.

Lantham and co-workers showed the detection of electron-rich aromatic VOCs through a "turn-on" process using a zinc-based MOF, $(Zn_2Cl_4Py\text{-}TPE)\cdot 4(TCE)$.[96] As is known, molecular networks containing TPE derivatives can show AIE in highly concentrated solution or in the solid state. In these states, the motion or rotation of the central phenyl ring is generally blocked, which stops the intramolecular rotation, and hence inhibition of the non-radiative decay of the excited state occurs.[97] Based on this concept, the synthesized zinc MOF showed luminescence property. However, its fluorescence emission intensity was further enhanced in the presence of aromatic VOCs (Fig. 9) together with the red shifting of its emission peak. The shifting in the emission peak and the "turn-on" luminescence response illustrate that the analytes gradually locked the rotation/vibration of the central phenyl ring, which led to an increase in the fluorescence intensity. Fig. 9 indicates that with an increase in the methyl substituent on the benzene ring, the emission intensity of the MOF was gradually reduced. For instance, the luminescence intensity of the MOF was greater with benzene than with mesitylene. The size of mesitylene is larger than the benzene ring, and thus the latter can smoothly enter the pores of the framework and block the rotation of the TPE moiety, whereas the diffusion of mesitylene is not favorable.

Similar to the detection of VOCs, another important class of compounds is organic amines, which are widely used in several industries such as pesticides, pharmaceuticals and tobacco.[98] However, the environmental and public health hazards caused by organic amines cannot be overlooked. This concern is one of

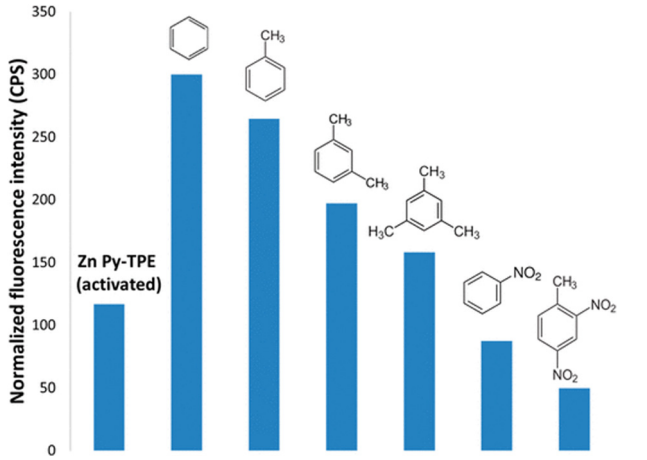

Fig. 9 Emission intensity of Zn_2Cl_4Py-TPE in the presence of a variety of aromatic VOCs. Reproduced with permission from ref. 96, the American Chemical Society, Copyright 2016.

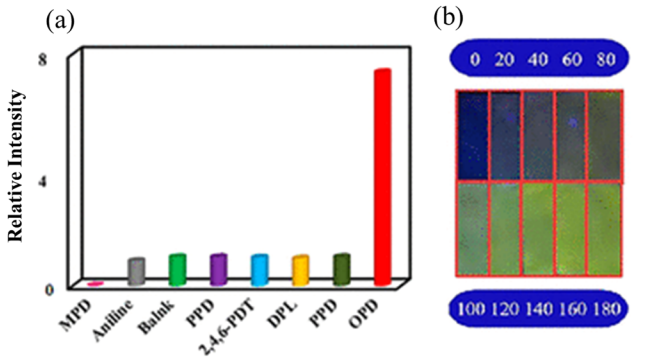

Fig. 10 (a) FL intensity of Cu-TBDA with a variety of amines and (b) recognition of OPD by Cu-TBDA coated on a strip paper, and then different concentrations of OPD were added under UV light 365 nm. Reproduced with permission from ref. 100, the American Chemical Society, Copyright 2021.

the frontier research fields in the scientific community. Huang and co-workers strategically developed an AIE luminogen-active linker, TPPE, for the construction of CuI-based MOFs towards the ''turn-on'' detection of ammonia.[99] In this network, the ligand TPPE acts as a receptor rather than transducer. The emission of the MOF is a linker-based emission and when the MOF was exposed to ammonia vapor, its emission peak was red-shifted. This illustrates that the ammonia vapor interacted with TPPE. The mechanism of sensing was established with the help of GCMC and DFT study. The suitable supramolecular interaction between the receptor and analyte restricted the free rotation of the AIEgen component. This reduced the non-radiative decay of the MOFs, resulting in the ''turn-on'' emission.

Xing and co-workers reported the synthesis of a triazine-based porous copper-based MOF, Cu-TBDA, for the detection of *o*-phenylenediamine (OPD).[100] Interestingly, the MOF showed a concentration-dependent luminescence ''turn-on'' and ''turn-off'' response for OPD. The Cu-TBDA MOF showed an emission peak at 430 nm under excitation at 345 nm. Upon screening of the fluorescence intensity with various aromatic amines, it displayed the highest luminescence intensity for OPD (Fig. 10).

Given that the sensitivity of Cu-TBDA is concentration dependent, the authors carefully examined the effect of the concentration of OPD on the luminescent intensity of Cu-TBDA. It was revealed that the addition of 0–200 μL of OPD caused the luminescence intensity of OPD to remarkably increase. Interestingly, the emission peak in this case appeared at 550 nm in place of 430 nm. This illustrates the existence of effective interaction between OPD and Cu-TBDA. According to the linear relation between the lower concentration of OPD and the luminescence intensity, the calculated LOD was found to be 5.00 μM. Remarkably, after the addition of more than 200 μL OPD, fluorescence intensity diminished. The detection of OPD was also achieved through a colorimetric response. A paper strip was coated with Cu-TBDA, and then different concentrations of OPD were added. The color of the strip paper gradually became brighter (Fig. 11). The bathochromic shift in the emission peak in the presence of OPD indicates that the porous network plays an important role. This was further confirmed by the addition of OPD to the free ligand, where the fluorescence intensity of the ligand did not change. Thus, the porous network enabled effective interactions between OPD and the MOF. OPD is electron rich and the Cu^{2+} metal ion in MOF is d^9, *i.e.*, electron-deficient moiety. Therefore, the smooth PET process occurs by the transfer of electrons from OPD to the vacant d orbital on the Cu^{2+} ion. Simultaneously, the strong interaction between OPD and the MOF inhibits the free rotation of the $-NH_2$ group, developing a stable planar network and enhancing the extent of conjugation. Therefore, upon the addition of OPD, the luminescence intensity of Cu-TBDA is largely augmented.

Although some MOF-based sensors employed the paper strip methodology for the detection of analytes, the fabrication of MOFs as membranes for the recognition of particular analytes is also an exciting approach in the field of MOF-based sensors. In this regard, Fan and co-workers published an interesting work, where they developed two copper-based MOFs with two different oxidation states of metal ions.[101]

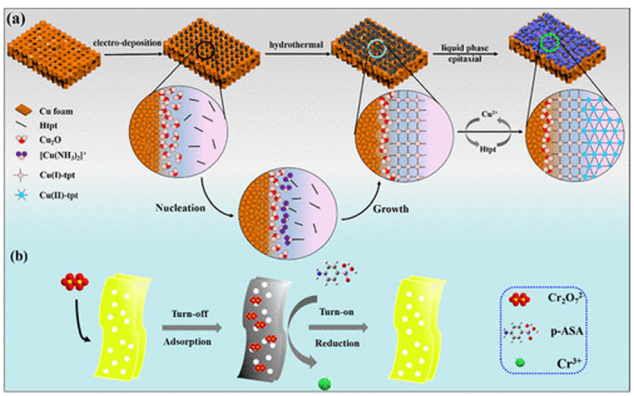

Fig. 11 (a) Fabrication of Cu(II)-tpt-on-Cu(I)-tpt and (b) adsorption of $Cr_2O_7^{2-}$ followed by the recognition of *p*-arsanilic acid. Reproduced with permission from [101], the American Chemical Society, Copyright 2020.

Interestingly, the MOF membrane showed the ''turn-on'' detection of *p*-arsanilic acid. The Cu(II)-tpt-on-Cu(I)-tpt membrane was fabricated *via* a layer-by-layer method. Firstly, by using a one-pot methodology, the Cu(I)-tpt layer was developed on a Cu_2O nanostructure, and then with the help of the liquid-phase epitaxy method, a second layer of Cu(II)-tpt layer was developed on the Cu(I)-tpt layer (Fig. 11). Actually, the Cu(II)-tpt-on-Cu(I)-tpt membrane was luminescent in nature, and when it adsorbed the poisonous $Cr_2O_7^{2-}$, it typically induced the fluorescence quenching of the membrane. Afterwards, in the presence of *p*-arsanilic acid, the membrane displayed a ''turn-on'' luminescent response. Therefore, the adsorption of $Cr_2O_7^{2-}$ led to the highly sensitive recognition of *p*-arsanilic acid with an LOD of 0.0566 μg L^{-1}.

The mechanism of sensing is very interesting and the role of $Cr_2O_7^{2-}$ is very important. The Cu(II) ion in Cu(II)-tpt-on-Cu(I)-tpt is electro-positive and can adsorb $Cr_2O_7^{2-}$ in the rhombic channel of the Cu(II)-tpt layer. Then, Cu(I)-tpt participates in the sensing. After the adsorption of $Cr_2O_7^{2-}$, the membrane showed the luminescence quenching phenomenon. This is because the excitation spectrum of Cu(I)-tpt perfectly overlapped with the absorption spectrum of $Cr_2O_7^{2-}$. Thus, $Cr_2O_7^{2-}$ captured all the light in the solution and there was no opportunity for the excitation of Cu(I)-tpt. In presence of *p*-arsanilic acid, an oxidation-reduction reduction occurred, where the reduction of $Cr_2O_7^{2-}$ to Cr^{3+} is attributed to the electron-donating power of the amino group of *p*-arsanilic acid. Concomitantly, the oxidation of the benzenoid amine ($-NH_2$) of *p*-arsanilic acid to quinoid imine ($-N{=}^{+}$) occurred. Consequently, the membrane showed a luminescence enhancement. This sensing mechanism was further supported by the XPS analysis, which demonstrated the existence of a Cr^{3+} ion (peaks at 576.9 eV and 587.3 eV) and quinoid imine ($-N{=}^{+}$, N1s peak at 401.3 eV) during the sensing mechanism. The presence of the amino group of *p*-arsanilic acid is crucial for the ''turn-on'' recognition of *p*-arsanilic acid.

The utilization of chiral molecule is very significant in several fields including the chemical, pharmaceutical, food additive, agrochemical, and biomedical industries. The enantiomers from the same molecule act in different ways, and surprisingly a specific isomer may have a negative impact on the living body. For instance, L-lactic acid is used as a food additive, whereas the D-lactic acid has adverse effects on humans.[102] Therefore, the detection of enantiomers is vital. Zhang and co-workers synthesized homochiral MOF nanosheets (HMOF-3-NS) for the ''turn-on'' detection of hydroxyl carboxylic enantiomers.[103] Initially, they synthesized a homochiral 2D MOF (HMOF-3) from the chiral ligand *R*,*R*-CHCAIP, bpy and zinc salt. Then, the exfoliation of HMOF-3 though a solvent-assisted sonication process afforded HMOF-3-NS. The free ligand *R*,*R*-CHCAIP and HMOF-3-NS in acetonitrile showed an emission wavelength at 430 and 435 nm, respectively, upon excitation at 325 nm. The luminescence in HMOF-3-NS is due to the n → π* transition. Interestingly, the luminescence intensity of HMOF-3-NS in acetonitrile was significantly enhanced in presence of *R* and *S*-mandelic acid. The fluorescence augmentation caused by *R*-mandelic acid was less than that by *S*-mandelic acid in comparison to the initial intensity of HMOF-3-NS (Fig. 12).

With the help of Benesi–Hildebrand plots, the calculated K_{BH} value of HMOF-3 with *R*- and *S*-mandelic acids was found to be 3.7×10^4 M^{-1} and 9.9×10^4 M^{-1}, respectively. These values strongly suggest the efficient interaction between the MOF networks with the analytes. The luminescence enhancement of HMOF-3-NS due to the decomposition of the framework was ruled out based on the well-matched PXRD peak pattern of the recovered HMOF-3-NS after sensing with the pristine HMOF-3-NS. Thus, the only possibility is the existence of strong host–guest interaction during the sensing event. The surface of HMOF-3-NS is exposed with numerous interaction sites such as pyridine N from bpy, carboxylic acid and acylamino group of the main ligand, and coordinated water molecules to the zinc metal ions. These interaction sites can induce supramolecular interaction (hydrogen bonding) with the analytes (Fig. 13). Consequently, HMOF-3-NS and the analyte come in close proximity for the PET effect to occur very smoothly. HMOF-3-NS acts as an electron acceptor and α-hydroxyl carboxylic behaves as an electron donor. Thus, the PET effect occurs from the LUMO of the analyte to the LUMO of HMOF-3-NS, resulting in the ''turn-on'' luminescence enhancement of HMOF-3-NS. This mechanism was further justified by DFT. The versatile sensing capability of HMOF-3-NS towards other

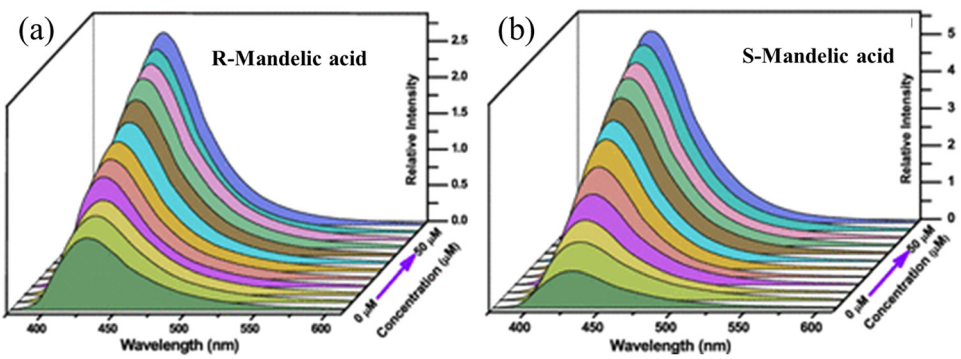

Fig. 12 Luminescence spectra of HMOF-3-NS with *R*-mandelic (a) and *S*-mandelic (b) in acetonitrile solvent. Reproduced with permission from ref. 103, the American Chemical Society, Copyright 2021.

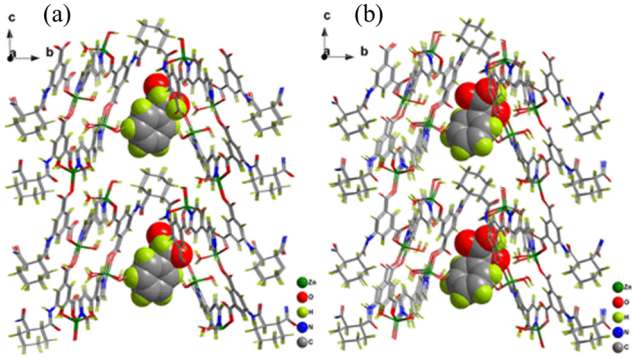

Fig. 13 Geometrical optimization of the structures between HMOF-3-NS *R*-mandelic acid (a) and *S*-mandelic acid (b). Reproduced with permission from ref. 103, the American Chemical Society, Copyright 2021.

hydroxyl carboxylic enantiomers was also demonstrated by the sensitive detection of D/L-lactic acid and D/L-tartaric acid. Remarkably, HMOF-3-NS could also detect D/L-tryptophan and D/L-alanine.

Organic solvent molecules are also considered a subclass of VOCs. The rapid industrial development globally, particularly in the chemical, pharmaceutical, and drug industry, has resulted in a significant increase in the use of solvents. In this case, although the outmost care is taken in handling the toxic solvent molecules, the safety issues and negative health effects of these solvent molecules are still a major concern. Some solvents have a low boiling point and easily evaporate into the atmosphere. During inhalation, humans are negatively affected by these solvent molecules, where direct and even indirect contact with these solvents molecules can cause several adverse health effects. Thus, their monitoring is critical. In this regard, MOFs are very effective, where their "turn-on" detection is essential for their practical application.[104,105]

For example, formaldehyde (HCHO) is a very simple aldehyde molecule and widely used in several chemical reactions. However, despite its many advantages, formaldehyde is very toxic to human health. Banerjee and co-workers showed the "turn-on" detection of HCHO in solution and the vapour phase using a Cd-based MOF, CMERI-1.[106] Moreover, for its real-time application, its detection applicability for HCHO was also demonstrated in a food sample. The CMERI-1 MOF showed a weak emission at 430 nm upon excitation at 350 nm. The reason for the weak emission is possible owing to the intra-ligand charge transfer in the MOF network. Fluorescence titration of CMERI-1 with HCHO demonstrated that its emission peak at 430 nm regularly increased with the bathochromic shift. The enhancement in fluorescence is due to the formation of an imine bond (–C═N–) between dangling $-NH_2$ moiety in the framework and HCHO. Consequently, the inhibition of the PET effect occurred, resulting in the restoration of fluorescence. Subsequently, to detect the HCHO in the vapour phase, a hydrogel MOF composite membrane was developed using PVA and CMERI-1, which showed the detection of HCHO within a minute (Fig. 14). The LOD value for the detection of HCHO was found to be 0.62 μM (0.019 ppm).

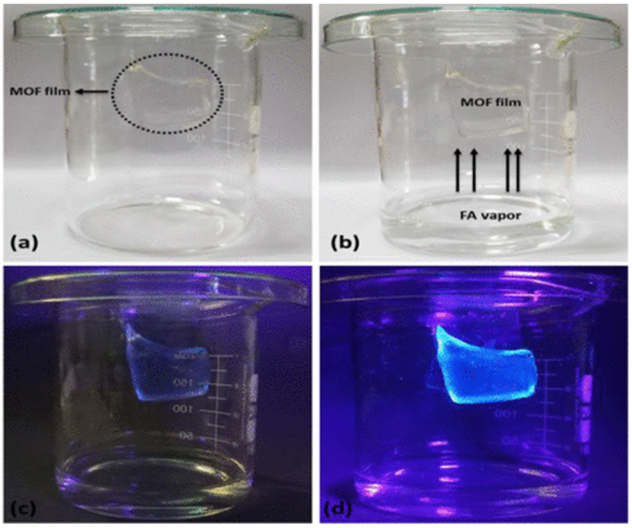

Fig. 14 (a) Gel composite kept inside the experimental set up (inside circle), (b) gel composite inside formaldehyde vapour, (c) luminescence of gel appeared in the presence of formaldehyde vapour and (d) after 30 minute exposure of the gel composite to formaldehyde vapour. Reproduced with permission from ref. 106, the American Chemical Society, Copyright 2021.

Recently, Mandal and co-workers synthesized $\{[Zn_2(oxdz)_2(tpbn)]\cdot 14H_2O\}n$ (1) for the "turn-on" detection of acetyl acetone and water solvent molecules.[107] The emission spectrum of the MOF revealed the maximum peak at 390 nm under excitation at 310 nm. This is due to the π–π* and n–π* transitions. Further the MOF showed diverse luminescence intensities in polar protic and polar aprotic solvents. When this MOF was treated with a variety of ketone molecules, it was found that its luminescence intensity was significantly enhanced with acetylacetone and the emission peak at 390 nm progressively increased upon the addition of acetylacetone with a blue shift (Fig. 15). Interestingly, this MOF also displayed the detection of water in a variety of organic solvents. The strong affinity between the pores in its walls (carboxylate oxygen) and the water molecules established a strong hydrogen bonding interaction, and thereby the energy transfer from the MOF to O–H bond oscillators decreased. Subsequently, the fluorescence intensity of the MOF improved. The sharp selectivity and high sensitivity of this MOF towards acetylacetone was well-justified by calculating the binding constant between the analyte and MOF with the help of the Benesi–Hildebrand plot. The K_{BH} was determined to be 1.131×10^4 M^{-1}, signifying the resilient interaction between the analyte and MOF. Further, the DFT experiment disclosed the operation of the PET effect from the LUMO of acetyl acetone to the LUMO of H_2oxdz, resulting in the enhancement of the fluorescence intensity.

Wu and co-workers synthesized Eu-HODA for the selective and sensitive "turn-on" recognition of methanol in the presence other polar protic solvents (Fig. 16).[108] When this MOF was excited at 305 nm, the emission peak was dominant at 614 nm ($^5D_0 \rightarrow {}^7F_2$) due the electrical dipole of Eu-HODA. This luminescence intensity largely changed in the presence of a

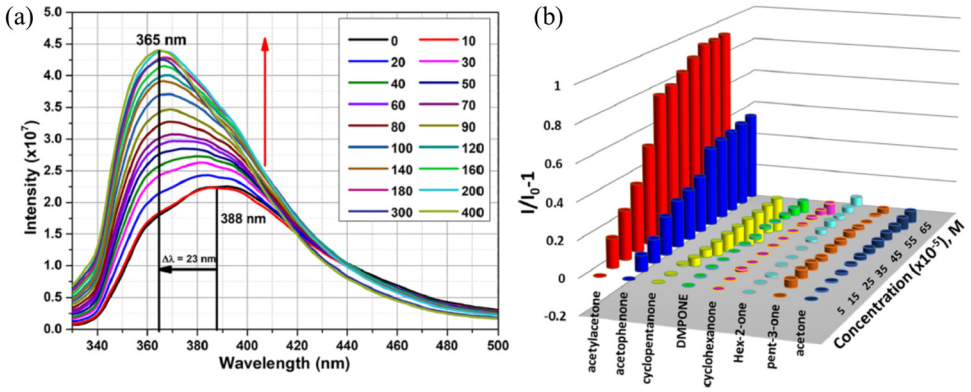

Fig. 15 (a) Emission spectra of the MOF after the gradual addition of acetyl acetone and (b) plot of intensity against concentration of 1 in the presence of a variety of ketones. Reproduced with permission from ref. 107, the American Chemical Society, Copyright 2022.

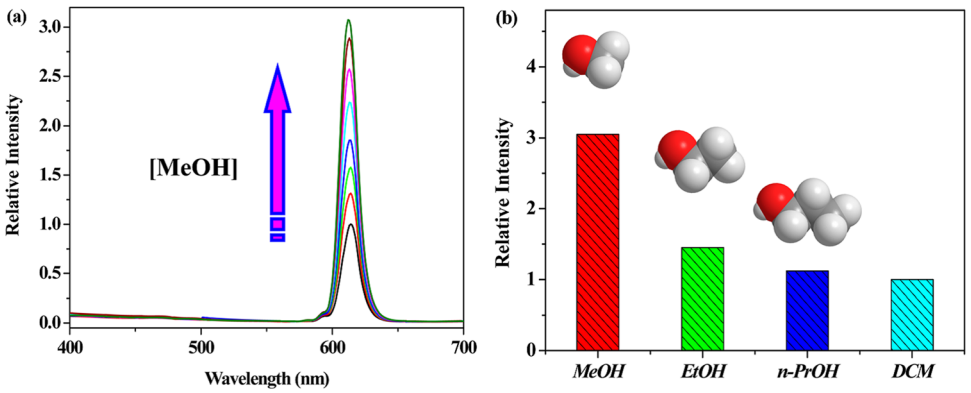

Fig. 16 (a) Emission of Eu-HODA gradual increased upon the addition of methanol and (b) comparison of the luminescent intensity of Eu-HODA in methanol with respect to other solvents. Reproduced with permission from ref. 108, the American Chemical Society, Copyright 2016.

variety of solvents and a significant enhancement was observed for methanol solvent (3.1-fold increment). Table 1 illustrates the various MOF-based "turn-on" probes for the recognition of a variety of neutral molecules including solvents.

3.2. Turn-on sensing of bio-markers and biological molecules

Biomarkers are measurable biochemical pointers that can illustrate the states of subcellular structure or functioning condition of living bodies. Therefore, the recognition of biomarkers is imperative for the primary analysis and cure of human diseases.[109] Gossypol (Gsp) is a poisonous substance present in cotton seeds, posing a severe threat to human health. Cottonseeds are widely used in the food industry, and thus the monitoring of Gsp in cottonseeds is very important. Rosi and co-worker demonstrated the selective "turn-on" detection of Gsp using Yb-NH_2-TPDC (Fig. 17).[110] Under excitation at 300–475 nm, Yb-NH_2-TPDC showed the signature emission peaks of Yb^{3+} in the NIR region in the range of 940–1060 nm, which is due to the $^2F_{5/2} \rightarrow {}^2F_{7/2}$ transition. This illustrates that the ligand (NH_2-TPDC) sensitized the Yb^{3+} ion through the antenna effect. With respect to the free ligand, the excitation peak of the MOF was red-shifted. Further, the excitation band of Yb^{3+} in Yb-NH_2-TPDC appeared at 475 nm, and when the MOF was treated with Gsp, the excitation band of Yb^{3+} red-shifted to 550 nm. It was revealed that upon the excitation of Yb-NH_2-TPDC at 475–550 nm, the luminescence intensity of Yb^{3+} was switched from the non-luminescence state to highly luminescence state in the presence of Gsp.

The simulation study showed that the hydroxyl group of Gsp forms strong intermolecular hydrogen bonding with the framework, which brings them in close proximity. Consequently, Gsp sensitizes (antenna effect) the Yb^{3+} ion through a sequential charge transfers process, *i.e.*, from the singlet state of Gsp to the triplet level of NH_2-TPDC, and then to the triplet level of Gsp, followed by the transfer of energy to Yb^{3+}. The LOD for Gsp by Yb-NH_2-TPDC was calculated to be 25 μg mL^{-1}.

Amino acids are the basic building blocks for proteins in the living body.[111,112] In the food industry, arginine tends to release urea by fermentation. However, if the arginine content is high, then a high amount of urea will be released, which reacts with ethanol to produce urethane, posing carcinogenic threat to human health.[113] Thus, for the detection of arginine, Zheng and co-workers synthesized uranyl-based MOFs, (UO_2)(nip)(2,2′-bpy) (MOF **1**) and $(H_2bpp)\cdot[(UO_2)_2\text{-}(nip)_3]\cdot H_2O$ (MOF-2), under solvothermal reaction conditions.[114] When MOF-1 and MOF-2 were treated with several amino acids, it

Table 1 Diverse MOFs with their excitation, emission wavelength and respective LOD values for the recognition of various analytes (neutral molecules, solvent molecules, biomarkers, biomolecules, hazardous compounds, and high-energy molecules)

MOFs	The metal in node/SBU	$\lambda_{excitation}$ (nm)	$\lambda_{emission}$ (nm)	Nature of analyte	LOD	Ref.
IRMOF-3(–N_3)	Zn	395	430	H_2S	28.3 μM	140
UiO-66@NO_2	Zr	334	436	H_2S	188 μM	141
CAU-10-N_3	Al	330	405	H_2S	2.65 μM,	142
Tb^{3+}@Cu-MOF	Tb	280	489, 544, 585 and 620	H_2S	1.20 μM	143
Fe^{III}-MIL-88-NH_2	Fe	333		H_2S	10 μM	144
DUT-52-$(NO2)_2$	Zr	390	474	H_2S	20 μM	145
Zr(TBAPy)$_5$(TCPP)	Zr	365		H_2S gas and its derivatives S^{2-}	1 ppb	146
Al-MIL-53-NO_2 MMMs	Al	396	466	H_2S	92.31 μM	147
MOF-5-NH_2	Zn	365		SO_2 gas	0.168 ppm	148
Al-MIL-53-NO_2	Al	339		H_2S	69.3 μM	149
Sm-MOF@Fe^{3+}	Sm	300	562, 595, 643 and 706	TBHQ	5.6 ng mL^{-1}	150
UiO-66-MA	Zr			H_2S	3.3 nM	151
RhB/UiO-66-N_3	Zr	302	425 and 575	H_2S	29.9 μM	152
Eu^{3+}/Cu^{2+}@Znpda	Zn	408	614 and 386	H_2S	1.45 μM	153
$^3{}_\infty$[Ce (Im)$_3$ImH]·ImH	Ce	366	422	H_2O, O_2, and CH_2Cl_2		154
[Sm_2(abtc)$_{1.5}$(H_2O)$_3$(DMA)]·H_2O·DMA	Sm	400	612	Benzyl alcohol and benzaldehyde		155
[Me_2NH_2][EuL(H_2O)]·1.5H_2O	Eu	324	591, 613, 649 and 697	Methanol		156
SB1, SB2, SB3 and SB4	Cd	365		Water		157
Zn(hpi$_2$cf)(DMF)(H_2O)	Zn	365	463 and 493	Water	<0.05% v/v (ZnO-based film)	158
QG-loaded MOF	Zn		424 nm	Water in ethanol and DMF	0.015% and 0.030%	159
SXU-4	Cd	365	430	DMSO		160
{[$Y_{0.9}Tb_{0.1}Mn_{1.5}$(PDA)$_3$ (H_2O)$_3$]·3.5H_2O}	Y and Mn	280	315,491, 545, 586 and 623	Trace water in EtOH, CH_3OH, CH_3CN, THF and *n*-heptane	1.12% (v/v), 0.47% (v/v), 0.04% (v/v), 0.13% (v/v) and 0.53% (v/v)	161
[(UO_2)(H_2DTATC)] (HNU-39)	U	373	430			162
Tb^{3+}@Ag-BTC	Ag	365	494, 547, 587 and 622	HCHO	1.9 mM	163
[In(BDC-NH_2)(OH)]$_n$	In	350	429	H_2O_2	0.42 μM	164
Zr-UiO-66-B(OH)$_2$	Zr	328	425	H_2O_2		165
PSM-1 and PSM-2	Cd	335	~435 and ~430	1,4-Dioxane	1.079 ppm and 2.487 ppm	166
MIL-100(In)@Eu^{3+}/Cu^{2+}	In	285	594, 619, and 699	H_2S	0.535 ppm	167
Fe-MIL-88	Fe	326	445	GSH, Cys and Hcy	30 nM, 40 nM, and 40 nM	168
Fe-MIL-88-H_2O_2-*o*-phenylenedia-mine	Fe	433	576	Dopamine	46 nm	169
[Cu(mal) (bpy)]·2H_2O	Cu	480	518	Glycine and serine	0.81 μg mL^{-1} and 1.51 μg mL^{-1}	170
[Cd(μ_3-abtz)·2I]}$_n$	Cd	242	350	Dopamine	57 nM	171
Ag@Au nanoprism-MOF	Zn	532	550	Glucose	0.038 mM	172
CD-MONT-2	Pb	330	526	Uric acid	4.3 μM	173
Cu-BTC/Tb	Cu	238	488, 545, 583, and 621	Amyloid β-peptide (Aβ1-40)	0.3 nM	174
RhB@Cu-BTC	Cu	365	575	L-Cysteine	0.702 μmol L^{-1}	175
Zr-MOF; UiO-68-An/Ma	Zr	375	420	Biothiols (Cys, Hcy, and GSH)	Low concentration of 50 μmol L^{-1}	176
ZJU-108	Zn	323	419	Tryptophan	42.9 nM	177
NH_2-MOF-76(Eu)	Eu	385	400	Dipicolinic acid	3.8 mM	178
$CrO_4{}^{2-}$@Cd-MOFs	Cd	358	414	Ascorbic acid	7.27 ppm	179
ZIF-67	Co	540	585	Biothiols	31 nM	180
Eu^{3+}@Ga-MOF(MIL-61)	Ga	370	614	Ciprofloxacin	2.4 μg mL^{-1}	181
RSPh@EuBTC	Eu	306	546, 592, 615 and 692	DPA	0.52 μM	182
Eu^{3+}@[$(Me)_4N$]$_2$[Pb_6K_6(m-BDC)$_9$($OH)_2$]·H_2O	Pb and K	377	612	Fleroxacin	43.91 ng mL^{-1}	183
UiO-67-sbdc		340	465	Glutathione (GSH)	107.2 μM	184
Eu^{3+}/Cu^{2+}@UiO-67-bpydc	Zr	372	592, 615, 651 and 700	GSH	54.3 nM	185
Cu(HBTC)-1 nanosheets	Cu		518	Oxytetracycline	0.40 μg L^{-1}	186
[$(CH_3)_2NH_2$]$_3$[(In_3Cl_2)(bpdc)$_5$]·(H_2O)$_5$(DMF)$_{2.5}$	In	340	410	Cysteine and 1-butanethiol	5.71 × 10^{-4} M and 4.38 × 10^{-4} M	187
[$Tb_{0.43}Eu_{1.57}$(1,4-phda)$_3$(H_2O)] (H_2O)$_2$	Tb and Eu	260	544 and 614	Dipicolinic acid	5.9 nM	188
FCS-3	Zn	400	450	Fluoroquinolone	0.52 μM	189
UiO-HQCA-Al	Zr	339	438	Creatinine	4.7 nM	190
Eu-in-BTEC	Eu	365	526 and 617	Doxycycline	47 nM	191
Tb-MOF	Tb	394	506	Dicarboxylic acid	2.4 μM	192
Eu@ZIF-90-PA	Zn	463	579	Flumequine	0.24 ppm	193

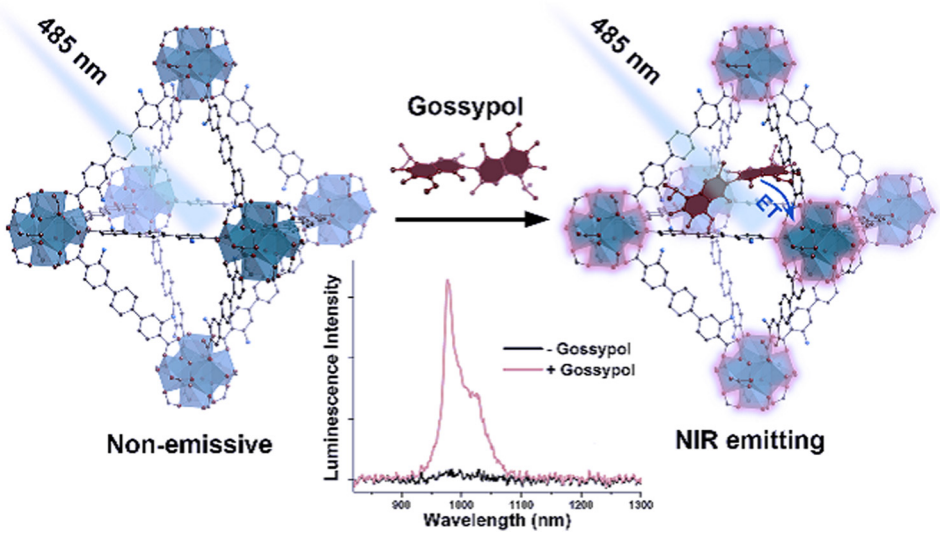

Fig. 17 Detection of gossypol *via* the luminescence "turn-on" effect in the NIR region by Yb-NH_2-TPDC MOF. Reproduced with permission from ref. 110, the American Chemical Society, Copyright 2020.

was revealed that the fluorescence intensity of both MOFs showed a fluorescence "turn-on" enhancement in the presence of arginine (Fig. 18). The LOD values for arginine by these two MOFs were found to be 1.06×10^{-6} mol L^{-1} and 6.42×10^{-6} mol L^{-1}, respectively. The calculations were based on the linear relation between the lower concentrations of the analytes with the emission peak at 515 nm of the MOFs.

The shape of the emission spectra of the MOFs changed in the presence of arginine during the sensing process. This indicates that there was an obvious interaction between the MOFs and arginine. Arginine is a basic amino acid, which contains a guanidine part. This moiety can be protonated, and resulting ionic species can establish an electrostatic interaction with the MOF. This interaction is responsible for the "turn-on" effect on the luminescence intensity. Furthermore, this postulation was proven upon the interaction between guanidine carbonate solutions and the MOFs. Interestingly, the emission peak of both MOFs was considerable enhanced. Therefore, the interaction between the guanidine part of arginine and the MOFs was the responsible for the sensing of arginine.

An abnormal concentration of histidine in the human body hampers several neurological activities. However, the recognition of histidine especially in the complex biological system is challenging. Liu and co-workers synthesised a highly luminescent Eu^{3+} ion-based MOF composite (Eu/Bi-MOF) *via* the post-synthetic insertion of Eu^{3+} in the pore of Bi-MOF.[115] This new Eu/Bi-MOF composite could selectively detect histidine *via* the luminescence "turn-on" process among several other amino acids. Interestingly, Eu/Bi-MOF showed strong red fluorescence due to the strong sensitization of Eu^{3+} by the ligand through the antenna effect. However, in water, the transfer of energy from the linker to Eu^{3+} in Eu/Bi-MOF was significantly hindered. Consequently, the composite became non-luminescent. When the luminescence titration of the composite was carried out with histidine in water, the fluorescence intensity of the composite recovered. In the presence of histidine, the aromatic

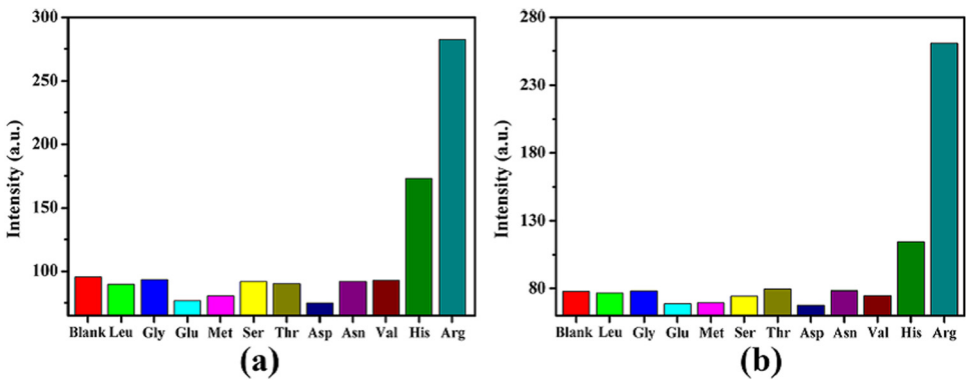

Fig. 18 (a) Fluorescence intensity of MOF-1 with various amino acid and (b) fluorescence intensity of MOF-2 with various amino acids. Reproduced with permission from ref. 114, the American Chemical Society, Copyright 2020.

surface area of histidine forms a π···π interaction with the aromatic surface area of the ligand. Consequently, the transfer of energy from the linker to Eu^{3+} in Eu/Bi-MOF is rejuvenated, which results in the fluorescence ''turn-on'' response of the composite. Besides the fluorometric response, the detection of histidine by Eu/Bi-MOF was also observed by a colorimetric response. The LOD for histidine was found to be 0.18 μM.

Besides the detection of basic amino acids, MOF sensors have been used significantly for the detection of acidic amino acids.[116,117] Similar to other amino acids, aspartic acid (Asp) plays a great role in the living organisms such as myocardial function and metabolism in mammals.[118] Thus, an abnormal concentration of Asp poses a threat to human health such as stroke and hepatic problems.[119] Liu and co-workers post-synthetically incorporated Cu^{2+} and Tb^{3+} ions in a Zn-MOF to deliver Cu/Tb@Zn-MOF, which displayed the selective and sensitive ''turn-on'' recognition of Asp.[120] The incorporation of the Tb^{3+} ion in the Zn-MOF resulted in the characteristic emission peak of the Tb^{3+} ion due to the antenna effect. When the Cu^{2+} ion was embedded in Tb@Zn-MOF, the Cu/Tb@Zn-MOF composite showed the quenching of fluorescence. This was due to the effective LMCT process from the ligand to Cu^{2+} ion (strong coordination between Cu^{2+} ion and S site of ligand), which reduced the charge transfer from the ligand to the Tb^{3+} ion. This Cu^{2+} ion and the size effect of the pore acted as a strong interaction site for Asp, resulting in the selective and sensitive detection of Asp. Given that the Cu^{2+} ion interacted with Asp, the LMCT process from the ligand to Cu^{2+} ion decreased. Simultaneously, the antenna effect from the ligand to Tb^{3+} ion was revived, leading to a ''turn-on'' luminescence response. The interaction between the Cu^{2+} ion and Asp was confirmed by the XPS analysis. The composite material showed the Cu 2p1 peak at 953.87 eV, and after treatment with Asp, this peak appeared at 953.03 eV. This shifting of the Cu 2p1 peak to a lower energy illustrates the weak interaction between Cu^{2+} and Asp.

MOFs have also been used for the detection of antibiotic molecules.[121–123] With the increase in the population globally, the intake of antibiotics has significantly increased, which has a negative effect on the environment.[124] Also, the side effects associated with antibiotics negatively impact human health and cause several diseases.[125,126] More importantly, taking antibiotics a for longer time will result in the development of antibiotic resistance in the body, which is fatal. In this regard, Neogi and co-workers strategically devised a highly luminescent porous zinc-based framework, CSMCRI-2, possessing free basic amino groups.[127] The activated MOF network could detect the antibiotics sulfadiazine (SDZ) and adenosine monophosphate (AMP) through a luminescence ''turn-on'' fashion with an increase in fluorescence intensity by almost 30 and 13.8 fold, respectively. The LOD values for SDZ and AMP were calculated to be 65 nM and 10 nM, respectively. The detection of these analytes was also realized through a colorimetric response. Besides the experimental evidence, the mechanism of sensing was established by deep theoretical investigation. The LUMO of SDZ is energetically higher than that of the MOF. Therefore, the transfer of electrons occurs from the LUMO of SDZ to the LUMO of the MOF, causing a luminescence enhancement in the MOF. The presence of free amino linkers in the MOF network resulted in intermolecular hydrogen bonding interaction with the analytes, which bring them in close proximity. Thus, the charge or transfer of electrons is possible between the MOF and analyte.

The recognition of antibiotic residue in food samples is imperative for real-time application. In this regard, Ghasemi and co-workers deliberately prepared a zirconium-based luminescent MOF coated with MIP polymer as a guest recognition site for the ''turn-on'' detection of chloramphenicol (CAP) antibiotic residue in food samples (honey and milk).[128] The porous structure and creation of a specific binding site in the composite resulted in the selective sensing of CAP. The LOD value for CAP was 0.013 μg L^{-1}. The mechanism of sensing for the detection of CAP is as follows: the coated MIP on ZrMOF interacts strongly with the CAP analyte. ZrMOF shows an emission peak at 440 nm and the linker ATA in the free state displays an emission peak at 436 nm. This indicates that the emission of the MOF is a ligand-based emission. Interestingly, the emission of ATA in the free state is almost 2.5-times higher than that of the MOF. This is due to the LMCT from the ligand ATA to the Zr–O clusters in the MOF. When CAP was added to the system, it prohibited the LMCT from the ligand to metal clusters, resulting in an enhancement in the emission intensity of ATA. The IR analysis was helpful to justify the sensing mechanism. In the presence of CAP, the carbonyl group of CAP forms a stronger interaction with the Zr^{4+} ion in the Zr–O clusters than with ATA. Consequently, the interaction between the Zr–O clusters and ATA declines, and hence the LMCT process almost stops. Therefore, the fluorescence intensity of ATA in ZrMOF is augmented. The diverse MOFs with their crucial features towards the ''turn-on'' recognition of several types of biomarkers and biomolecules are presented in Table 1.

3.3. Turn-on sensing of hazardous entities and high-energy compounds

The sensing of hazardous and toxic compounds is critical given that they have a very bad environmental effect and negative human health impact.[129–131] Generally, nitrogen-rich organic compounds, nerve agents and NACs belong to the category of hazardous/toxic compounds.[132,133] Thus, researchers are devoted on the development of sophisticated detection techniques for the sensing of these lethal entities. Luminescent MOFs are considered potential candidates in this regard. The qualitative structural features and controllable electronic properties of MOFs make them suitable sensors for the recognition of explosives and nitrogen-rich energetic organic compounds. Furthermore, with the help of crystal engineering, their selectivity and sensitivity can be tuned efficiently.

Zhou and co-workers reported an excellent work for the ''turn-on'' recognition of nitrogen-rich heterocyclic compounds (NRHCs) using a cobalt-based MOF (Co-TCPE), which was derived from the AIE-active ligand H_4TCPE.[134] Although this MOF contained highly conjugated linkers, it was almost non-

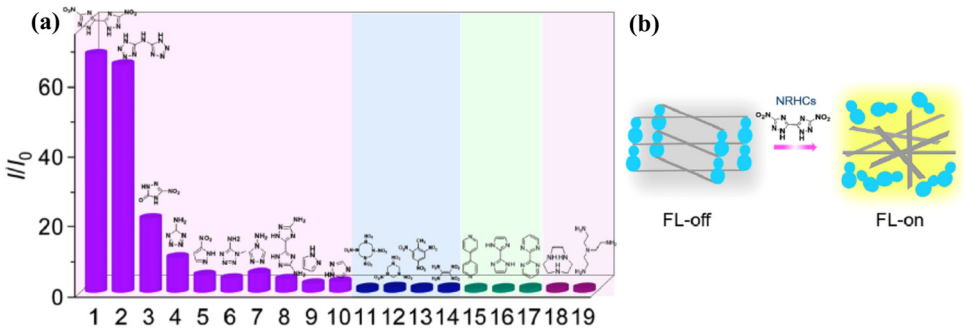

Fig. 19 (a) Intensity ratio of Co-TCPE in the presence of a variety of nitrogen-rich organic compounds (compound numbers 1 to 19 in the *x*-axis are given in the abbreviations list) and (b) illustration of competitive coordination of Co-TCPE with NRHCs. Reproduced with permission from ref. 134, the American Chemical Society, Copyright 2022.

fluorescent (signal off) because of the presence of the Co3 scaffold, which acted as a quencher (LMCT) for the emission of AIE-MOF. The Co-TCPE MOF showed an emission peak at 515 nm upon excitation at 375 nm, which remained unchanged over a wide pH range (3 to 12). This indicates that the MOF has the potential to act as an efficient sensor under different conditions. Interestingly, when Co-TCPE was titrated with NRHCs such as NTO (single ring) and DNBT (dual ring), the luminescence intensity of the MOF was significantly enhanced (Fig. 19). In contrast, polyamines and non-energetic heterocyclic molecules did not affect the fluorescence intensity of the MOF much (Fig. 19).

Additionally, the increase in fluorescence intensity caused by the double-ring NRHCs was much greater than that by the single-ring NRHCs. The mechanism for fluorescence the "turn-on" phenomenon by NRHCs was explained based on PXRD, TEM, mass and NMR studies. The PXRD pattern of the recovered Co-TCPE showed the absence of the signature peak at 7.56°, indicating that the framework collapsed. Further, the NMR and mass spectrometry study revealed the formation of a complex between the linker H_4TCPE and DNBT (dual-ring NRHCs). Therefore, all these experimental evidence suggested that upon the addition of NRHCs, the deformation or collapse of the MOF occurred through the competitive coordination substitution. Consequently, the H_4TCPE linker was released from the MOF network and became self-aggregated (restricted intramolecular motion) in the water medium, which caused aggregation-induced emission. The detection of NRHCs was also realized through colorimetric changes to yellow (Fig. 19b).

Li and co-workers published an excellent work based on the "turn-on" detection of explosive molecules (aliphatic nitro-organics) with the help of the dye@bio-MOF-1 composite.[135] The aperture channels of the MOF were decorated with free amine functional moieties, which induced non-covalent bonding with the incoming (guest) molecules. This facilitated the encapsulation of nitro explosive molecules (Fig. 20).

The composite showed a "turn-off" luminescence response for aromatic nitro explosive molecules. On the contrary, the framework demonstrated the luminescence "turn-on"

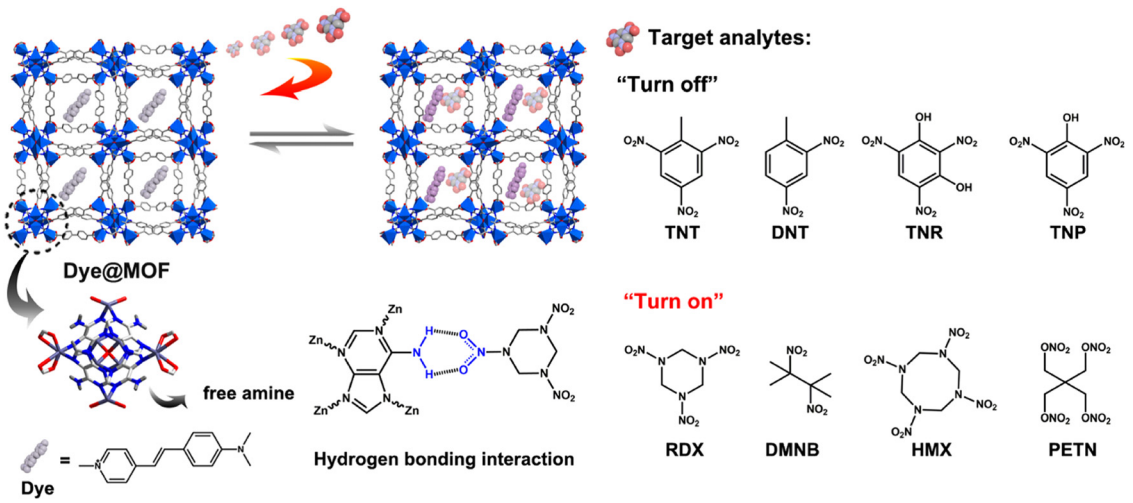

Fig. 20 Dye@bio-MOF-1 showing luminescence "turn-on" detection for aliphatic nitro compounds. Reproduced with permission from ref. 135, the American Chemical Society, Copyright 2022.

phenomenon with aliphatic nitro explosive molecules. After the inclusion of dye molecules inside the MOF cavity, very limited space was available in the MOF. Thus, it was difficult for the aromatic nitro compounds to enter the pores of the composite, whereas the smaller aliphatic nitro compounds could easily enter the cavity and occupied the available space to induce host–guest interactions. Due to this space confinement, the vibrations and torsions of the dye molecules were restricted, and consequently the nonradiative decay decreased. Thus, an increment in fluorescence (confinement-induced enhancement) was observed.

With the increasing world population, the demand for the food has significantly increased. Thus, the farmers are focused on increasing the productivity from cultivation. In this case, large amounts of pesticides are utilized in the agro field. Although pesticides are important to enhance the crop productivity, they profoundly affect human health.[136] Thus, smart sensors are necessary for the monitoring of pesticide molecules. Neogi and co-workers detected the pesticides DEP and IPT by using de-solvated CSMCRI-8 through the fluorescence "turn-on" mechanism with the LOD values of 79.8 nM and 226 nM, respectively.[137]

Moorthy and co-workers synthesized a bisimidazole-based tetracarboxylic acid ligand (H_4ANTBI) having anthracene in its core, and using this ligand, they constructed a cadmium-based MOF, Cd-ANTBI. This MOF showed the sensitive "turn-on" detection of toxic nerve agent mimics.[138] Due to the self-quenching of the MOF in the crystalline state, the fluorescence intensity of the MOF significantly diminished. The solvent aided the exfoliation of the MOF, affording 2D MOF nanosheets (MOFNS), which exhibited a significant enhancement in fluorescence intensity. Interestingly, MOFNS displayed the "turn-on" recognition of nerve agent mimics (diethyl chlorophosphate, DCP) with an LOD of 0.52 ppm.

The mechanism of "turn-on" emission in the presence of DCP is presented in Fig. 21. The protonation reaction between the imidazolium moiety of the linker and the DCP, followed by nucleophilic attack leads to the structural modification of the linker in MOFNS. This ligand structural orientation induces rigidification of the overall framework by inhibiting the torsional motions of the benzene ring. Consequently, the deactivation pathways are block, and a hence fluorescence enhancement is observed. With an increase in the concentration of DCP in the experimental solution, the luminescence intensity proportionally increased because the rigidification was enhanced in the linker.

Hydrazine is also another hazardous compound that is widely used in several fields such organic synthesis, pharmaceuticals, and catalysts. Because of its large enthalpy value, it is used as a fuel in space craft and rockets. However, although it has lots of potential value-added qualities, it is regarded as carcinogenic and toxic. Thus, the detection of hydrazine is essential. Biswas and co-workers reported the selective and sensitive detection of hydrazine through the "turn-on" luminescence process using a zirconium-based MOF, Zr-UiO-66-$(OCOCH_3)_2$.[139] They judiciously used the H_2BDC-$(OCOCH_3)_2$ ligand to introduce the acetoxy functionality as a guest reaction site in the zirconium framework. The detection of hydrazine was also visualized through the naked eye.

The sensing mechanism is presented in Fig. 22. The nucleophilic attack by the hydrazine occurs on the acetoxy functionality, which is then converted to a hydroxyl moiety. Therefore, the H_2BDC-$(OCOCH_3)_2$ linker is transformed to H_2BDC-$(OH)_2$. The enhancement in the luminescence of the MOF is due to the formation of H_2BDC-$(OH)_2$. The generation of the hydroxyl group was also further supported by the IR and ^{1}H NMR analysis. Table 1 presents different MOFs for the "turn-on" detection of hazardous entities and high-energy compounds.

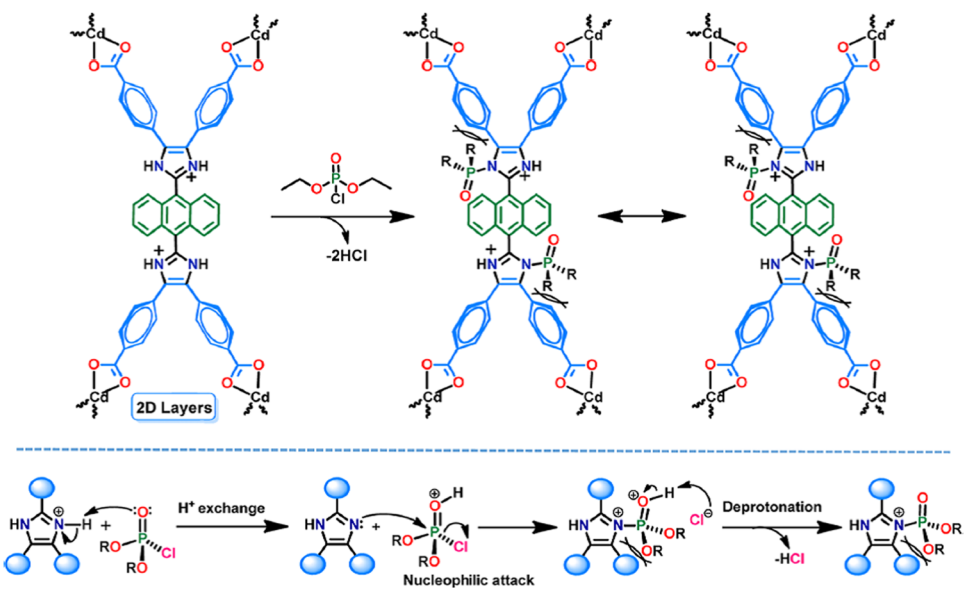

Fig. 21 Turn-on mechanism for the detection of DCP. Reproduced with permission from ref. 138, the American Chemical Society, Copyright 2021.

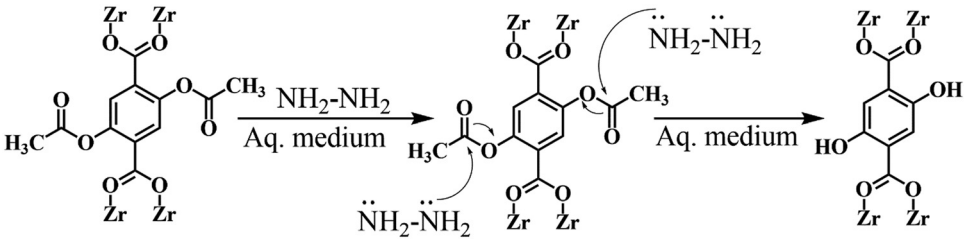

Fig. 22 Probable sensing mechanism for hydrazine by Zr-UiO-66-$(OCOCH_3)_2$.

3.4. Turn on sensing of cations

In recent years, luminescent MOFs have been developed to recognize several cationic species with high selectivity and ultra-sensitivity. The detection limit in some cases is very low, and sometimes in real field studies, the MOFs can detect ions at much lower concentrations than the optimized concentration fixed by the EPA and WHO. The efficient supramolecular host–guest interaction is one of the strongest reason for this high detection efficiency. Furhtmoer, the supramolecular interaction, and hence the selectivity and sensitivity can be controlled by introducing several functional moieties.[194,195] This has been witnessed in the following examples.

Das and coworkers reported the preparation of a 3D porous anionic stable cobalt-based MOF, $\{[Me_2NH_2]_{0.5}[Co(DATRz)_{0.5}(NH_2BDC)]\cdot Gx\}_n$, for the discriminating "turn-on" recognition of Al^{3+} ion.[196] The MOF network was nicely oriented with free $-NH_2$ groups (Fig. 23), which interact efficiently with the guest metal ions.

The MOF displayed the maximum emission peak at 430 nm (blue emission) upon excitation at 340 nm, which is due to the intra and inter LLCT occurring in its framework. Upon screening the luminescence intensity of this MOF with various metal ions, it was observed that its emission intensity at 430 nm sharply increased in the presence of Al^{3+} ions. This illustrates that the MOF showed unique selectivity and sensitivity for Al^{3+} ions with an LOD of 17.5 ppb. The rectangular large cavity of the MOF consists of a dimethyl ammonium cation ($Me_2NH_2^+$), *i.e.*, an ionic environment, which allows the facile transfer of metal ions through the cavity and forms a strong host–guest interaction. The mechanism for the sensing of Al^{3+} was explained based on the absorbance-caused fluorescence increment. The Al^{3+} ion embedded entity (Al^{3+}@MOF) absorbs more excitation light than the free MOF and gets excited. From the excited level, the Al^{3+}@MOF reaches the ground level by releasing a large amount of energy (wavelength), showing a "turn-on" luminescence response. The Al^{3+}@MOF unit releases a larger amount of energy than the free MOF in the emission process. Further, the authors exhibited the detection of Al^{3+} using the paper strip method to make the sensing approach portable, convenient and economic.

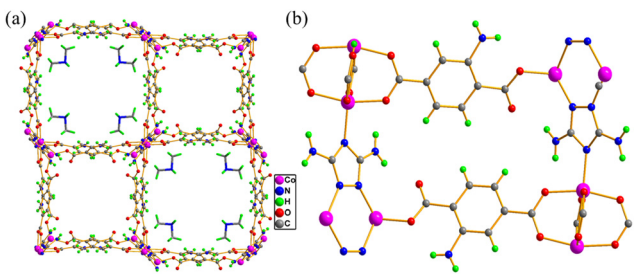

Fig. 23 (a) Three-dimensional packing of MOF, which contains $Me_2NH_2^+$ in its rectangular cavity and (b) decoration of guest interaction–NH_2 sites in the framework.

Guo and co-workers synthesized a cadmium-based highly stable MOF, $[Cd(3\text{-}NH_2\text{-}pba)_2]_4\cdot 8DMF$, under solvothermal conditions for the selective and sensitive "turn-on" detection of silver metal ions.[197] The crystallographic investigation disclosed that the framework is decorated with basic amine functional moieties. The emission spectrum of the MOF revealed the maximum emission at 470 nm (blue emission) upon excitation at 322 nm. This emission is due to the π–π^* transition in the organic ligand. The luminescence intensity of the MOF was quenched in water, thus it acted as a water sensor in ethanol solvent. Interestingly, when this MOF was treated with several metal ions in water medium, its emission intensity at 479 nm considerably increased (almost 50 times) in the presence of silver metal ions (Fig. 24).

The interaction between the amino group and Ag^+ ion was confirmed by IR and XPS analysis. The IR spectrum showed the signature peaks for the amino group at 3230 and 1673 cm^{-1}, which are vanished for Ag^+@MOF. According to the XPS data, the N1s binding energy of the $-NH_2$ group shifted from 399.2 eV for the MOF to 399.4 eV for Ag^+@MOF. Further, the lifetime decay measurement indicated an increase in the lifetime of the excited state of Ag^+@MOF (5.877 ns) compared to the simple MOF (3.803 ns). This study illustrated that the interaction between $-NH_2$ and the Ag^+ ion is very strong to overcome the luminescence quenching induced by the O–H oscillators of the water molecule. Besides the fluorometric method, the detection of silver ions was also investigated through a colorimetric response (Fig. 26).

Hong and co-workers described the synthesis of zinc-based porous 3D MOF, $[Zn_3(L_3)_2(bpy)]$, for the discriminating "turn-on" recognition of Cd^{2+} ions.[198] Interestingly, the diffusion of Cd^{2+} ions into the pores of the MOF was directly visualized by two-photon confocal microscopy. Among a pool of several metal ions, the Cd^{2+} ion significantly enhanced the luminescence intensity (60 fold) of the framework compared to the free MOF. The mechanism of sensing was confirmed with the help

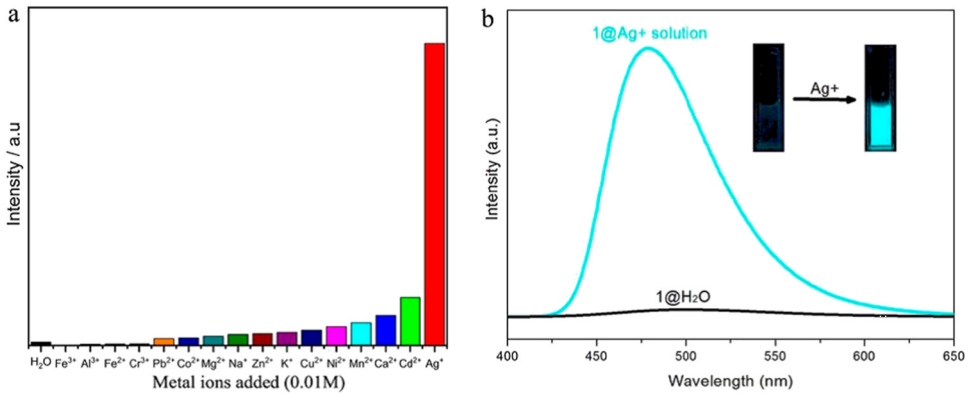

Fig. 24 (a) Fluorescence intensity of MOF in the presence of different metal ions in aqueous medium and (b) significant enhancement in the luminescent intensity of the MOF in the presence of silver metal ions (inset: colorimetric response of the MOF with silver ions). Reproduced with permission from ref. 197, the American Chemical Society, Copyright 2021.

of XPS. The L_3 and bpy linkers contain nitrogen atoms in their backbone. The nitrogen atom of bpy is sterically congested given that it is linked with the metal ion (Zn^{2+} ion) to form the MOF network. The N1s peak position of the nitrogen atom of the L_3 linker in the MOF slightly shifted to 398.63 eV (Cd^{2+}@MOF) from 398.34 eV (MOF), indicating the interaction between the nitrogen atoms of the L_3 linker with the Cd^{2+} ion. The XPS analysis of the O atoms (O1s peak) of the methoxy and carboxylate groups of the L_3 linker in the free MOF and in the MOF in the presence of Cd^{2+} ions did not show any obvious change, which ruled out the interaction between the O atoms and Cd^{2+} ions.

Duan and co-workers synthesized an Eu^{3+}-based MOF, $[Eu_2(L_4)_3(DMF)_3]$ $2DMF{\cdot}5H_2O$, for the detection of Cr^{3+} ions through luminescence recovery of the MOF material.[199] In the MOF network, the anthracene moiety of the ligand stacked nicely, as confirmed by SCXRD, which reduced the emission intensity of the MOF.[200] The H_2L_4 linker and MOF exhibited an emission peak at 460 and 475 nm under excitation at 365 nm, respectively. The emission intensity of the MOF indicated that is almost non-fluorescent in nature and its luminescence under a UV lamp was also not visible. The characteristic emission peak of the lanthanide ion in the MOF was not observed, which may be due to the presence of an anthracene moiety in the ligand of the MOF, acting as s triplet-state quencher (triplet–triplet annihilation). Consequently, the metal based luminescence was significantly reduced.[201,202] Also, this MOF showed an extremely low ligand-based emission due to the self-absorption process, *i.e.*, the absorption band of the MOF overlaps with its emission band. When the MOF was treated with various metal ions in aqueous medium, its luminescence intensity at 450 nm significantly increased for Cr^{3+} ions. Furthermore, the detection ability for Cr^{3+} ions remained unaffected in the presence of other metal ions with the LOD for Cr^{3+} ions of 7.52×10^{-8} M. The mechanism of sensing was well-established with the assistance of IR, SEM, XPS and UV visible analysis. The appearance of the free MOF and $Cr(NO_3)_3$-embedded MOF was the same in the SEM images. The atomic mapping of $Cr(NO_3)_3$@MOF showed the presence of five elements (carbon, nitrogen, oxygen, europium and chromium). This suggests that the Cr^{3+} metal ion was incorporated in its framework. The IR stretching vibration peak appeared at 1287 cm^{-1}, which is the signature peak of NO_2. This illustrated the successful encapsulation of the nitrate anion in the MOF to counter the charge balance of the chromium ion. Further, the interaction of the Cr^{3+} ion within the framework was confirmed by XPS. The UV-visible spectrum showed that in presence of Cr^{3+} ions, the self-absorption effect of $Cr(NO_3)_3$@MOF was greatly reduced compared to the free MOF, which indicates its strong luminescence response for Cr^{3+}. Alternatively, its emission spectrum was red-shifted during the recognition process, signifying that apart from the reduction of the self-absorption effect, the ICT between the different aryl groups and/or the changes in the excitation-state energy levels largely contributed to the enhancement of the luminescent intensity of the MOF in presence of Cr^{3+}.

Mercury is a lethal pollutant to the human body, which is present in the ecosystem through various anthropogenic activities and natural sources. Although the Hg^{2+} ion, as the inorganic form of mercury, is very dangerous, its organic form the methylmercury ion (CH_3Hg^+) is fatal. These two ions are generally accumulated in the human body through the food chain, causing serious health issues including cardiovascular, nerve, and kidney failure.[203] Therefore, the selective and sensitive detection of these toxic species are very important, and particularly on-site cost-effective methods are desirable. Qu and co-workers synthesized a boric acid (BA)-functionalized Eu^{3+} ion-based MOF (BA-Eu-MOF) for the ultra-sensitive "turn-on" recognition of CH_3Hg^+ and Hg^{2+}.[204] Upon excitation at 275 nm, the BA-Eu-MOF displayed signature emission peaks at 620 ($^5D_0 \rightarrow {}^7F_2$) and 595 nm ($^5D_0 \rightarrow {}^7F_1$), which illustrate the occurrence of the antenna effect. However, the red emission of the complex was very weak in water medium, which is attributed to the electron-withdrawing nature of BA, deactivating the antenna effect. Upon the addition CH_3Hg^+ and Hg^{2+} ions, the C–B bond of BA is destroyed and the formation of a C–Hg bond occurs, *i.e.*, transmetalation reaction occurs (Fig. 25). Therefore, the electron-withdrawing nature of BA is completely lost,

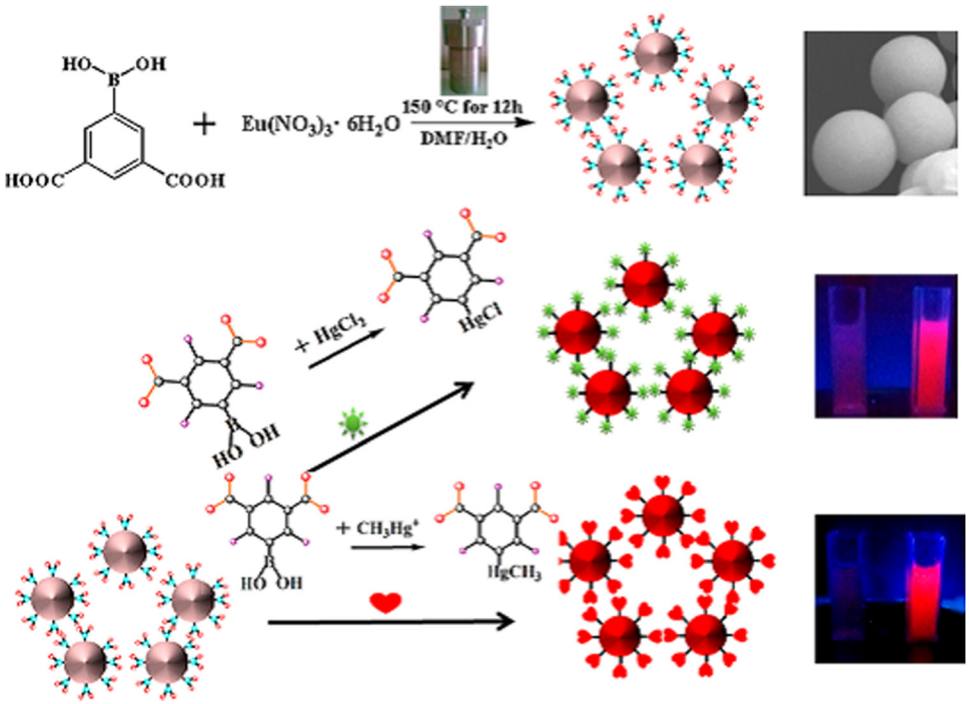

Fig. 25 Synthesis of BA-Eu-MOF and schematic presentation for the sensing of CH_3Hg^+ and Hg^{2+} through the transmetalation reaction, *i.e.*, C–B bond of BA is ruptured and the formation of a C–Hg bond occurs. Reproduced with permission from ref. 204, the American Chemical Society, Copyright 2020.

and concomitantly the antenna effect of the ligand is revived, which boost the red emission.

Although the Fe^{3+} ion is a very important element in living organisms,[205,206] its excess leads to harmful health effects such cardiac arrest and Alzheimer's disease.[207,208] Hence, the detection and on-site monitoring of Fe^{3+} ions are critical. Zhang and co-workers used an AIE-active ligand (L_5) for the construction of a stable cadmium-based luminescent MOF, $[Cd(NDA)(L_5)(H_2O)_2]_n$, for the discriminating sensitive recognition of Fe^{3+} ions in water medium through the fluorescence "turn-on" process.[209] The emission peak of the MOF appeared at 440 nm upon excitation at 324 nm. When the MOF was treated with a large number of metal ions (Fig. 26), its emission intensity was considerably enhanced in the presence of Fe^{3+} ions with an LOD of 2.06 × 10^{-3} mM.

The PXRD pattern of the recovered MOF after the sensing of Fe^{3+} ion was exactly the same as that of the pristine MOF, which ruled out the degradation of the framework. XPS analysis of Fe^{3+}@MOF showed two peaks at 726.4 eV and 713.9 eV, which are ascribed to the Fe 2p1/2 and Fe 2p3/2 configurations, respectively. This study directly suggests the presence of Fe^{3+} cation in the framework. The SCXRD data of the MOF revealed the existence of a π···π interaction (3.613 Å) between the parallel aryl moiety of the ligand. The authors suggested that

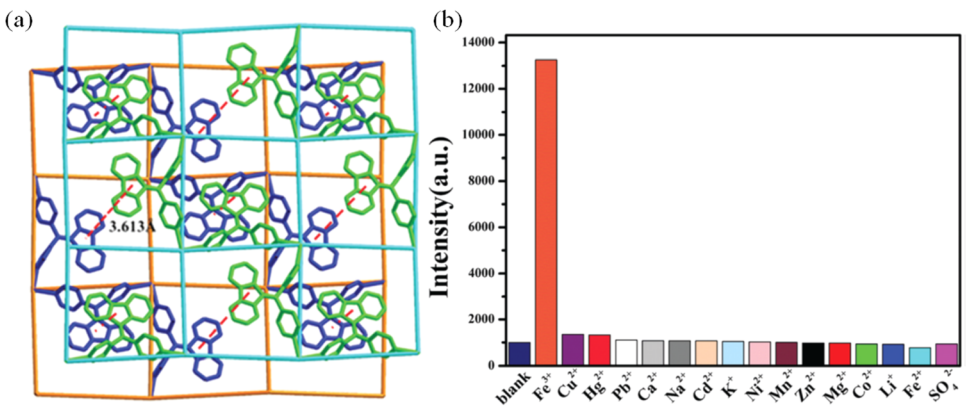

Fig. 26 (a) Network of MOF showing π···π interaction between the parallel fluorene moiety and (b) selective detection turn-on detection of Fe^{3+} ions in aqueous medium.

the Fe^{3+} ion forms a π···cation···π-type interaction within the framework, which helps to transport electrons and enhances the emission intensity of the MOF.

Similar to other metal ions, the Mg^{2+} ion plays a significant role in the human body in several physiological processes, cell proliferation, activating membrane proteins and influencing biochemical processes.[210,211] Consequently, an imbalance in Mg^{2+} ions can lead to several diseases including osteoporosis, diabetes, and coronary heart problems.[212,213] Thus, the monitoring of the Mg^{2+} ion concentration is very important. In this regard, Han and co-workers reported the synthesis of a dye-entrapped magnetically active MOF, Fe_3O_4/RhB@Al-MOF, for the discriminating sensitive ''turn-on'' recognition of Mg^{2+} ions.[214] This composite showed two emission peaks at 610 nm (from RhB) and 440 nm (Al-MOF) upon excitation at 330 nm. When the MOF composite was treated with a variety of metal ions, it selectively detected Mg^{2+} ions. Consequently, its emission peak at 440 nm increased, while the peak at 610 nm remained constant. The composite displayed an initial recognition time of about 90 s for Mg^{2+} ions and almost 5-fold enhancement in luminescence intensity with an LOD value for Mg^{2+} ions of 8×10^{-7} M. Further, the detection of Mg^{2+} ions was also exhibited in biosystems (HL-7702 and A375 cells). The mechanism of sensing was corroborated by the XPS analysis. The emission peak at 440 nm sharply increased, which indicates that Mg^{2+} efficiently interacts with the nitrogen element of the $-NH_2$ group of the 2-ATA linker in the Al-MOF. This interaction permits facile energy transfer and enhances the ligand-based emission. According to the XPS data, the N1s peak of the 2-ATA linker in Fe_3O_4/RhB@Al-MOF appeared at 402.25 eV, which illustrates the coordination of Mg^{2+} with N of the $-NH_2$ group. A list of the various MOFs and their vital features for the ''turn-on'' recognition of different types of cations is presented in Table 2.

3.5. Turn-on sensing of anions

The aforementioned discussion clearly illustrates that MOFs are potential candidates for the recognition of several analytes (*vide supra*). However, interestingly, MOFs also have the ability to recognize anionic species.[239–241] The detection of anionic species is very important because of their biological significance and lethal effects on the environment. In recent years, MOFs have shown potential for the detection of a variety of toxic anions and rapid development has been witnessed regarding this. As is well-known, the cyanide ion (CN^-) is a very lethal among the list of anionic species and has been listed as a toxic compound by both the EPA and WHO. CN^- has the ability to link with cytochrome oxidase and prevent the utilization of oxygen. Consequently, due to the lack of oxygen, the cells will die. Thus, the development of CN^- sensors is essential[242] but the detection of CN^- using MOFs as sensory materials has rarely been reported.[243] In this regard, Zhou and co-workers

Table 2 Diverse MOFs with their excitation, emission wavelength and LOD values for the recognition of various cations

MOFs	Metal ion in node/SBU	$\lambda_{excitation}$ (nm)	$\lambda_{emission}$ (nm)	Nature of analyte detects	LOD	Ref.
[Co(OBA)-(DATZ)$_{0.5}$(H$_2$O)]	Co	283	407	Al^{3+}	57.5 ppb	215
PCN-222-Pd(II)	Zr	275	351	Cu(II)	50 nM	216
UPC-17	Ba	330	546	Fe^{3+}		217
[Cd$_3$L$_2$(μ-H$_2$O)(H$_2$O)]·3DMF·5H$_2$O	Cd	369	484	Mg^{2+}	0.021 μM	218
NUM-2	Zn	324	377	Al^{3+}	0.10 ppm	219
UiO-66-N=CH$_2$	Zr	342	468	Cd^{2+}	0.336 mM	220
CTGU-1	Tb		595, 619, 654 and 703	Eu^{3+}/Dy^{3+}	5×10^{-8} and 1×10^{-4} M	221
1 and **2**	Zn(1) and Cd(2)	364 for **1** 372 nm for **2**	478 and 514 nm for both **1** and **2**	Al^{3+} and Cr^{3+} for **1**, Al^{3+} and Cr^{3+} and Pb^{2+} for **2**		222
IRMOF-3	Zn	379	450	Cr^{3+}, Al^{3+}, Ga^{3+} and In^{3+}	0.293 ppm, 0.267 ppm, 0.598 ppm and 0.616 ppm	223
Gold nanoclusters/Zn-MOF	Zn	410	570	Zn^{2+}	6 nM	224
Mg-TPP-DHBDC	Mg	367	505	Al^{3+}	28 nM	225
JXUST-1	Cd	354	404	Al^{3+}	0.048 ppm	226
Cd-TCHO	Cd	350	450	Al^{3+}	0.54 ppb	227
JXUST-2	Co	394	530	Fe^{3+}, Cr^{3+}, and Al^{3+}	0.13 μM, 0.10 μM and 0.10 μM	228
Zn$_2$(BDC)$_2$(DABCO)	Zn	360	436	Zn^{2+}	0.7 μM	229
Zn(NH$_2$-bdc)(4,4′-bpy)]	Zn	365	426	Al^{3+}	30 nM	230
UiO-(OH)$_2$@RhB	Zr	420	583	Al^{3+}	10 nM	231
[Cd$_4$(NDC)$_3$(4-Hptz)$_2$(H$_2$O)$_2$]·H$_2$O	Cd	325	400	Cr^{3+}	0.164 μM	232
[Zn(bimpy)(1,4-ndc)]·H$_2$O	Zn	370	422	Fe^{3+}	8.82×10^{-7} M	233
Tb-TCPP	Tb	428	652	Al^{3+}, Cr^{3+}, and Fe^{3+}	7.79 nM, 9.94 nM and 16.4 nM	234
Cu-HBIBA	Cu	337	460	Bi^{3+} and Fe^{3+}	43 nM and 0.16 mM	235
Zn-DHNDC MOF	Zn	350	367	Al^{3+} and Fe^{3+}	95 nM, 33 nM	236
JXUST-5	Zn	365	420	Al^{3+} and Ga^{3+}	0.17 and 0.69 ppm	237
JXUST-6	Cd	452	499	Al^{3+} and Ga^{3+}	0.081 and 0.047 ppm	238

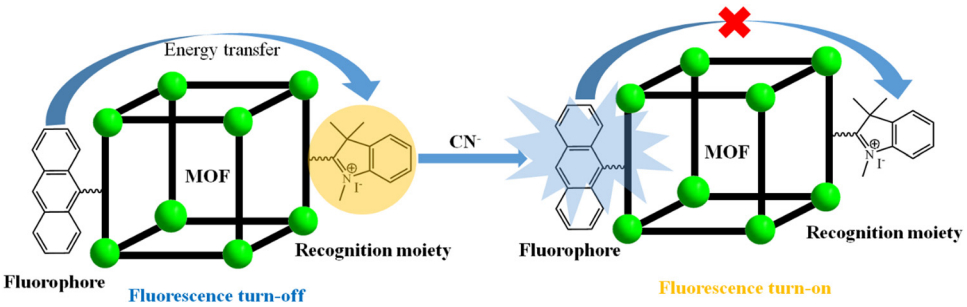

Fig. 27 Installation of the fluorophore and the recognition site in the MOF for the selective sensing of CN^-.

systematically developed a CN^- sensor by sequentially modifying PCN-700.[244] The fluorophore anthracene moiety and selective binding site (hemicyanine) for CN^- ions were installed on the network of PCN-700. After screening with several anions, the fluorescence intensity of the MOF was significantly enhanced with CN^- and the detection limit was found to be 0.05 μm. In the pristine MOF, the energy transfer between the anthracene and hemicyanine moieties quenches the luminescence of the anthracene part. Alternatively, in the presence of CN^-, the electron-deficient nature of the hemicyanine part is greatly reduced, and hence the charge transfer from the anthracene to hemicyanine stops. Consequently, the luminescence intensity of the anthracene is regained (Fig. 27).

Perborate is essential in daily life, which is present in detergent materials, cosmetics, and bleaching agents.[245] Due to its low cost and oxidising property, it is widely used in industry and considered as an alternative to H_2O_2.[246] Thus, because of the large use of perborate, it has become a common pollutant in drinking water and the environment. Biswas and co-workers synthesized an acetoxy-functionalized Al-based MOF, CAU-10-$OCOCH_3$, for the selective and sensitive "turn-on" detection of perborate anions in aqueous medium.[247] Upon the treatment of the MOF with several anions, in the case of perborate, its fluorescence intensity at 402 nm dramatically increased by 65 fold (Fig. 28). The "turn-on" detection of perborate by CAU-10-$OCOCH_3$ remained unaffected in the presence of various competitive anions present in the sample solution. The selective and sensitive detection of perborate is due to the conversion of the acetoxy functional group on the linker in the MOF to the auxo-chromic moiety –OH group (5-hydroxy isophthalic acid), leading to the fluorescence enhancement in the system. This functionality conversion was confirmed by IR and ^1H NMR analysis. The LOD for perborate was found to be 1.19 μM. Further, the MOF showed detection ability for perborate in various environmental samples.

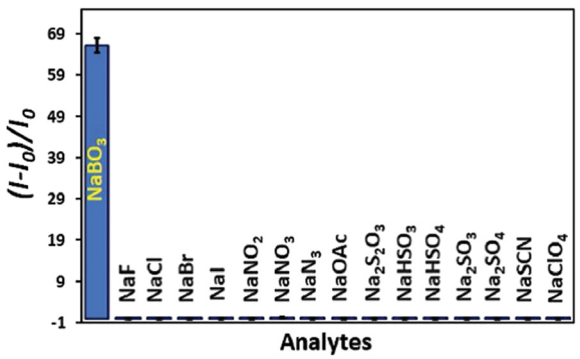

Fig. 28 Selective "turn-on" enhancement of CAU-10-$OCOCH_3$ for $NaBO_3$.

The same group further reported the "turn-on" detection of the ROS superoxide using a Zr-based MOF.[248] Here, the new zirconium-based MOF UiO-66-NH-SO_2-Ph-NO_2 was synthesized using BDC-NH-SO_2-Ph-NO_2 ligand under solvothermal reaction conditions. The MOF and linker displayed an emission peak 422 and 436 nm, respectively, upon excitation at 350 nm in methanol solvent. After the injection of 350 μL of 1 mM superoxide ($O_2^{\bullet -}$) in a dispersed solution of the MOF, the fluorescence intensity of the MOF was significantly enhanced by almost 10 fold with a shift in its emission peak by 14 nm to the blue region. This shifting in its emission peak is due to the elimination of the coordinated linker from the MOF. However, the luminescence intensity of the MOF remained unaffected in the presence of other ROS. The mechanism of sensing was established with the help of PXRD, IR and mass analysis. The PXRD study indicated that the after first sensing process, the MOF was not recoverable, illustrating the collapse of the MOF network. The IR study revealed that the intensity of the carboxylate stretching vibrations of the ligand in the MOF gradually declined upon the steady addition of $O_2^{\bullet -}$. Finally, the IR peak was almost similar to that of the free ligand. This again confirmed the collapse of the MOF. Further, the release of the ligand from the MOF was confirmed by the mass analysis with the appearance of a sharp peak at 365.1619. All these studies vividly elaborated that the framework collapsed in the presence of $O_2^{\bullet -}$ and the BDC-NH-SO_2-Ph-NO_2 linker became free in the methanol solution, resulting in a "turn-on" fluorescence emission.

Dong and co-workers reported the sensing of the reactive oxygen species HClO using an MOF-based fluorescent mixed matrix membrane composed of UiO-68-PT and poly(vinyl alcohol) (PVA).[249] This detection was very sensitive with a colorimetric response, and importantly the sensing was reversible when triggered by Vitamin C (VC) (Fig. 29 and 30). Among several cationic and anionic analytes, UiO-68-PT showed an enhancement in its emission peak at 392 nm upon excitation at

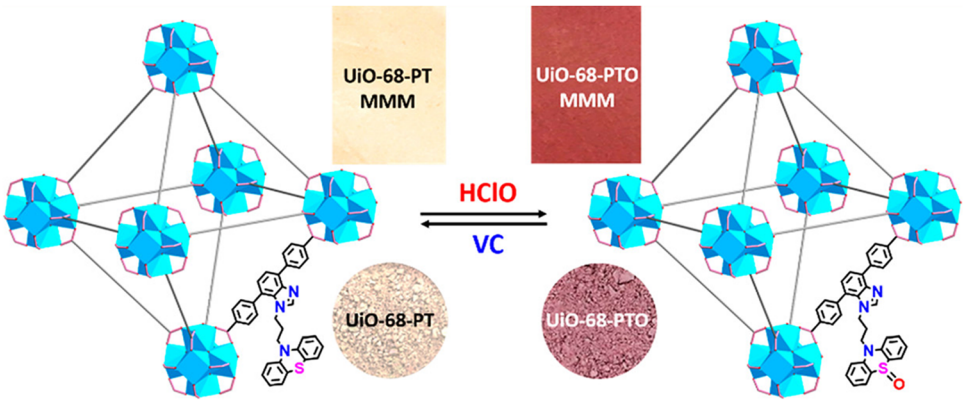

Fig. 29 Colour change in UiO-68-PT (and its membrane) during the sensing of HClO and the conversion of the MOF to UiO-68-PTO (and its membrane) upon treatment with VC. Reproduced with permission from ref. 249, the American Chemical Society, Copyright 2020.

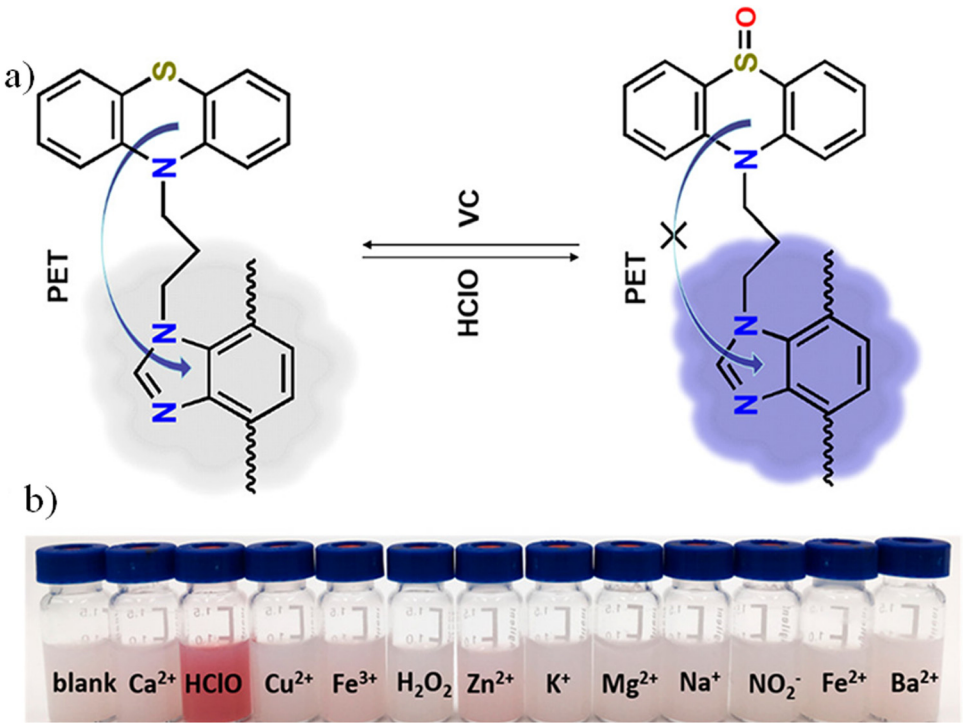

Fig. 30 (a) Mechanism of sensing during the recognition of HClO and (b) colorimetric response of UiO-68-PT with HClO. Reproduced with permission from ref. 249, the American Chemical Society, Copyright 2020.

323 nm in the presence of the ClO^- anion. The detection limit for the ClO^- anion was 0.28 μM.

The pristine MOF UiO-68-PT was almost non-fluorescent in nature. This is because the electron-donating ability of phenothiazine to benzimidazole through the PET process reduced its luminescence intensity. When ClO^- anion was added to the system, it converted the phenothiazine moiety to phenothiazine sulfoxide (UiO-68-PTO). Consequently, the PET effect was completely inhibited from the phenothiazine sulfoxide to benzimidazole moiety, and thus the fluorescence property of the latter was significantly amplified. The IR spectrum of UiO-68-PTO showed a peak at 1045 cm^{-1}, which corresponds to the signature peak for the S=O bond. Interestingly, upon the addition of VC, the phenothiazine sulfoxide reverted to phenothiazine, and consequently the emission intensity was quenched. This reversible redox conversion was also observed through a visual colour change.

Pyrophosphate (PPi) plays an essential role in physiological functions and it acts as a crucial character in DNA sequencing.[250] Thus, its concentration is very important and its monitoring in living cells imperative. Hu and co-workers reported the synthesis of MOF-5-NH_2 for the selective detection

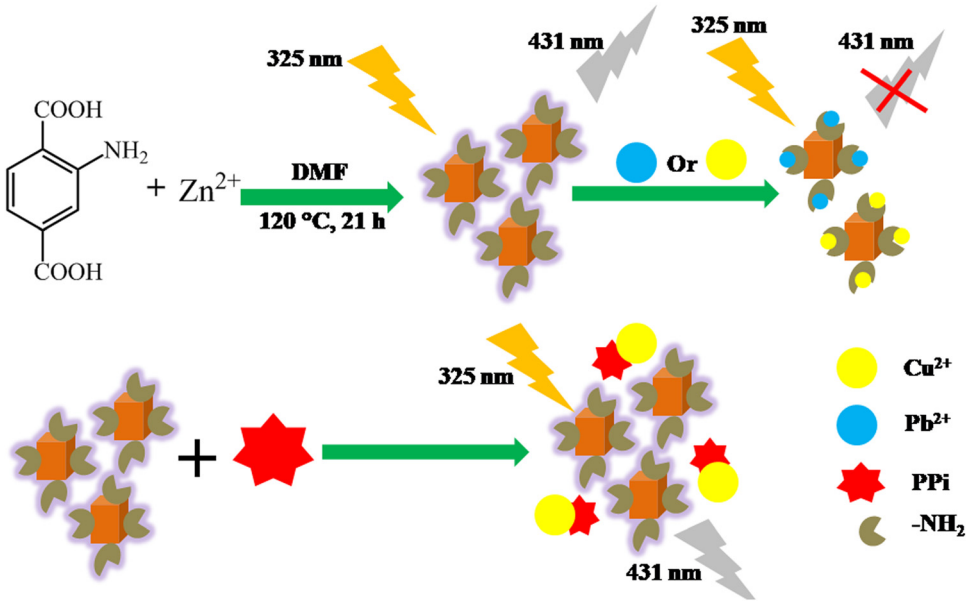

Fig. 31 Synthesis of MOF-NH_2, followed by its complexation with Cu^{2+}/Pb^{2+} ions for the sensing of PPi.

of pyrophosphate (PPi) through the turn-on process.[251] This framework showed an emission peak at 431 nm upon excitation at 325 nm. Actually, the MOF acts as a dual-type sensor, *i.e.*, it detects two varieties of analytes. Firstly, the MOF recognises metal ions (Cu^{2+} and Pb^{2+}) through the "turn-off" process. Interestingly, in the presence of PPi, the non-luminescent entity Cu^{2+}@MOF-5-NH_2/Pb^{2+}@MOF-5-NH_2 displayed the fluorescence "turn-on" phenomenon (Fig. 31).

The overall sensing mechanism was established with the help of the host–guest interaction. The luminescence of MOF-5-NH_2 is primarily due to its amino-based linker. In the presence of Cu^{2+}/Pb^{2+}, the excited electrons on the ligand of the MOF are donated to the vacant orbital on Cu^{2+} (3d orbital) and Pb^{2+} (6p orbital). This leads to a reduction in the fluorescence intensity of MOF-5-NH_2. However, when PPi is added to the system, it pulls out the Cu^{2+}/Pb^{2+} metal ion from the system. Thereby, the inhibition of electron transfer between MOF-5-NH_2 and Cu^{2+}/Pb^{2+} occurs. Thus, the fluorescence of MOF-5-NH_2 is rejuvenated. Further, this mechanism of sensing was supported by excited lifetime decay study, zeta potential measurement and FRET analysis.

Ghosh and co-workers strategically designed an MOF as a scaffold for the selective "turn-on" detection of the bisulfite anion (HSO_3^-) in aqueous solution.[252] They used the well-known MOF NH_2-MIL-68(In) for the PSM process of –NH_2 groups in the MOF with glyoxal to enable –CHO interaction site for the guest molecules (Fig. 32). Interestingly, upon the formation of the Schiff base, the MOF sensor lost its fluorescence intensity with respect to the pristine MOF. When the post-synthetic-modified MOF was treated with a variety of anions, it was found that it regained its florescence intensity with HSO_3^- anions. Accordingly, the emission peak at 437 nm was significantly enhanced upon excitation at 320 nm. The LOD value in this case was 0.047 ppm. The sensitivity and selectivity of the post-synthetic-modified MOF for HSO_3^- anions remained unaffected in the presence of several other competitive anions. The mechanism of the sensing process was validated using IR spectroscopy. The IR spectrum of the MOF treated with HSO_3^- anions showed a stretching peak at ~1130 cm^{-1}, correspong to the S=O bond of the HSO_3^- anions.

The detection of fluoride ions is very important given that they play various important roles in biological and environmental systems.[253] The recognition and quantification of fluoride ions are necessary, and in this context, MOFs are very efficient. Yan and co-workers post-synthetically incorporated the Tb^{3+} ion in a Zr-MOF to form Tb^{3+}@Zr-MOF for the discriminating sensitive "turn-on" recognition of fluoride ions in aqueous medium.[254] In the solid state, the luminescence spectrum (λ_{ex} = 302 nm) of Tb^{3+}@Zr-MOF showed the signature peaks for the Tb^{3+} ion at 620, 584, 544 and 488 nm, which correspond to the $^5D_4 \rightarrow {}^7F_J$ transition where, J = 3, 4, 5 and 6,

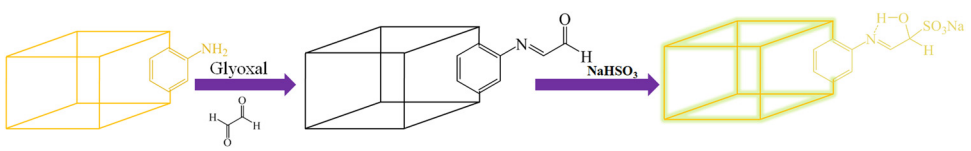

Fig. 32 PSM process of NH_2-MIL-68(In) with glyoxal to produce the final probe and its sensing mechanism for the HSO_3^- anion.

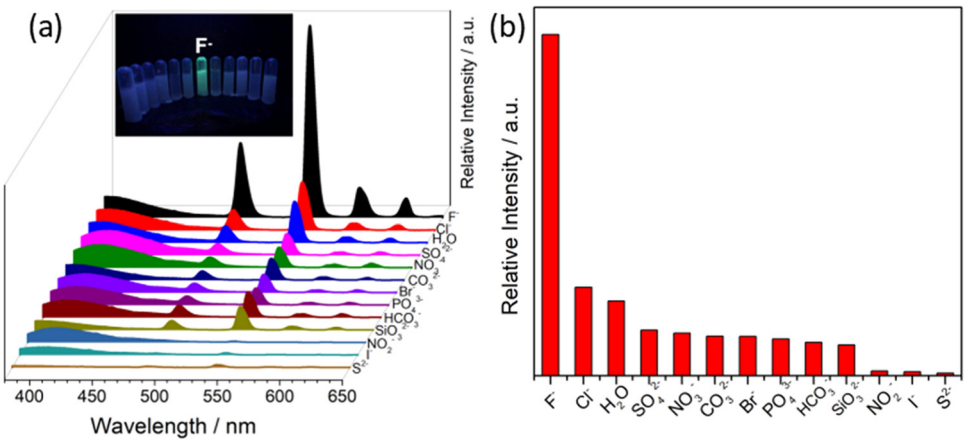

Fig. 33 Emission peak pattern of Tb^{3+}@Zr-MOF with diverse anions (inset: colorimetric response of Tb^{3+}@Zr-MOF with F^- ion) and (b) highest increment of fluorescence intensity of Tb^{3+}@Zr-MOF with F^- ion among a variety of competitive anions. Reproduced with permission from ref. 254, the American Chemical Society, Copyright 2018.

Table 3 Diverse MOFs with their excitation, emission wavelength and LOD values corresponding to the recognition of various anions

MOFs	The metal ion in node/SBU	$\lambda_{excitation}$ (nm)	$\lambda_{emission}$ (nm)	Nature of analyte detects	LOD	Ref.
1	Zr	310	465	CN^-	0.14 μM	256
UiO-66-NH_2	Zr	360	470		8.2×10^{-7} M and 7.3×10^{-7} M	257
ZIF-90-BA	Zn	475	544	OCl^-	6.25 μM	258
Zr-UiO-66-N_2H_3	Zr	360	430	PO_4^{3-}	0.196 μM	259
NH_2-MIL-101(Al)	Al	490	520	F^-	0.05 μmol L^{-1}	260
Zr-UiO-66-NH-CH_2-Py	Zr	330	430	$O_2^{\bullet-}$	0.21 μM	261
PDA/Eu/PDA-UiO-66-NH_2(x)	Zr	280	591, 614, 650 and 698	ClO^-	0.10 μM	262

respectively. This indicates that the ligand effectively sensitized (antenna) Tb^{3+} in the luminescence process. However, when the luminescence spectrum (λ_{ex} = 302 nm) of Tb^{3+}@Zr-MOF was recorded in water medium, the ligand-centred emission at 398 nm appeared, whereas the intensity of the Tb^{3+} emission decreased. This reduction is owing to the stretching vibration of the O–H bond of the water molecule. On screening the luminescence intensity of Tb^{3+}@Zr-MOF in water medium with several anions (Fig. 33), its fluorescence intensity sharply increased with F^- ions. Under UV light in the presence of F^-, the MOF also showed a colorimetric response with bright green color, which corresponds to the major peak at 544 nm ($^5D_4 \rightarrow {}^7F_5$) (Fig. 33, inset). The detection limit for F^- ion was found to be 0.35 ppm.

The PXRD pattern of the recovered MOF after the first sensing process ruled out the degradation of the framework. Interestingly, the MOF having imperfect bonds indicates that the coordination number around Zr^{4+} remained vacant, which acts as a Lewis acid and furnished the guest interaction site.[255] In water, the intensity ratio value of I_{545}/I_{398} was 1.5, which significantly increased to 29 upon the interaction of Tb^{3+}@Zr-MOF with F^- ions. The F^- ion is a Lewis base, and thus strongly interacts with the Lewis acid Zr^{4+} ion, causing the energy transfer from the ligand to Zr^{4+} to considerably decline. Concomitantly, the energy transfer was enhanced from the ligand to Tb^{3+}. Thus, the luminescence intensity of Tb^{3+}@Zr-MOF increased. The MOF-based "turn-on" probes for the recognition of diverse anions are listed in Table 3.

4. Conclusion and outlook

This review article furnished a summary and classification of various luminescent MOF materials with their fabrication strategies and the "turn-on" sensing application towards a variety of organic and inorganic analytes such as cations, anions, VOCs, biomolecules, biomarkers and environmental pollutants. The tunable structural features of MOFs make them suitable luminescence sensors and their emission can be increased depending on the presence of highly conjugated organic linkers, metal ions and/or suitable luminescence guest moieties in their framework. Compared with the "turn-off" (signal-off) sensing process, the "turn-on" signalling event is very important and has more practical applicability. Thus, the optical response associated with "turn-on" sensing is a significant research motif. "Turn-on" MOF sensors with a low LOD are very appealing given that they enable the visual detection of analytes. The host–guest interaction and the transfer of energy/

electrons between them are the prime contributors to the signal transduction in the sensing process. However, although significant developments have been achieved, there is an ample chance for further advancement in this research field.

The MOF-based ''turn-on'' sensing phenomenon can be explored for device-based sensors or OLED devices, which is in its infancy. Similarly, MOF-based membrane or thin film sensors need to be considered, and many aspects can evolve from this methodology in terms of sensitivity, selectivity, response time and recyclability. Nanoscale luminescent MOFs have potential application in tissue and cell imaging, *i.e.*, *in vivo* sensing. In this regard, hydrolytic stability and robustness in the biological environment are crucial. The aqua solvent has the ability to coordinate with metal ions and there is a chance of the collapse of the MOF network. However, currently, there are ample MOFs that are very water stable. Nevertheless, we have to look at other parameters for diverse applications in the line with ''turn-on'' sensing. For example, the cytotoxicity of MOFs should be properly investigated for biological sensing and considerably absent in this case. Moreover, multidisciplinary collaboration between bioengineers, materials scientist and biomedical scientists will enable the execution of luminescence MOFs for practical biological applications.

Abbreviations

TPPE	1,1,2,2-Tetrakis(4-(pyridin-4-yl)phenyl)ethane
DMA	*N*,*N*-Dimethylacetamide
CSMCRI-3	$[Ni_2(\mu_2\text{-}OH)(azdc)(tpim)](NO_3)\cdot 6DMA\cdot 6MeOH$
tpim	4,4′,4″-(1*H*-Imidazole-2,4,5-triyl)tripyridine
H_2azdc	azobenzene-4,4′-dicarboxylic acid
H_2DHT	2,5-Dihydroxyterephthalic acid
TFA	Trifluoroacetic acid
LLCT	Ligand to ligand charge transfer
H_3L	4,4′,4″-Nitrilotribenzoic acid
ETTC	4,4,4,4-(Ethane-1,1,2,2-tetrayl)tetrabiphenyl-4-carboxylic acid
XPS	X-Ray photoelectron spectroscopy
H_2L_1	4,4′-Dicarboxy-4″-nitrotriphenylamine
L_2	4-Hydroxypyridine-2,6-dicarboxylate
2,3-pydcH_2	Pyridine-2,3- dicarboxylic acid
Bpp	1,3-Bis(4-pyridyl)propane)
H_3L_3	4′,4‴,4⁗-Nitrilotris(3-methoxy-[1,1′-biphenyl]-4-carboxylic acid
H_2L_4	5-[(Anthracen-9-ylmethyl)-amino]-isophthalic acid
L_5	4,4′-((9*H*-Fluoren-9-ylidene)-methylene)dipyridine
bpy	4,4′-Bipyridine
SCXRD	Single crystal X-ray diffraction
3-NH_2-Hpba	3-Amino-4-(pyridin-4-yl)benzoic acid
MMCT	Metal to metal charge transfer
RhB	Rhodamine B
HDATRz	3,5-Diamino-1,2,4-triazole
H_2NH_2-BDC	2-Amino-1,4-benzenedicarboxylic acid
G	Guest molecule
CAU	Christian-Albrechts-University
UiO	University of Oslo
ROS	Reactive oxygen species
TPDC	3,3″-Diamino-1,1′:4′,1″-terphenyl-4,4″-dicarboxylic acid
2,2′-bpy	2,2′-Bipyridine
bpp	4,4′-Trimethylenedipyridine
H_2nip	5-Nitroisophthalic acid
NIR	Near infrared
LMCT	Ligand to metal charge transfer
Ag_{12}	$[(Ag_{12}(StBu)_6(CF_3COO)_6(CH_3CN)_6]\cdot CH_3CN$
Py-TPE	Tetrapyridine-tetraphenylethene
AIE	Aggregation enhanced emission
Htpt	5-[4(1*H*-1,2,4-Triazol-1-yl)]phenyl-2*H*-tetrazole)
R,*R*-CHCAIP	5,5′-((1*R*,2*R*)-Cyclohexane dicarbonyl bis-(azanediyl)) diisophthalic acid
NACs	Nitro aromatic compounds
MLCT	Metal to ligand charge transfer
H_4TCPE	Tetrakis[4-(4-carboxyphenyl)phenyl]ethane
DCP	Diethyl chlorophosphate
H_2BDC-$(OCOCH_3)_2$	2,5-Diacetoxy-1,4-benzenedicarboxylic acid
H_2BDC-$(OH)_2$	2,5-Dihydroxyterephthalic acid
DEP	3-(Diethylamino)phenol
IPT	Isoproturon
PVA	Poly(vinyl alcohol)
OXDZ	Nitrogen-rich heterocyclic dicarboxylate linker
HODA	2,2′,3,3′-Oxidiphthalic acids
MIP	Molecularly imprinted polymer
MMM	Polymer mixed-matrix membranes
pda	1,10-Phenanthroline-2,9-dicarboxylic acid
HDATRz	3,5-Diamino-1,2,4-triazole
PDA	2,6-Pyridinedicarboxylic acid
H_4DTATC	5,5′-(9,10-Dihydroxy-4a,9,9a,10-tetrahydroanthracene-9,10-diyl)-diisophthalic acid
H_2hpi_2cf	(5-(2-(5-Fluoro-2-hydroxyphenyl)-4,5-bis(4-fluorophenyl)-1*H*-imidazol-1-yl)isophthalic acid)
1	DNBT (dual-ring NRHC)
2	H_3bta (bis(1*H*-tetrazol-5-yl) amine)
3	NTO (single-ring NRHC)
4	5*H*-tetrazol-5-amine
5	3-Nitro-1*H*pyrazole
6	1-Methyl-1*H*-tetrazol-5-amine
7	4*H*-1,2,4-Triazol-4-amine
8	DABT (3,3′-diamino-5,5′-bis(1*H*-1,2,4-triazole))
9	Pyrazole
10	4*H*-1,2,4-Triazole

11	HMX (1,3,5,7-Tetranitro-1,3,5,7-tetrazocane)
12	RDX (1,3,5-Trinitroperhydro-1,3,5-triazine)
13	TNT (Trinitrotoluene)
14	FOX-7 (1,1-diamino-2,2-dinitroethylene)
15	4,4′-Bipyridine
16	2,2′-Biimidazole
17	2,2′-Bipyrimidine
18	1,4,7-Triazacyclononane
19	Tris(2-aminoethyl)amine

Conflicts of interest

There are no conflicts to declare.

Acknowledgements

TKP gratefully acknowledges financial support received from the SERB, India (TAR/2021/000090).

References

1 O. M. Yaghi, G. Li and H. Li, Selective binding and removal of guests in a microporous metal–organic framework, *Nature*, 1995, **378**, 703–706.
2 S. Kitagawa, R. Kitaura and S.-I. Noro, Functional porous coordination polymers, *Angew. Chem., Int. Ed.*, 2004, **43**, 2334–2375.
3 M. Dincă and J. Long, Introduction: Porous Framework Chemistry, *Chem. Rev.*, 2020, **120**, 8037–8038.
4 Z. Ji, H. Wang, S. Canossa, S. Wuttke and O. Yaghi, Pore Chemistry of Metal–Organic Frameworks, *Adv. Funct. Mater.*, 2020, **30**, 2000238.
5 T. K. Pal, Syntheses, structures and topology variations of metal organic frameworks built from a semi-rigid tetracarboxylate ligand, *Chemistry Select*, 2019, **4**, 536–542.
6 M. Kalaj and S. Cohen, Postsynthetic Modification: An Enabling Technology for the Advancement of Metal–Organic Frameworks, *ACS Cent. Sci.*, 2020, **6**, 1046–1057.
7 M. Bláha, V. Valeš, Z. Bastl, M. Kalbáč and H. Shiozawa, Host–Guest Interactions in Metal–Organic Frameworks Doped with Acceptor Molecules as Revealed by Resonance Raman Spectroscopy, *J. Phys. Chem. C*, 2020, **124**, 24245–24250.
8 S. Yuan, L. Feng, K. Wang, J. Pang, M. Bosch, C. Lollar, Y. Sun, J. Qin, X. Yang, P. Zhang, Q. Wang, L. Zou, Y. Zhang, L. Zhang, Y. Fang, J. Li and H. Zhou, Stable Metal–Organic Frameworks: Design, Synthesis, and Applications, *Adv. Mater.*, 2018, **30**, 1704303.
9 N. Patel, P. Shukla, P. Lama, S. Das and T. K. Pal, Engineering of metal organic frameworks (MOFs) as ratiometric sensors, *Cryst. Growth Des.*, 2022, **22**, 3518–3564.
10 B. Yan, Lanthanide-Functionalized Metal−Organic Framework Hybrid Systesms To Create Multiple Luminescent Centers for Chemical Sensing, *Acc. Chem. Res.*, 2017, **50**, 2789–2798.
11 J. Dong, X.-D. Zhang, X.-F. Xie, F. Guo and W.-Y. Sun, Amino group dependent sensing properties of metal–organic frameworks: selective turn-on fluorescence detection of lysine and arginine, *RSC Adv.*, 2020, **10**, 37449–37455.
12 A. Bavyskina, N. Kolobov, I. Khan, J. A. Bau, A. Ramirez and J. Gascon, Metal−Organic Frameworks in Heterogeneous Catalysis: Recent Progress, New Trends, and Future Perspectives, *Chem. Rev.*, 2020, **120**, 8468–8535.
13 L. Zhu, X. Liu, H. Jiang and L. Sun, Metal−Organic Frameworks for Heterogeneous Basic Catalysis, *Chem. Rev.*, 2017, **117**, 8129–8176.
14 T. K. Pal, D. De and P. Bharadwaj, *Engineering the Confined Space of MOFs for Heterogeneous Catalysis of Organic Transformations*, Wiley, 2021, 17, pp. 293–326.
15 T. K. Pal, D. De and P. Bharadwaj, Metal-organic frameworks as heterogeneous catalysts for the chemical conversion of carbon dioxide, *Fuel*, 2022, **320**, 123904.
16 A. Rawat, S. Dhakla, P. Lama and T. K. Pal, Fixation of carbon dioxide to aryl/aromatic carboxylic acids, *J. CO2 Uti.*, 2022, **59**, 101939.
17 A. Thorarinsdottir and T. Harris, Metal–Organic Framework, *Chem. Rev.*, 2020, **120**, 8716–8789.
18 T. K. Pal, D. De, S. Neogi, P. Pachfule, S. Senthilkumar, Q. Xu and P. Bharadwaj, Significant Gas Adsorption and Catalytic Performance by a Robust CuII–MOF Derived through Single-Crystal to Single-Crystal Transmetalation of a Thermally Less-Stable ZnII–MOF, *Chem. – Eur. J.*, 2015, **21**, 19064–19070.
19 P. Lama, H. Aggarwal, C. X. Bezuidenhout and L. J. Barbour, Giant Hysteretic Sorption of CO2: In Situ Crystallographic Visualization of Guest Binding Within a Breathing Framework At 298 K, *Angew. Chem., Int. Ed.*, 2016, **55**, 13271–13275.
20 R. Lin, S. Xiang, W. Zhou and B. Chen, Microporous Metal-Organic Framework Materials for Gas Separation, *Chem*, 2020, **6**, 337–363.
21 J. Li, J. Sculley and H. Zhou, Metal–Organic Frameworks for Separations, *Chem. Rev.*, 2012, **112**, 869–932.
22 Q. Yin, Y.-L. Li, L. Li, J. Lü, T.-F. Liu and R. Cao, Novel Hierarchical Meso-Microporous Hydrogen-Bonded Organic Framework for Selective Separation of Acetylene and Ethylene versus Methane, *ACS Appl. Mater. Interfaces*, 2019, **11**, 17823–17827.
23 D. Gallis, L. Rohwer, M. Rodriguez, M. Dailey, K. Butler, T. Luk, J. Timlin and K. Chapman, Multifunctional,Tunable Metal–Organic Framework Materials Platform for Bioimaging Applications, *ACS Appl. Mater. Interfaces*, 2017, **9**, 22268–22277.
24 H. Lawson, S. Walton and C. Chan, Metal–Organic Frameworks for Drug Delivery: A Design Perspective, *ACS Appl. Mater. Interfaces*, 2021, **13**, 7004–7020.
25 T. Qiu, Z. Liang, W. Guo, H. Tabassum, S. Gao and R. Zou, Metal–Organic Framework-Based Materials for Energy Conversion and Storage, *ACS Energy Lett.*, 2020, **5**, 520–532.
26 D. Lim and H. Kitagawa, Proton Transport in Metal–Organic Frameworks, *Chem. Rev.*, 2020, **120**, 8416–8467.

27 J. Ellis, S. Crawford and K. Kim, Metal–organic framework thin films as versatile chemical sensing materials, *Mater. Adv.*, 2021, **2**, 6169–6196.
28 S. Majhi, A. Ali, P. Rai, Y. Greish, A. Alzamly, S. Surya, N. Qamhieha and S. Mahmoud, Metal–organic frameworks for advanced transducer based gas sensors: review and perspectives, *Nanoscale Adv.*, 2022, **4**, 697–732.
29 A. Douvali, A. C. Tsipis, S. V. Eliseeva, S. Petoud, G. S. Papaefstathiou, C. D. Malliakas, I. Papadas, G. S. Armatas, I. Margiolaki, M. G. Kanatzidis, T. Lazarides and M. J. Manos, Turn-On Luminescence Sensing and Real-Time Detection of Traces of Water in Organic Solvents by a Flexible Metal–Organic Framework, *Angew. Chem., Int. Ed.*, 2015, **54**, 1651–1656.
30 J.-F. Feng, T.-F. Liu, J. Shi, S.-Y. Gao and R. Cao, Dual-Emitting UiO-66(Zr&Eu) Metal−Organic Framework Films for Ratiometric Temperature Sensing, *ACS Appl. Mater. Interfaces*, 2018, **10**, 20854–20861.
31 R. Goswami, T. K. Pal and S. Neogi, Stimuli-triggered fluoro-switching in metal–organic frameworks: applications and outlook, *Dalton Trans.*, 2021, **50**, 4067–4090.
32 X.-Z. Wang, M.-Y. Sun, Z. Huang, M. Xie, R. Huang, H. Lu, Z. Zhao, X.-P. Zhou and D. Li, Turn-On Circularly Polarized Luminescence in Metal–Organic Frameworks, *Adv. Optical Mater.*, 2021, 2002096.
33 J. Liu, J. Xue, G.-P. Yang, L.-L. Dang, L.-F. Ma, D.-S. Li and Y.-Y. Wang, Recent advances of functional heterometallic-organic framework (HMOF) materials: Design strategies and applications, *Coord. Chem. Rev.*, 2022, **463**, 214521.
34 H. Fu, L. Yan, N. Wu, L. Ma and S. Zang, Dual-emission MOF ⊃ dye sensor for ratiometric fluorescence recognition of RDX and detection of a broad class of nitro-compounds, *J. Mater. Chem. A*, 2018, **6**, 9183–9191.
35 Z. Qiu, S. Zhao, Z. Xu, Y. Zhao, Z. Wang and W. Y. Sun, Crystal Structures and Luminescent Probe Behaviors of Three-Dimensional Zn(II) Frameworks with Multicarboxylate and Tetradentate Imidazole-Containing Ligands, *Cryst. Growth Des.*, 2021, **21**, 5306–5316.
36 K. Yi and L. Zhang, Embedding dual fluoroprobe in metal-organic frameworks for continuous visual recognition of Pb^{2+} and PO43- via fluorescence 'turn-off-on' response: Agar test paper and fingerprint, *J. Haz. Mat.*, 2020, **389**, 122141.
37 X. Zhang, Q. Maab, X. Liu, H. Niu, A. Luo, R. Li and X. Feng, A turn-off Eu-MOF@Fe^{2+} sensor for the selective and sensitive fluorescence detection of bromate in wheat flour, *Food Chem.*, 2022, **382**, 132379.
38 H. Wang, W. Lustig and J. Li, Sensing and capture of toxic and hazardous gases and vapors by metal–organic frameworks, *Chem. Soc. Rev.*, 2018, **47**, 4729–4756.
39 M. Hu, S. Razavi, M. Piroozzadeh and A. Morsali, Sensing organic analytes by metal–organic frameworks: a new way of considering the topic, *Inorg. Chem. Front.*, 2020, **7**, 1598–1632.
40 Y. Cui, B. Chen and G. Qian, Lanthanide metal-organic frameworks for luminescent sensing and light-emitting applications, *Coord. Chem. Rev.*, 2014, **273–274**, 76–86.
41 L. Kreno, K. Leong, O. Farha, M. Allendorf, R. Duyne and J. Hupp, Metal–Organic Framework Materials as Chemical Sensors, *Chem. Rev.*, 2012, **112**, 1105–1125.
42 D. Frackowiak, The Jablonski diagram, *J. Photochem. Photobiol., B*, 1988, **2**, 399.
43 M. Berezin and S. Achilefu, Fluorescence lifetime measurements and biological imaging, *Chem. Rev.*, 2010, **110**, 2641–2684.
44 J. Dong, D. Zhao, Y. Lu and W.-Y. Sun, Photoluminescent metal–organic frameworks and their application for sensing biomolecules, *J. Mater. Chem. A*, 2019, **7**, 22744–22767.
45 X. Wu, H. Fu, M. Han, Z. Zhou and L. Ma, Tetraphenylethylene Immobilized Metal–Organic Frameworks: Highly Sensitive Fluorescent Sensor for the Detection of Cr2O72– and Nitroaromatic Explosives, *Cryst. Growth Des.*, 2017, **17**, 6041–6048.
46 R. Goswami, N. Seal, S. Dash, A. Tyagi and S. Neogi, Devising Chemically Robust and Cationic Ni(II)-MOF with Nitrogen-Rich Micropores for Moisture Tolerant CO2 Capture: Highly Regenerative and Ultra- Fast Colorimetric Sensor for TNP and Multiple Oxo-Anions in Water with Theoretical Revelation, *ACS Appl. Mater. Interfaces*, 2019, **11**, 40134–40150.
47 C. A. Bauer, T. V. Timofeeva, T. B. Settersten, B. D. Patterson, V. H. Liu, B. A. Simmons and M. D. Allendorf, Influence of Connectivity and Porosity on Ligand-Based Luminescence in Zinc Metal−Organic Frameworks, *J. Am. Chem. Soc.*, 2007, **129**, 7136–7144.
48 K. Jayaramulu, P. Kanoo, S. George and T. Maji, Tunable emission from a porous metal–organic framework by employing an excited-state intramolecular proton transfer responsive ligand, *Chem. Commun.*, 2010, **146**, 7906–7908.
49 A. Legrand, A. Pastushenko, V. Lysenko, A. Geloen, E. Quadrelli, J. Canivet and D. Farrusseng, Enhanced Ligand-Based Luminescence in Metal–Organic Framework Sensor, *ChemNanoMat*, 2016, **2**, 866–872.
50 M. Alnaqbi, A. Alzamly, S. Ahmed, M. Bakiro, J. Kegerea and H. Nguyen, Frameworks chemistry and applications of s-block metal–organic frameworks, *J. Mater. Chem. A*, 2021, **9**, 3828–3854.
51 F. Saraci, V. Novoa, P. Donnarumma and A. Howarth, Rare-earth metal–organic frameworks: from structure to applications, *Chem. Soc. Rev.*, 2020, **49**, 7949–7977.
52 K. Lv, C. Urbank, M. Patzschke, J. März, P. Kaden, S. Weiss and M. Schmidt, MOFs with 12-Coordinate 5f-Block Metal Centers, *J. Am. Chem. Soc.*, 2022, **144**, 2879–2884.
53 T. K. Pal, R. Katoch, A. Garg and P. Bharadwaj, Metal–Organic Frameworks Built from a Linear Rigid Dicarboxylate and Different Colinkers: Trap of the Keto Form of Ethylacetoacetate, Luminescence and Ferroelectric Studies, *Cryst. Growth Des.*, 2015, **15**, 4526–4535.
54 S. Pal, T. K. Pal and P. K. Bharadwaj, Solvothermal synthesis of coordination polymers at different temperatures and their luminescence studies, *CrystEngComm*, 2016, **18**, 1825–1831.
55 J. Rocha, L. Carlos, F. Paz and D. Ananias, Luminescent multifunctional lanthanides-based metal–organic frameworks, *Chem. Soc. Rev.*, 2011, **40**, 926–940.

56 X. Zhou, X. Guo, L. Liu, H. Zhai, Q. Meng, Z. Shi and X. Tai, Two d10 luminescent metal–organic frameworks as dual functional luminescent sensors for (Fe^{3+}, Cu^{2+}) and 2,4,6-trinitrophenol (TNP) with high selectivity and sensitivity, *RSC Adv.*, 2020, **10**, 4817–4824.
57 S. V. Eliseeva and J.-C. G. Bünzli, Lanthanide luminescence for functional materials and bio-sciences, *Chem. Soc. Rev.*, 2010, **39**, 189–227.
58 J. Bünzli, Lanthanide Luminescence for Biomedical Analyses and Imaging, *Chem. Rev.*, 2010, **110**, 2729–2755.
59 E. Moore, A. Samuel and K. Raymond, From Antenna to Assay: Lessons Learned in Lanthanide Luminescence, *Acc. Chem. Res.*, 2009, **42**, 542–552.
60 J. Bünzli and C. Piguet, Lanthanide-containing molecular and supramolecular polymetallic functional assemblies, *Chem. Rev.*, 2002, **102**, 1897–1928.
61 P. Escribano, B. Julián-López, J. Planelles-Aragó, E. Cordoncillo, B. Viana and C. Sanchez, Photonic and nanobiophotonic properties of luminescent lanthanide-doped hybrid organic–inorganic materials, *J. Mater. Chem.*, 2008, **18**, 23–40.
62 S. Zhang, L. Chen, J. Xie, Y. Zhang, F. Huang, X. Wang, K. Li, F. Zhai, Q. Yang, L. Chen, Y. Wang, X. Dai, Z. Chai and S. Wang, Turn-up Luminescent Sensing of Ultraviolet Radiation by Lanthanide Metal−Organic Frameworks, *Inorg. Chem.*, 2022, **61**, 4561–4565.
63 K. Binnemans, Lanthanide-Based Luminescent Hybrid Materials, *Chem. Rev.*, 2009, **109**, 4283–4374.
64 B. Chandler, D. Cramb and G. Shimizu, Microporous Metal−Organic Frameworks Formed in a Stepwise Manner from Luminescent Building Blocks, *J. Am. Chem. Soc.*, 2006, **128**, 10403–10412.
65 J. Büunzli, Lanthanide Luminescence for Biomedical Analyses and Imaging, *Chem. Rev.*, 2010, **110**, 2729–2755.
66 M. Yuan, Q. Lu, Z. Zhang, X. Li, S. Liu, X. Sun and S. Liu, Using the Luminescence and Ion Sensing Experiment of a Lanthanide Metal–Organic Framework to Deepen and Extend Undergraduates' Understanding of the Antenna Effect, *J. Chem. Educ.*, 2019, **96**, 1256–1261.
67 P. Mahata, K. V. Ramya and S. Natarajan, Pillaring of CdCl2-Like Layers in Lanthanide Metal–Organic Frameworks: Synthesis, Structure, and Photophysical Properties, *Chem. – Eur. J.*, 2008, **14**, 5839–5850.
68 J. Xu, W. Su and M. Hong, A Series of Lanthanide Secondary Building Units Based Metal–Organic Frameworks Constructed by Organic Pyridine-2,6-Dicarboxylate and Inorganic Sulfate, *Cryst. Growth Des.*, 2011, **11**, 337–346.
69 S. Eliseeva and J. Büunzli, Lanthanide luminescence for functional materials and bio-sciences, *Chem. Soc. Rev.*, 2010, **39**, 189–227.
70 P. Escribano, B. López, J. Aragó, E. Cordoncillo, B. Vianab and C. Sanchez, Photonic and nanobiophotonic properties of luminescent lanthanide-doped hybrid organic–inorganic materials, *J. Mater. Chem.*, 2008, **18**, 23–40.
71 X. Zhu, J. Lu, X. Li, S. Gao, G. Li, F. Xiao and R. Cao, Syntheses, Structures, Near-Infrared, and Visible Luminescence of Lanthanide-Organic Frameworks with Flexible Macrocyclic Polyamine Ligands, *Cryst. Growth Des.*, 2008, **8**, 1897–1901.
72 S. Záliš, C. Consani, E. Nahhas, A. Cannizzo, M. Chergui, F. Hartl and A. Vlček Jr, Origin of electronic absorption spectra of MLCT-excited and one-electron reduced 2,2′-bipyridine and 1,10- phenanthroline complexes, *Inorg. Chim. Acta*, 2011, **374**, 578–585.
73 M. Robin, The Color and Electronic Configurations of Prussian Blue, *Inorg. Chem.*, 1962, **1**, 337–342.
74 A. Vogler and H. Kunkely, Ligand-to-ligand and intraligand charge transfer and their relation to charge transfer interactions in organic zwitterions, *Coord. Chem. Rev.*, 2017, **251**, 577–583.
75 Y. Zhao, J. Wang, W. Zhu, L. Liub and R. Pei, The modulation effect of charge transfer on photoluminescence in metal–organic frameworks, *Nanoscale*, 2021, **13**, 4505–4511.
76 N. Shustova, B. McCarthy and M. Dincă, Turn-On Fluorescence in Tetraphenylethylene-Based Metal–Organic Frameworks: An Alternative to Aggregation-Induced Emission, *J. Am. Chem. Soc.*, 2011, **133**, 20126–20129.
77 G. Wang, Z. Li, H. Jia, N. Hu and J. Xu, Metal–organic frameworks based on the pyridine-2,3-dicarboxylate and a flexible bipyridyl ligand: syntheses, structures, and photoluminescence, *CrystEngComm*, 2009, **11**, 292–297.
78 X. Yang, H. Zhu and M. Liu, Transition-metal-based (Zn^{2+} and Cd^{2+}) metal-organic frameworks as fluorescence "turn-off" sensors for highly sensitive and selective detection of hydrogen sulphide, *Inorg. Chim. Acta*, 2017, **466**, 410–416.
79 J. Zou, Q. Peng, Z. Wen, G. Zeng, Q. Xing and G. Guo, Two Novel Metal–Organic Frameworks (MOFs) with (3,6)-Connected Net Topologies: Syntheses, Crystal Structures, Third-Order Nonlinear Optical and Luminescent Properties, *Cryst. Growth Des.*, 2010, **10**, 2613–2619.
80 Y. Ma, G. Xu, F. Wei, Y. Cen, X. Xu, M. Shi, X. Cheng, Y. Chai, M. Sohail and Q. Hu, One-Pot Synthesis of a Magnetic, Ratiometric Fluorescent Nanoprobe by Encapsulating Fe3O4 Magnetic Nanoparticles and Dual-Emissive Rhodamine B Modified Carbon Dots in Metal–Organic Framework for Enhanced HClO Sensing, *ACS Appl. Mater. Interfaces*, 2018, **10**, 20801–20805.
81 X. Zheng, Y. Zhao, P. Jia, Q. Wang, Y. Liu, T. Bu, M. Zhang, F. Bai and L. Wang, Dual-Emission Zr-MOF-Based Composite Material as a Fluorescence Turn-On Sensor for the Ultrasensitive Detection of Al^{3+}, *Inorg. Chem.*, 2020, **59**, 18205–18213.
82 R. Chen, J. Zhang, J. Chelora, Y. Xiong, S. Kershaw, K. Li, P. Lo, K. Cheah, A. Rogach, J. Zapien and C. Lee, Ruthenium (II) Complex Incorporated UiO-67 Metal–Organic Framework Nanoparticles for Enhanced Two-Photon Fluorescence Imaging and Photodynamic Cancer Therapy, *ACS Appl. Mater. Interfaces*, 2017, **9**, 5699–5708.
83 Y. Yang, W. Liu, Q. Zhong, J. Zhang, B. Yao, X. Lian and H. Niu, Self-Assembly of Lanthanide-Based Metallogel Nanoplates into Microcubic Blocks as Self-Calibrating

Luminescent Methanol Sensors, *ACS Appl. Nano Mater.*, 2021, **4**, 4735–4745.

84 X. Zhang, Q. Hu, T. Xia, J. Zhang, Y. Yang, Y. Cui, B. Chen and G. Qian, Turn-on and Ratiometric Luminescent Sensing of Hydrogen Sulfide Based on Metal–Organic Frameworks, *ACS Appl. Mater. Interfaces*, 2016, **8**, 32259–32265.

85 J. An, C. Shade, D. Czegan, S. Petoud and N. Rosi, Zinc-Adeninate Metal-Organic Framework for Aqueous Encapsulation and Sensitization of Near-infrared and Visible Emitting Lanthanide Cations, *J. Am. Chem. Soc.*, 2011, **133**, 1220–1223.

86 X. Xu and B. Yan, Fabrication and application of a ratiometric and colorimetric fluorescent probe for Hg^{2+} based on dual-emissive metal–organic framework hybrids with carbon dots and Eu^{3+}, *J. Mater. Chem. C*, 2016, **4**, 1543–1549.

87 X. Lin, G. Gao, L. Zheng, Y. Chi and G. Chen, Encapsulation of Strongly Fluorescent Carbon Quantum Dots in Metal–Organic Frameworks for Enhancing Chemical Sensing, Chen, *Anal. Chem.*, 2014, **86**, 1223–1228.

88 L. Xua, G. Fang, J. Liua, M. Pana, R. Wanga and S. Wang, One-pot synthesis of nanoscale carbon dots-embedded metal−organic frameworks at room temperature for enhancing chemical sensing, *J. Mater. Chem. A*, 2014, **4**, 15880–15887.

89 X. Liu, K. Xing, Y. Yang, C. Tsung and J. Li, Three Models To Encapsulate Multicomponent Dyes into Nanocrystal Pores: A New Strategy for Generating High-Quality White Light, *J. Am. Chem. Soc.*, 2019, **141**, 14807–14813.

90 W. Xie, W. He, S. Li, K. Shao, Z. Su and Y. Lan, An Anionic Interpenetrated Zeolite-Like Metal–Organic Framework Composite As a Tunable Dual-Emission Luminescent Switch for Detecting Volatile Organic Molecules, *Chem. – Eur. J.*, 2016, **22**, 17298–17304.

91 P. Jia, K. Yang, J. Hou, Y. Cao, X. Wang and L. Wang, Ingenious dual-emitting Ru@UiO-66-NH2 composite as ratiometric fluorescence sensor for detection of mercury in aqueous, *J. Hazard. Mater.*, 2021, **408**, 124469.

92 Z. Li, G. Wang, Y. Ye, B. Li, H. Li and B. Chen, Loading Photochromic Molecules into a Luminescent Metal–Organic Framework for Information Anticounterfeiting, *Angew. Chem., Int. Ed.*, 2019, **58**, 18025–18031.

93 S. Sharma and S. K. Ghosh, Metal–Organic Framework-Based Selective Sensing of Biothiols via Chemidosimetric Approach in Water, *ACS Omega*, 2018, **3**, 254–258.

94 K. Wang, T.-F. Zheng, J.-L. Chen, H.-R. Wen, S.-J. Liu and T.-L. Hu, A pH-Stable TbIII-Based Metal–Organic Framework as a Turn-On and Blue-Shift Fluorescence Sensor toward Benzaldehyde and Salicylaldehyde in Aqueous Solution, *Inorg. Chem.*, 2022, **61**, 16177–16184.

95 R. Huang, Y.-S. Wei, X.-Y. Dong, X.-H. Wu, C.-X. Du, S.-Q. Zang and T. C. W. Mak, Hypersensitive dual-function luminescence switching of a silver-chalcogenolate cluster-based metal–organic framework, *Nat. Chem.*, 2017, **9**, 689–697.

96 S. L. Jackson, A. Rananaware, C. Rix, S. V. Bhosale and K. Latham, Highly Fluorescent Metal−Organic Framework for the Sensing of Volatile Organic Compounds, *Cryst. Growth Des.*, 2016, **16**, 3067–3071.

97 Z.-H. Xu, Z.-Q. Huang, X.-H. Liu, Y. Zhao, Y. Lu and W.-Y. Sun, Luminescent silver(i) complexes with pyrazole-tetraphenylethene ligands: turn-on fluorescence due to the coordination-driven rigidification and solvent-oriented structural transformation, *Dalton Trans.*, 2021, **50**, 2183–2191.

98 N. B. Shustova, A. F. Cozzolino, S. Reineke, M. Baldo and M. Dincă, Selective Turn-On Ammonia Sensing Enabled by High-Temperature Fluorescence in Metal–Organic Frameworks with Open Metal Sites, *J. Am. Chem. Soc.*, 2013, **135**, 13326–13329.

99 X. Lian, Y.-J. Zhou, H.-F. Zhang, M. Li and X.-C. Huang, Luminescence turn-on detection by an entanglement-protected MOF operating via a divided receptor-transducer protocol, *J. Mater. Chem. C*, 2020, **8**, 3622–3625.

100 Q. Guan, Y. Sun, R. Huo, Y. Xin, F. Bai, Y. Xing and L. Sun, Cu-MOF Material Constructed with a Triazine Polycarboxylate Skeleton: Multifunctional Identify and Microdetecting of the Aromatic Diamine Family (*o*,*m*,*p*-Phenylenediamine) Based on the Luminescent Response, *Inorg. Chem.*, 2021, **60**, 2829–2838.

101 K. Zhu, R. Fan, J. Wu, B. Wang, H. Lu, X. Zheng, T. Sun, S. Gai, X. Zhou and Y. Yang, MOF-on-MOF Membrane with Cascading Functionality for Capturing Dichromate Ions and p-Arsanilic Acid Turn-On Sensing, *ACS Appl. Mater. Interfaces*, 2020, **12**, 58239–58251.

102 C. Sun, D. Wang, M. Zhang, Y. Ni, X. Shen, Y. Song, Z. Geng, W. Xu, F. Liu and C. Mao, Novel l-Lactic Acid Biosensors Based On Conducting Polypyrrole-block Copolymer Nanoparticles, *Analyst*, 2015, **140**, 797–802.

103 Y. Zhao, L. Guo, F. Zhang, J. Yao and X. Zhang, Turn-On Fluorescence Enantioselective Sensing of Hydroxyl Carboxylic Enantiomers by Metal−Organic Framework Nanosheets with a Homochiral Tetracarboxylate of Cyclohexane Diamide, *ACS Appl. Mater. Interfaces*, 2021, **13**, 20821–20829.

104 J. Wang, M. Jiang, L. Yan, R. Peng, M. Huangfu, X. Guo, Y. Li and P. Wu, Multifunctional Luminescent Eu (III)-Based Metal−Organic Framework for Sensing Methanol and Detection and Adsorption of Fe (III) Ions in Aqueous Solution, *Inorg. Chem.*, 2016, **55**, 12660–12668.

105 M. Gutiérrez, Y. Zhang and J. Tan, Confinement of Luminescent Guests in Metal−Organic Frameworks: Understanding Pathways from Synthesis and Multimodal Characterization to Potential Applications of LG@MOF Systems, *Chem. Rev.*, 2022, **122**, 10438–10483.

106 S. Bej, S. Mandal, A. Mondal, T. K. Pal and P. Banerjee, Solvothermal Synthesis of High-Performance d10-MOFs with Hydrogel Membranes @ ''Turn-On'' Monitoring of Formaldehyde in Solution and Vapor Phase, *ACS Appl. Mater. Interfaces*, 2021, **13**, 25153–25163.

107 A. Gogia and S. Mandal, Subtle Ligand Spacer Change in 2D Metal−Organic Framework Sheets for Dual Turn-On/Turn-Off Sensing of Acetylacetone and Turn-On Sensing of

Water in Organic Solvents, *ACS Appl. Mater. Interfaces*, 2022, **14**, 16357–16368.

108 J. Wang, M. Jiang, L. Yan, R. Peng, M. Huangfu, X. Guo, Y. Li and P. Wu, Multifunctional Luminescent Eu(III)-Based Metal−Organic Framework for Sensing Methanol and Detection and Adsorption of Fe(III) Ions in Aqueous Solution, *Inorg. Chem.*, 2016, **55**, 12660–12668.

109 J. Ludwig and J. Weinstein, Biomarkers in cancer staging, prognosis and treatment selection, *Nat. Rev. Cancer*, 2005, **11**, 845–856.

110 T. Luo, P. Das, D. White, C. Liu, A. Star and N. Rosi, Luminescence ''Turn-On'' Detection of Gossypol using Ln^{3+} -Based Metal-Organic Frameworks and Ln Salts, *J. Am. Chem. Soc.*, 2020, **142**, 2897–2904.

111 J. Wu, H. Wang, H. Yang, J. Chen and H. Yang, A Novel Arginine Bioprobe Based on up-Conversion Fluorescence Resonance Energy Transfer, *Anal. Chim. Acta*, 2019, **1079**, 200–206.

112 J. Dong, X.-Y. Dao, X.-Y. Zhang, X.-D. Zhang and W.-Y. Sun, Sensing Properties of NH2-MIL-101 Series for Specific Amino Acids via Turn-On Fluorescence, *Molecules*, 2021, **26**, 5336.

113 N. Stasyuk, G. Gayda, L. Fayura, Y. R. Boretskyy, M. Gonchar and A. A. Sibirny, Novel Arginine Deiminase-Based Method to Assay L-arginine in Beverages, *Food Chem.*, 2016, **201**, 320–326.

114 L. Wang, B. Tu, W. Xu, Y. Fu and Y. Zheng, Uranyl Organic Framework as a Highly Selective and Sensitive Turnon and Turn-off Luminescent Sensor for Dual Functional Detection Arginine and MnO4-, *Inorg. Chem.*, 2020, **59**, 5004–5017.

115 L. Song, J. Xiao, R. Cui, X. Wang, F. Tian and Z. Liu, Eu3+ doped bismuth metal-organic frameworks with ultrahigh fluorescence quantum yield and act as ratiometric turn-on sensor for histidine detection, *Sens. Actuators, B*, 2021, **336**, 129753.

116 Y. Zhao, M. Wan, J. Bai, H. Zeng, W. Lu and D. Li, pH-Modulated luminescence switching in a Eu-MOF: rapid detection of acidic amino acids, *J. Mater. Chem. A*, 2019, **7**, 11127–11133.

117 C. Fan, B. Zhu, X. Zhang, C. Bi, D. Zhang, Z. Zong and Y. Fan, Highly Stable Acid-Induced Emission-Enhancing Cd-MOFs: Synthesis, Characterization, and Detection of Glutamic Acid in Water and Fe Ions in Acid, *Inorg. Chem.*, 2021, **60**, 6339–6348.

118 M. Rekharsky, H. Yamamura, M. Kawai and Y. Inoue, Critical difference in chiral recognition of N-Cbz-d/l-aspartic and -glutamic acids by mono- and bis(trimethylammonio)-β-cyclodextrins, *J. Am. Chem. Soc.*, 2001, **123**, 5360–5361.

119 J. L. Johnson, Aspartic acid as a precursor for glutamic acid and glycine, *Brain Res.*, 1974, **67**, 358–362.

120 G. Ji, T. Zheng1, X. Gao and Z. Liu, A highly selective turn-on luminescent logic gates probe based on post synthetic MOF for aspartic acid detection, *Sens. Actuators, B*, 2019, **284**, 91–95.

121 P. Lakshmi, P. Nanjan, S. Kannan and S. Shanmugaraju, Recent advances in luminescent metal–organic frameworks (LMOFs) based fluorescent sensors for antibiotics, *Coord. Chem. Rev.*, 2021, **435**, 213793.

122 D. B. Kanzariya, R. Goswami, D. Muthukumar, R. S. Pillai and T. K. Pal, Highly Luminescent MOF and Its In Situ Fabricated Sustainable Corn Starch Gel Composite as a Fluoro-Switchable Reversible Sensor Triggered by Antibiotics and Oxo-Anions, *ACS Appl. Mater. Interfaces*, 2022, **14**, 48658–48674.

123 Y. Liu, H. Liu, X. Shi, H. Yan, W. Guo, S. Wang, X. Ma, L. Zhang, L. Kong, G. Chen, X. Ju, X. Li, Y. Yang, H. Zhu, Y. Li, F. Dai and H. Hao, Series of TM-OFs as a Platform for Efficient Catalysis and Multifunctional Luminescence Sensing, *Inorg. Chem.*, 2022, **61**, 15880–15894.

124 L. Liu, Q. Chen, J. Lv, Y. Li, K. Wang and J. Li, Stable Metal-Organic Frameworks for Fluorescent Detection of Tetracycline Antibiotics, *Inorg. Chem.*, 2022, **61**, 8015–8021.

125 S. Gai, J. Zhang, R. Fan, K. Xing, W. Chen, K. Zhu, X. Zheng, P. Wang, X. Fang and Y. Yang, Highly stable zinc-based metal–organic frameworks and corresponding flexible composites for removal and detection of antibiotics in water, *ACS Appl. Mater. Interfaces*, 2020, **12**, 8650–8662.

126 J. Dong, S. Hou and B. Zhao, Bimetallic lanthanide-organic framework membranes as a self-calibrating luminescent sensor for rapidly detecting antibiotics in water, *ACS Appl. Mater. Interfaces*, 2020, **12**, 38124–38131.

127 R. Goswami, S. Mandal, N. Seal, B. Pathak and S. Neogi, Antibiotic-Triggered Reversible Luminescence Switching in Amine Grafted Mixed-Linker MOF: Exceptional Turn-On and Ultra-Fast Nanomolar Detection of Sulfadiazine and AMP with Molecular Keypad-Lock Function, *J. Mater. Chem. A.*, 2019, **7**, 19471–19484.

128 F. Amiripour, S. Ghasemi and S. Azizi, Design of turn-on luminescent sensor based on nanostructured molecularly imprinted polymer-coated zirconium metal–organic framework for selective detection of chloramphenicol residues in milk and honey, *Food Chem.*, 2021, **347**, 129034.

129 Y. Guo, X. Feng, T. Han, S. Wang, Z. Lin, Y. Dong and B. Wang, Tuning the Luminescence of Metal–Organic Frameworks for Detection of Energetic Heterocyclic Compounds, *J. Am. Chem. Soc.*, 2014, **136**, 15485–15488.

130 Z. Hu, K. Tan, W. P. Lustig, H. Wang, Y. Zhao, C. Zheng, D. Banerjee, T. J. Emge, Y. J. Chabal and J. Li, Effective sensing of RDX via instant and selective detection of ketone vapors, *Chem. Sci.*, 2014, **5**, 4873–4877.

131 H.-R. Fu, L.-B. Yan, N.-T. Wu, L.-F. Ma and S.-Q. Zang, Dual-emission MOF ⊃ dye sensor for ratiometric fluorescence recognition of RDX and detection of a broad class of nitro-compounds, *J. Mater. Chem. A*, 2018, **6**, 9183–9191.

132 D. Kanzariya, T. Khan, S. Das, P. Lama, R. Bandyopadhyay and T. K. Pal, Highly regenerative, fast colorimetric response for organo-toxin and oxo-anions in an aqueous medium using a discrete luminescent Cd(II) complex in a heterogeneous manner with theoretical revelation, *Dalton Trans.*, 2022, **51**, 7436–7454.

133 D. Majumdar, S. Dey, A. Kumari, T. K. Pal, K. Bankura and D. Mishra, Dicyanamide-intertwined assembly of two new Zn complexes based on N2O4-type pro-ligand: Synthesis, crystal networks, spectroscopic insights, and selective nitroaromatic turn-off fluorescence sensing, *Spectrochim. Acta, Part A*, 2021, **254**, 119612.

134 B. Zhu, L. Zhu, T. Hou, K. Ren, K. Kang, C. Xiao and J. Luo, Cobalt Metal−Organic Frameworks with Aggregation-Induced Emission Characteristics for Fluorometric/Colorimetric Dual Channel Detection of Nitrogen-Rich Heterocyclic Compounds, *Anal. Chem.*, 2022, **94**, 3744–3748.

135 C. Wang, L. Tian, W. Zhu, S. Wang, P. Wang, Y. Liang, W. Zhang, H. Zhao and G. Li, Dye@bio-MOF-1 Composite as a Dual-Emitting Platform for Enhanced Detection of a Wide Range of Explosive Molecules, *ACS Appl. Mater. Interfaces*, 2017, **9**, 20076–20085.

136 S. Rojas, A. Diéguez and P. Horcajada, Metal−Organic Frameworks in Agriculture, *ACS Appl. Mater. Interfaces*, 2022, **14**, 16983–17007.

137 M. Singh, A. Palakkal, R. Pillai and S. Neogi, N-Functionality actuated improved CO2 adsorption and turn-on detection of organo-toxins with guest-induced fluorescence modulation in isostructural diamondoid MOFs, *J. Mater. Chem. C*, 2021, **9**, 7142–7153.

138 M. Jindal, V. Maka, G. Anjum and J. Moorthy, Anthracene-Bisimidazole Tetraacid Linker-Based Metal−Organic Nanosheets for Turn-On Fluorescence Sensing of Nerve Agent, *ACS Appl. Nano Mater.*, 2021, **4**, 449–458.

139 S. Nandi, S. K. Mostakim and S. Biswas, Rapid Switch-On Fluorescent Detection of Nanomolar Level Hydrazine in Water by a Diacetoxy Functionalized MOF: Application in Paper Strips and Environmental Samples, *Dalton Trans.*, 2020, **49**, 12565–12573.

140 X. Zhang, J. Zhang, Q. Hu, Y. Cui, Y. Yang and G. Qian, Postsynthetic modification of metal–organic framework for hydrogen sulfide detection, *Appl. Surf. Sci.*, 2015, **355**, 814–819.

141 S. Nagarkar, A. Desai and S. Ghosh, A Nitro-Functionalized Metal–Organic Framework as a Reaction-Based Fluorescence Turn-On Probe for Rapid and Selective H2S Detection, *Chem. – Eur. J.*, 2015, **21**, 9994–9997.

142 S. Nandi, H. Reinsch, S. Banesh, N. Stock, V. Trivedi and S. Biswas, Rapid and highly sensitive detection of extracellular and intracellular H2S by an azide-functionalized Al (III)-based metalorganic framework, *Dalton Trans.*, 2017, **46**, 12856–12864.

143 X. Zheng, R. Fan, Y. Song, A. Wang, K. Xing, X. Du, P. Wang and Y. Yang, Highly sensitive turn-on ratiometric luminescent probe based on post-synthetic modification Tb^{3+} @Cu-MOF for H2S detection, *J. Mater. Chem. C*, 2017, **5**, 9943–9995.

144 Y. Cao, X. Guo and H. Wang, High Sensitive Luminescence Metal-Organic Framework Sensor for Hydrogen Sulfide in Aqueous Solution: A Trial of Novel Turn-on Mechanism, *Sens. Actuators, B*, 2017, **243**, 8–13.

145 R. Dalapati, S. Balaji, V. Trivedi, L. Khamari and S. Biswas, A dinitro-functionalized Zr(IV)-based metal-organic framework as colorimetric and fluorogenic probe for highly selective detection of hydrogen sulphide, *Sens. Actuators, B*, 2017, **245**, 1039–1049.

146 L. Guo, M. Wang and D. Cao, A Novel Zr-MOF as Fluorescence Turn-On Probe for Real-Time Detecting H2S Gas and Fingerprint Identification, *Small*, 2018, **14**, 1703822.

147 X. Zhang, Q. Zhang, D. Yue, J. Zhang, J. Wang, B. Li, Y. Yang, Y. Cui and G. Qian, Flexible Metal–Organic Framework-Based Mixed-Matrix Membranes: A New Platform for H2S Sensors, *Small*, 2018, 1801563.

148 M. Wang, L. Guo and D. Cao, Amino-functionalized luminescent MOF test paper for rapid and selective sensing SO2 gas and its derivatives by luminescence turn-on effect, *Anal. Chem.*, 2018, **90**, 3608–3614.

149 Z. Zhu, X. He and W. Wang, Unraveling the origin of the ''Turn-On'' effect of Al-MIL-53-NO2 during H2S detection, *CrystEngComm*, 2020, **22**, 195–204.

150 X. Liu, X. Zhang, R. Li, L. Du, X. Feng and Y. Ding, A highly sensitive and selective ''turn off-on'' fluorescent sensor based on Sm-MOF for the detection of tertiary butylhydroquinone, *Dyes Pigm.*, 2020, **178**, 108347.

151 X. Yang, C. Ding, R. Guan, W. Zhang, Y. Feng and M. Xie, Selective dual detection of H2S and Cu^{2+} by a post-modified MOF sensor following a tandem process, *J. Haz. Mat.*, 2021, **403**, 123698.

152 X. Gao, G. Sun, X. Wang, X. Lin, S. Wang and Y. Liu, RhB/UiO-66-N3 MOF-based ratiometric fluorescent detection and intracellular imaging of hydrogen sulphide, *Sens. Actuators, B*, 2021, **331**, 129448.

153 X. Han, C. Gu, Y. Ding, J. Yu, K. Li, D. Zhao and B. Chen, Stable Eu^{3+}/Cu^{2+} -Functionalized Supramolecular Zinc (II) Complexes as Fluorescent Probes for Turn-On and Ratiometric Detection of Hydrogen Sulfide, *ACS Appl. Mater. Interfaces*, 2021, **13**, 20371–20379.

154 L. Meyer, F. Schönfeld, A. Zurawski, M. Mai, C. Feldmann and K. Buschbaum, A blue luminescent MOF as a rapid turn-off/turn-on detector for H2O, O2 and CH2Cl2, MeCN:3∞[Ce (Im)3ImH]·ImH, *Dalton Trans.*, 2015, **44**, 4070–4079.

155 P. Du, S. Liao, W. Gu and X. Liu, A multi-functional chemical sensor based on a three-dimensional lanthanide metal-organic framework, *J. Solid State Chem.*, 2016, **244**, 31–34.

156 Y. Yang, L. Chen, F. Jiang, X. Wan, M. Yu, Z. Cao, T. Jinga and M. Hong, Fabricating a super stable luminescent chemo sensor with multi-stimuli-response to metal ions and small organic molecules by turn on and turn-off effects, *J. Mater. Chem. C*, 2017, **5**, 4511–4519.

157 A. Wang, R. Fan, P. Wang, R. Fang, S. Hao, X. Zhou, X. Zheng and Y. Yang, Research on the Mechanism of Aggregation-Induced Emission through Supramolecular Metal−Organic Frameworks with Mechanoluminescent Properties and Application in Press-Jet Printing, *Inorg. Chem.*, 2017, **56**, 12881–12892.

158 L. Chen, J.-W. Ye, H.-P. Wang, M. Pan, S.-Y. Yin, Z.-W. Wei, L.-Y. Zhang, K. Wu, Y.-N. Fan and C.-Y. Su, Ultrafast water

sensing and thermal imaging by a metal-organic framework with switchable luminescence, *Nat. Commun.*, 2017, **8**, 15985.

159 Y. Cai, L. Feng, Y. Hua, H. Liu, M. Yin, X. Lv, S. Li and H. Wang, Q-Graphene-loaded metal organic framework nanocomposites with water-triggered fluorescence turn-on: fluorimetric test strips for directly sensing trace water in organic solvents, *Chem. Commun.*, 2018, **54**, 13595–13598.

160 X. Wang, J. Tian, X. Guo, F. Zhang, L. Liang and X. Zhang, Cd-Based Metal-Organic Framework for Selective Turn-On Fluorescent DMSO Residual Sensing, *Chem. Eu. J.*, 2021, **27**, 3753–3760.

161 P. Majee, P. Daga, D. Singha, D. Saha, P. Mahata and S. K. Mondal, A Lanthanide Doped Metal-Organic Framework Demonstrated as Naked Eye Detector of a Trace of Water in Organic Solvents Including Alcohols by Monitoring the Turn-on of Luminescence, *J. Photochem. Photobiol., A*, 2020, **402**, 112830.

162 D. Gu, W. Yang, G. Ning, F. Wang, S. Wu, X. Shi, Y. Wang and Q. Pan, In Situ Ligand Formation-Driven Synthesis of a Uranyl Organic Framework as a Turn-on Fluorescent pH Sensor, *Inorg. Chem.*, 2020, **59**, 1778–1784.

163 M. Li, A. Shen, M. Du, X. Hao, H. Wang, X. Du, S. Ma, J. Yuan and Y. Yang, Tb^{3+} -Doped Ag-MOFs for fluorescent detection of formaldehyde in a novel smartphone platform and its removal applications in milk products and wastewater, *RSC Adv.*, 2021, **11**, 34291–34299.

164 X. Jiang, R. Fan, X. Zhou, K. Zhu, T. Sun, X. Zheng, K. Xing, W. Chen and Y. Yang, Mixed functionalization strategy on indium organic framework for multiple ion detection and H2O2 turn-on sensing, *Dalton Trans.*, 2021, **50**, 7554–7562.

165 W. Zuo, L. Liang, F. Ye and S. Zhao, An integrated platform for label-free fluorescence detection and inactivation of bacteria based on boric acid functionalized Zr-MOF, *Sens. Actuators, B*, 2021, **345**, 130345.

166 U. Mondal, S. Bej, A. Hazra, S. Mandal, T. K. Pal and P. Banerjee, Amine-substituent induced highly selective and rapid ''turn-on'' detection of carcinogenic 1,4-dioxane from purely aqueous and vapour phase with novel post-synthetically modified d10-MOFs, *Dalton Trans.*, 2022, **51**, 2083–2093.

167 J. Zhang, F. Liu, J. Gan, Y. Cui, B. Li, Y. Yang and G. Qian, Metal-organic framework film for fluorescence turnon H_2S gas sensing and anti-counterfeiting patterns, *Sci. China Mater.*, 2019, **62**, 1445–1453.

168 Z. Sun, J. Jiang and Y. Li, Sensitive and selective sensor for biothiols based on turn-on fluorescence of the Fe-MIL-88 metal-organic frameworks–hydrogen peroxide system, *Analyst*, 2015, **140**, 8201–8208.

169 C. Zhao, Z. Jiang, R. Mu and Y. Li, A novel sensor for dopamine based on the turn-on fluorescence of Fe-MIL-88 metal-organic frameworks–hydrogen peroxide–o-phenylenediamine system, *Talanta*, 2016, **159**, 365–370.

170 W. Li, X. Qi, C. Zhao, X. Xu, A. Tang and D. Kong, A Rapid and Facile Detection for Specific Small-Sized Amino Acids Based on Targets-Triggered Destruction of Metal Organic Frameworks, *ACS Appl. Mater. Interfaces*, 2017, **9**, 236–243.

171 Y. Cheng, J. Wu, C. Guo, X. Li, B. Ding and Y. Li, A facile water-stable MOF-based ''off-on'' fluorescent switch for label-free detection of dopamine in biological fluid, *J. Mater. Chem. B*, 2017, **5**, 2524–2535.

172 P. Huang, C. Hong, J. Zhu, T. Chen, C. Chan, Y. Ko, T. Lin, Z. Pan, N. Sun, Y. Wang, J. Luo, T. Lin, C. Kang, J. Shyue and M. Ho, Ag@Au nano prisms-metal organic frameworks-based paper for extending glucose sensing range in human serum and urine, *Dalton Trans.*, 2017, **46**, 6985–6993.

173 X. Xin, M. Zhang, J. Zhao, C. Han, X. Liu, Z. Xiao, L. Zhang, B. Xu, W. Guo, R. Wang and D. Sun, Fluorescent Turn-on Detection of Uric Acid by a Water-Stable Metal-Organic Nanotube with High Selectivity and Sensitivity, *J. Mater. Chem. C*, 2017, **5**, 601–606.

174 B. Liu, H. Shen, Y. Hao, X. Zhu, S. Li, Y. Huang, P. Qu and M. Xu, Lanthanide Functionalized Metal-Organic Coordination Polymer: Toward Novel Turn-on Fluorescent Sensing of Amyloid β-Peptide, *Anal. Chem.*, 2018, **90**, 12449–12455.

175 X. Zhao, Y. Zhang, J. Han, H. Jing, Z. Gao, H. Huang, Y. Wang and C. Zhong, Design of ''turn-on'' fluorescence sensor for L-Cysteine based on the instability of metal-organic framework, *Microporous Mesoporous Mater.*, 2018, **268**, 88–92.

176 B. Gui, Y. Meng, Y. Xie, J. Tian, G. Yu, W. Zeng, G. Zhang, S. Gong, C. Yang, D. Zhang and C. Wang, Tuning the Photoinduced Electron Transfer in a Zr-MOF: Toward Solid-State Fluorescent Molecular Switch and Turn-On Sensor, *Adv. Mater.*, 2018, **30**, 1802329.

177 J. Zhang, Y. Huang, D. Yue, Y. Cui, Y. Yang and G. Qian, A luminescent turn-up metal-organic framework sensor for tryptophan based on singlet-singlet Förster energy transfer, *J. Mater. Chem. B*, 2018, **6**, 5174–5180.

178 D. Wu, Z. Zhang, X. Chen, L. Meng, C. Li, G. Li, X. Chen, Z. Shi and S. Feng, A non-luminescent Eu-MOF-based ''turn-on'' sensor towards an anthrax biomarker through single-crystal to single-crystal phase transition, *Chem. Commun.*, 2019, **55**, 14918–14921.

179 J. Xiao, J. Liu, M. Liu, G. Ji and Z. Liu, Fabrication of a Luminescence-Silent System Based on a Post-Synthetic Modification Cd-MOFs: A Highly Selective and Sensitive Turn-on Luminescent Probe for Ascorbic Acid Detection, *Inorg. Chem.*, 2019, **58**, 6167–6174.

180 T. Jin, Y. Li, W. Jing, Y. Li, L. Fan and X. Li, Cobalt-based metal organic frameworks: a highly active oxidase-mimicking nanozyme for fluorescence ''turn-on'' assays of biothiol, *Chem. Commun.*, 2020, **56**, 659–662.

181 B. Wang and B. Yan, A turn-on fluorescence probe Eu^{3+} functionalized Ga-MOF integrated with logic gate operation for detecting ppm-level ciprofloxacin (CIP) in urine, *Talanta*, 2020, **208**, 120438.

182 X. Li, J. Zhao, Y. Zhu, B. Wang, X. Wei, Y. Shao, Y. Ma and T. Jiang, Colorimetric and ratiometric fluorescent response

for anthrax bioindicator: A combination of rare earth MOF and rhodamine derived Dye, *Spectrochim. Acta, Part A*, 2020, **229**, 117999.

183 T. Liu, X. Qua and B. Yan, A highly sensitive and selective ''turn-on'' fluorescent probe for detection of fleroxacin in human serum and urine based on a lanthanide functionalized metal–organic framework, *Dalton Trans.*, 2019, **48**, 17945–17952.

184 J. Zhu, T. Xia, Y. Cui, Y. Yang and G. Qian, A Turn-on MOF-Based Luminescent Sensor for Highly Selective Detection of Glutathione, *J. Solid State Chem.*, 2019, **270**, 317–323.

185 J. Zhu, Y. Tang, Y. Yang, B. Li, Y. Cui and G. Qian, Post-modified metal-organic framework as a turn-on fluorescent probe for potential diagnosis of neurological diseases, *Microporous Mesoporous Mater.*, 2019, **288**, 109610.

186 B. Tan, D. Wang, Z. Cai, X. Quan and H. Zhao, Extending suitability of physisorption strategy in fluorescent platforms design: surface passivation and covalent linkage on MOF nanosheets with enhanced OTC detection sensitivity, *Sens. Actuators, B*, 2020, **303**, 127230.

187 Z. Wu, B. Tan, E. Velasco, H. Wang, N. Shen, Y. Gao, X. Zhang, K. Zhu, G. Zhang, Y. Liu, X. Hei, X. Huang and J. Li, Fluorescent In based MOFs showing ''turn on'' luminescence to thiols and acting as a ratiometric fluorescence thermometer, *J. Mater. Chem. C*, 2019, **7**, 3049–3055.

188 J. Othonga, J. Boonmaka, F. Kielarb, S. Hadsadeec, S. Jungsuttiwong and S. Youngmea, Self-calibrating sensor with logic gate operation for anthrax biomarker based on nanoscaled bimetallic lanthanoid MOF, *Sens. Actuators, B*, 2020, **316**, 128156.

189 C. Li, W. Long, Z. Lei, L. Guo, M. Xie, J. Lü and X. Zhu, Anionic metal–organic framework as a unique turn-on fluorescent chemical sensor for ultra-sensitive detection of antibiotics, *Chem. Commun.*, 2020, **56**, 12403–12406.

190 S. Qu, Q. Cao, J. Ma and Q. Jia, A Turn-on Fluorescence Sensor for Creatinine Based on the Quinoline-Modified Metal Organic Frameworks, *Talanta*, 2020, **219**, 121280.

191 L. Yu, H. Chen, J. Yue, X. Chen, M. Sun, J. Hou, K. Alamry, H. Marwanic, X. Wang and S. Wang, Europium metal-organic framework for selective and sensitive detection of doxycycline based on fluorescence enhancement, *Talanta*, 2020, **207**, 120297.

192 X. Zhao, H. Yang, W. Zhao, J. Wang and Q. Yang, A weakly luminescent Tb-MOF-based ''turn-on'' sensor for the highly selective and sensitive sensing of an anthrax biomarker, *Dalton Trans.*, 2021, **50**, 1300–1306.

193 S. Li, Y. Li and B. Yan, A turn-on fluorescence sensing strategy for rapid detection of flumequine in water environments using covalent-coordination functionalized MOFs, *CrystEngComm*, 2021, **23**, 5345–5352.

194 J. Zhao, Y. Wang, W. Dong, Y. Wu, D. Li and Q. Zhang, A Robust Luminescent Tb (III)-MOF with Lewis Basic Pyridyl Sites for the Highly Sensitive Detection of Metal Ions and Small Molecules, *Inorg. Chem.*, 2016, **55**, 3265–3271.

195 B. Wang, Q. Yang, C. Guo, Y. Sun, L.-H. Xie and J.-R. Li, Stable Zr(IV)-Based Metal–Organic Frameworks with Predesigned Functionalized Ligands for Highly Selective Detection of Fe(III) Ions in Water, *ACS Appl. Mater. Interfaces*, 2017, **9**, 10286–10295.

196 S. Chand, G. Verma, A. Pal, S. Pal, S. Ma and M. Das, Porous Anionic Co(II) Metal-Organic Framework, with a High Density of Amino Groups, as a Superior Luminescent Sensor for Turn-on Al(III) Detection, *Chem. – Eur. J.*, 2021, **27**, 11804–11810.

197 T. Zhou, S. Liu, X. Guo, Q. Wang, L. Fu, S. Mi, P. Gao, Q. Su and H. Guo, Dual-Function Metal−Organic Framework as Efficient Turn-Off Sensor for Water and Unusual Turn-On Sensor for Ag^{+}, *Cryst. Growth Des.*, 2021, **21**, 5108–5115.

198 K. Lim, S. Jeong, D. Kang, J. Song, H. J. Lee, W. Phang, D. Moon and C. Hong, Luminescent Metal-Organic Framework Sensor: Exceptional Cd^{2+} Turn-on Detection and First In Situ Visualization of Cd^{2+} Ion Diffusion to a Crystal, *Chem. – Eur. J.*, 2017, **23**, 4803–4809.

199 P. Zhang, B. Song, Z. Li, J. Zhang, A. Ni, J. Chen, J. Ni, S. Liu and C. Duan, A ''turn-on'' Cr^{3+} ion probe based on non-luminescent metal–organic framework-new strategy to prepare a recovery probe, *J. Mater. Chem. A*, 2021, **9**, 13552–13561.

200 Y. Yamauchi, M. Yoshizawa, M. Akita and M. Fujita, Engineering Double to Quintuple Stacks of a Polarized Aromatic in Confined Cavities, *J. Am. Chem. Soc.*, 2010, **132**, 960–966.

201 B. Song, G. L. Wang, M. Q. Tan and J. L. Yuan, A Europium(III) Complex as an Efficient Singlet Oxygen Luminescence Probe, *J. Am. Chem. Soc.*, 2006, **128**, 13442–13450.

202 B. Song, G. Wang and J. Yuan, A new europium chelate-based phosphorescence probe specific for singlet oxygen, *Chem. Commun.*, 2005, 3553–3555.

203 T. Clarkson, L. Magos and G. J. Myers, The Toxicology of Mercury Current Exposures and Clinical Manifestations, *N. Engl. J. Med.*, 2003, **349**, 1731–1737.

204 H. Wang, X. Wang, M. Liang, G. Chen, R. Kong, L. Xia and F. Qu, A Boric Acid-Functionalized Lanthanide Metal−Organic Framework as a Fluorescence ''Turn-on'' Probe for Selective Monitoring of Hg^{2+} and CH3Hg, *Anal. Chem.*, 2020, **92**, 3366–3372.

205 D. Mukherjee, A. Pal, S. C. Pal, A. Saha and M. C. Das, A Highly Selective MOF-Based Probe for Turn-On Luminescent Detection of Al^{3+}, Cr^{3+}, and Fe^{3+} in Solution and Test Paper Strips through Absorbance Caused Enhancement Mechanism, *Inorg. Chem.*, 2022, **61**, 16952–16962.

206 D.-G. Cai, C.-Q. Qiu, Z.-H. Zhu, T.-F. Zheng, W.-J. Wei, J.-L. Chen, S.-J. Liu and H.-R. Wen, Fabrication and DFT Calculation of Amine-Functionalized Metal–Organic Framework as a Turn-On Fluorescence Sensor for Fe^{3+} and Al^{3+} Ions, *Inorg. Chem.*, 2022, **61**, 14770–14777.

207 P. Nayak, Aluminum: impacts and disease, *Environ. Res.*, 2002, **89**, 101–115.

208 X. Zhao, D. Tian, Q. Gao, H. Sun, J. Xu and X. Bu, A chiral lanthanide metal–organic framework for selective sensing of Fe(III) ions, *Dalton Trans.*, 2016, **45**, 1040–1046.

209 J. Zhang, S. Ren, H. Xia, W. Jia and C. Zhang, AIE-ligand-based luminescent Cd(II)–organic framework as the first "turn-on" Fe^{3+} sensor in aqueous medium, *J. Mater. Chem. C*, 2020, **8**, 1427–1432.

210 T. Fujii, Y. Shindo, K. Hotta, D. Citterio, S. Nishiyama, K. Suzuki and K. Oka, Design and Synthesis of a FlAsH-Type Mg^{2+} Fluorescent Probe for Specific Protein Labeling, *J. Am. Chem. Soc.*, 2014, **136**, 2374–2381.

211 F. Mann, S. Prisic, E. Davenport, M. Determan, R. Coates and R. Peters, A single residue switch for Mg^{2+} dependent inhibition characterizes plant class II diterpene cyclases from primary and secondary metabolism, *J. Biol. Chem.*, 2010, **285**, 20558–20563.

212 R. Swaminathan, Magnesium Metabolism and its Disorders, *Clin. Biochem Rev.*, 2003, **24**, 47–66.

213 G. Farruggia, S. Iotti, L. Prodi, M. Montalti, N. Zaccheroni, P. B. Savage, V. Trapani, P. Sale and F. I. Wolf, 8-Hydroxyquinoline Derivatives as Fluorescent Sensors for Magnesium in Living Cells, *J. Am. Chem. Soc.*, 2006, **128**, 344–350.

214 X. Gao, Y. Gao, R. Qi and L. Han, One-pot synthesis of a recyclable ratiometric fluorescent probe based on MOFs for turn-on sensing of Mg^{2+} ions and bioimaging in live cells, *New J. Chem.*, 2019, **43**, 18377–18383.

215 D. Singha and P. Mahata, Highly Selective and Sensitive Luminescence Turn-On-Based Sensing of Al^{3+} Ions in Aqueous Medium Using a MOF with Free Functional Sites, *Inorg. Chem.*, 2015, **54**, 6373–6379.

216 Y. Chen and H. Jiang, Porphyrinic Metal-Organic Framework Catalyzed Heck- Reaction: Fluorescence "Turn-on" Sensing of Cu(II) Ion, *Chem. Mater.*, 2016, **28**, 6698–6704.

217 R. Wang, X. Liu, A. Huang, W. Wang, Z. Xiao, L. Zhang, F. Dai and D. Sun, Unprecedented Solvent-Dependent Sensitivities in Highly Efficient Detection of Metal Ions and Nitroaromatic Compounds by a Fluorescent Barium Metal−Organic Framework, *Inorg. Chem.*, 2016, **55**, 1782–1787.

218 S. Eom, S. Park, J. Song, W. Lee, H. Lee, D. Kang, J. Joung, S. Park, D. Moon and C. Hong, Synthesis, Structure, and Photoluminescence Properties of a Metal-Organic Framework with Hexagonal Channels: Selective Turn-On Sensing for Mg^{2+} Ion, *Eur. J. Inorg. Chem.*, 2019, 330–335.

219 M.-H. Yu, T.-L. Hu and X.-H. Bu, A Metal-Organic Framework as a "Turn on" Fluorescent Sensor for Aluminum Ions, *Inorg. Chem. Front.*, 2017, **4**, 256–260.

220 J. Wang, T. Xia, X. Zhang, Q. Zhang, Y. Cui, Y. Yang and G. Qian, A turn-on fluorescent probe for Cd^{2+} detection in aqueous environments based on an imine functionalized nanoscale metal–organic framework, *RSC Adv.*, 2017, **7**, 54892–54897.

221 G. Xu, Y. Wu, W. Dong, J. Zhao, X. Wu, D. Li and Q. Zhang, A Multifunctional Tb-MOF for Highly Discriminative Sensing of Eu^{3+}/Dy^{3+} and as a Catalyst Support of Ag Nanoparticles, *Small*, 2017, **13**, 1602996.

222 K. Shen, Z. Ju, L. Qin, T. Wang and H. Zheng, Two stable 3D porous metal-organic frameworks with high selectivity for detection of PA and metal ions, *Dyes Pigm.*, 2017, **136**, 515–521.

223 M. Wang, L. Guo and D. Cao, Metal-organic framework as luminescence turn-on sensor for selective detection of metal ions: Absorbance caused enhancement mechanism, *Sens. Actuators, B*, 2018, **256**, 839–845.

224 Y. Li, X. Hu, X. Zhang, H. Cao and Y. Huang, Unconventional application of gold nanoclusters/Zn-MOF composite for fluorescence turn-on sensitive detection of zinc ion, *Anal. Chim. Acta*, 2018, **1024**, 145–152.

225 Y. Li, X. Zhu, S. Li, Y. Jiang, M. Hu and Q. Zhai, Highly Selective and Sensitive Turn-Off-On Fluorescent Probes for Sensing Al^{3+} Ions Designed by Regulating the ESIPT Process in Metal-Organic Frameworks, *ACS Appl. Mater. Interfaces*, 2019, **11**, 11338–11348.

226 S. Yao, X. Tian, L. Li, S. Liu, T. Zheng, Y. Chen, D. Zhang, J. Chen, H. Wen and T. Hu, A CdII-Based Metal-Organic Framework with pcu Topology as Turn-On Fluorescent Sensor for Al^{3+}, *Chem. An Asian J.*, 2019, 3648–3654.

227 Y. Liu, M. Huangfu, P. Wu, M. Jiang, X. Zhao, L. Liang, L. Xie, J. Baia and J. Wang, Post-imparting Brønsted Acidity into an Amino-functionalized MOF as Bifunctional Luminescent Turn-ON Sensors for the Detection of Aluminum Ions and Lysine, *Dalton Trans.*, 2019, **48**, 13834–13840.

228 X. Tian, S. Yao, C. Qiu, T. Zheng, Y. Chen, H. Huang, J. Chen, S. Liu and H. Wen, Turn-On Luminescent Sensor toward Fe^{3+}, Cr^{3+}, and Al^{3+} Based on a Co(II) Metal−Organic Framework with Open Functional Sites, *Inorg. Chem.*, 2020, **59**, 2803–2810.

229 H. Shayegan, Y. Farahani and V. Safarifard, A pillar-layer metal-organic framework as a turn-on luminescent sensor for highly selective and sensitive detection of Zn(II) ion, *J. Solid State Chem.*, 2019, **279**, 120968.

230 T. Wiwasuku, J. Othong, J. Boonmak, V. Ervithayasuporn and S. Youngme, Sonochemical synthesis of microscale Zn(II)-MOF with dual Lewis basic sites for fluorescent turn-on detection of Al^{3+} and methanol with low detection limits, *Dalton Trans.*, 2020, **49**, 10240–10249.

231 X. Zheng, Y. Zhao, P. Jia, Q. Wang, Y. Liu, T. Bu, M. Zhang, F. Bai and L. Wang, Dual-Emission Zr-MOF-Based Composite Material as a Fluorescence Turn-On Sensor for the Ultrasensitive Detection of Al^{3+}, *Inorg. Chem.*, 2020, **59**, 18205–18213.

232 H. Li, D. Li, B. Qin, W. Li, H. Zheng, X. Zhang and J. Zhang, Turn-on fluorescence in a stable Cd(II) metal-organic framework for highly sensitive detection of Cr^{3+} in water, *Dyes Pigm.*, 2020, **178**, 108359.

233 J. Tang, D. Feng, J. Yang, X. Ma and X. Wang, A Turn-on Luminescent Probe for Fe^{3+} and Ascorbic Acid with Logic Gate Operation Based on a Zinc(II)-Based Metal-Organic Framework, *New J. Chem.*, 2020, **44**, 8728–8735.

234 C. Fu, X. Sun, G. Zhang, P. Shi and P. Cui, Porphyrin-Based Metal−Organic Framework Probe: Highly Selective and Sensitive Fluorescent Turn-On Sensor for M^{3+} (Al^{3+}, Cr^{3+}, and Fe^{3+}) Ions, *Inorg. Chem.*, 2021, **60**, 1116–1123.

235 G. Wang, X. Huang, C. Wu, Y. Shen, S. Cai, J. Fan, W. Zhang and S. Zheng, A hydrolytically stable hydrogen-

bonded inorganic-organic network as a luminescence turn-on sensor for the detection of Bi^{3+} and Fe^{3+} cations in water, *Polyhedron*, 2021, **205**, 115284.

236 S. Bhowal and A. Ghosh, Highly selective fluorescent turn-on–off sensing of OH−, Al^{3+} and Fe^{3+} ions by tuning ESIPT in metal organic frameworks and mitochondria targeted bio-imaging, *RSC Adv.*, 2021, **11**, 27787–27800.

237 L. Wu, S. Yao, H. Xu, T. Zheng, S. Liu, J. Chen, N. Li and H. Wen, Highly selective and turn-on fluorescence probe with red shift emission for naked-eye detecting Al^{3+} and Ga^{3+} based on metal-organic framework, *Chin. Chem. Lett.*, 2022, **33**, 541–546.

238 B. Chai, S. Yao, X. Xie, H. Xu, T. Zheng, J. Li, J. Chen, S. Liu and H. Wen, Luminescent Metal−Organic Framework-Based Fluorescence Turn- On and Red-Shift Sensor toward Al^{3+} and Ga^{3+}: Experimental Study and DFT Calculation, *Cryst. Growth Des.*, 2022, **22**, 277–284.

239 K. Naskar, A. Bhanja, S. Paul, K. Pal and C. Sinha, Trace Quantity Detection of H2PO4– by Fluorescent Metal–Organic Framework (F-MOF) and Bioimaging Study, *Cryst. Growth Des.*, 2020, **20**, 6453–6460.

240 K.-L. Wong, G.-L. Law, Y.-Y. Yang and W.-T. Wong, A Highly Porous Luminescent Terbium–Organic Framework for Reversible Anion Sensing, *Adv. Mater.*, 2006, **18**, 1051–1054.

241 S.-M. Zhao, Z.-F. Qiu, Z.-H. Xu, Z.-Q. Huang, Y. Zhao and W.-Y. Sun, Fluorescent Zn(II) frameworks with multicarboxylate and pyridyl N-donor ligands for sensing specific anions and organic molecules, *Dalton Trans.*, 2022, **51**, 3572–3580.

242 F. Moriya and Y. Hashimoto, Potential for error when assessing blood cyanide concentrations in fire victims, *J. Forensic Sci.*, 2001, **46**, 1421–1425.

243 A. Karmakar, N. Kumar, P. Samanta, A. V. Desai and S. K. Ghosh, A Post-Synthetically Modified MOF for Selective and Sensitive Aqueous-Phase Detection of Highly Toxic Cyanide Ions, *Chem. – Eur. J.*, 2016, **22**, 864–868.

244 J. Li, S. Yuan, J. Qin, J. Pang, P. Zhang, Y. Zhang, Y. Huang, H. Drake, W. Liu and H. C. Zhou, Stepwise Assembly of Turn-on Fluorescence Sensors in Multicomponent Metal–Organic Frameworks for in Vitro Cyanide Detection, *Angew. Chem., Int. Ed.*, 2020, 59, 9319–9323.

245 S. Kocakuşak, H. J. Köroğlu, K. Akçay, Ö. T. Savaşçì and R. Tolun, Production of Sodium Perborate Monohydrate by Fluidized-Bed Dehydration, *Ind. Eng. Chem. Res.*, 1997, **36**, 2862–2865.

246 C. Yazbeck, W. Kloppmann, R. Cottier, J. Sahuquillo, G. Debotte and G. Huel, Health Impact Evaluation of Boron in Drinking Water: A Geographical Risk Assessment in Northern France, *Environ. Geochem. Health*, 2005, **27**, 419–427.

247 S. Nandi, H. Reinsch and S. Biswas, An acetoxy functionalized Al(III) based metal–organic framework showing selective ''turn on'' detection of perborate in environmental samples, *Dalton Trans.*, 2020, **49**, 17612–17620.

248 S. Ghosh, A. Das and S. Biswas, A functionalized UiO-66 MOF acting as a luminescent chemo sensor for selective and sensitive turn-on detection of superoxide and acetylacetone, *Microporous Mesoporous Mater.*, 2021, **323**, 111251.

249 Q. Li, Y. Li, Q. Guan, W. Li, X. Dong and Y. Dong, UiO-68-PT MOF-Based Sensor and Its Mixed Matrix Membrane for Detection of HClO in Water, *Inorg. Chem.*, 2019, **58**, 9890–9896.

250 S. Jindal and J. Moorthy, Zwitterionic Luminescent 2D Metal−Organic Framework Nanosheets (LMONs): Selective Turn-On Fluorescence Sensing of Dihydrogen Phosphate, *Inorg. Chem.*, 2022, **61**, 3942–3950.

251 X. An, Q. Tan, S. Pan, H. Liu and X. Hu, A turn-on luminescence probe based on amino-functionalized metal-organic frameworks for the selective detections of Cu^{2+}, Pb^{2+} and pyrophosphate, *Spectrochim. Acta, Part A*, 2021, **247**, 119073.

252 A. Sen, A. Desai, P. Samanta, S. Dutta, S. Let and S. Ghosh, Post-synthetically modified metal-organic framework as a scaffold for selective bisulphite recognition in water, *Polyhedron*, 2018, **156**, 1–5.

253 B. Chen, L. Wang, F. Zapata, G. Qian and B. Lobkovsky, A Luminescent Microporous Metal-Organic Framework for the Recognition and Sensing of Anions, *J. Am. Chem. Soc.*, 2008, **130**, 6718–6719.

254 H.-Y. Zheng, X. Lian, S. Qin and B. Yan, Novel ''Turn-On'' Fluorescent Probe for Highly Selectively Sensing Fluoride in Aqueous Solution Based on Tb^{3+} -Functionalized Metal− Organic Frameworks, *ACS Omega*, 2018, **3**, 12513–12519.

255 J. Song, I. Ahmed, P. Seo and S. Jhung, UiO-66-Type Metal-Organic Framework with Free Carboxylic Acid: Versatile Adsorbents via H-bond for Both Aqueous and Nonaqueous Phases, *ACS Appl. Mater. Interfaces*, 2016, **8**, 27394–27402.

256 A. Das and S. Biswas, A multi-responsive carbazole-functionalized Zr (IV)-based metal-organic framework for selective sensing of Fe (III), cyanide and p-nitrophenol, *Sens. Actuators, B*, 2017, **250**, 121–131.

257 R. Dalapati and S. Biswas, Post-synthetic modification of a metal-organic framework with fluorescent-tag for dual naked-eye sensing in aqueous medium, *Sens. Actuators, B*, 2017, **239**, 759–767.

258 Y. Li, K. Jiang, J. Zhang, T. Xia, Y. Cui, Y. Yang and G. Qian, A turn-on fluorescence probe based on post-modified metal–organic frameworks for highly selective and fast-response hypochlorite detection, *Polyhedron*, 2018, **148**, 76–80.

259 A. Das, S. Das, V. Trivedi and S. Biswas, A dual functional MOF-based fluorescent sensor for intracellular phosphate and extracellular 4-nitrobenzaldehyde, *Dalton Trans.*, 2019, **48**, 1332–1343.

260 Y. Sun, X. Xu, Y. Zhao, H. Tan, Y. Li and J. Du, Luminescent metal organic frameworks–based chemiluminescence resonance energy transfer platform for turn–on detection of fluoride ion, *Talanta*, 2020, **209**, 120582.

261 A. Das, N. Anbu, S. K. Mostakim, A. Dhakshinamoorthy and S. Biswas, A functionalized UiO-66 MOF for turn-on fluorescence sensing of superoxide in water and efficient catalysis for Knoevenagel condensation, *Dalton Trans.*, 2019, **48**, 17371–17380.

262 Y. Zeng, H. Zheng, X. He, G. Cao, B. Wang, K. Wu and Z. Lin, Dual-Emissive Metal-Organic Framework: A Novel Turn-on and Ratiometric Fluorescent Sensor for Highly Efficient and Specific Detection of Hypochlorite, *Dalton Trans.*, 2020, **49**, 9680–9687.